EXPERIMENTAL STUDIES OF HYDROXYL RADICAL INITIATED TROPOSPHERIC OXIDATION OF UNSATURATED HYDROCARBONS

A Dissertation

by

BUDDHADEB GHOSH

Submitted to the Office of Graduate Studies of
Texas A&M University
in partial fulfillment of the requirements for the degree of

DOCTOR OF PHILOSOPHY

August 2010

Major Subject: Chemistry

EXPERIMENTAL STUDIES OF HYDROXYL RADICAL INITIATED TROPOSPHERIC OXIDATION OF UNSATURATED HYDROCARBONS

A Dissertation

by

BUDDHADEB GHOSH

Submitted to the Office of Graduate Studies of
Texas A&M University
in partial fulfillment of the requirements for the degree of

DOCTOR OF PHILOSOPHY

Approved by:

Chair of Committee:	Simon W. North
Committee Members:	Dong Hee Son
	Yi-Qin Gao
	Sarah Brooks
Head of Department:	David H. Russell

August 2010

Major Subject: Chemistry

ABSTRACT

Experimental Studies of Hydroxyl Radical Initiated Tropospheric Oxidation of Unsaturated Hydrocarbons. (August 2010)

Buddhadeb Ghosh, B.Sc., Chemistry, Calcutta University, 2003

M.Sc., Chemistry, Indian Institute of Technology, Bombay, 2005

Chair of Advisory Committee: Dr. Simon W. North

The tropospheric oxidation of unsaturated hydrocarbons is a central issue in atmospheric chemistry. These hydrocarbons are emitted into the atmosphere from both natural and anthropogenic sources, and their atmospheric oxidation leads to different atmospheric pollutants, including ground level ozone, photochemical smog and secondary organic aerosols. Isoprene and 1,3-butadiene represent a biogenic and an anthropogenic hydrocarbon, respectively, which primarily undergo electrophilic addition of OH radical, followed by chain propagating radical reactions. Their oxidation is the major source for ground level ozone formation in both rural and urban area and understanding their chemistry is essential for regional air quality modeling.

Until recently, most of the studies of isoprene chemistry have been non-isomer specific, reflecting the reactivity of combined pathways and therefore were insensitive to specific details of the isomeric pathways. An isomeric selective approach to studying unsaturated hydrocarbon oxidation is described in this dissertation. A synthesized precursor, whose photolysis can provide a route to the formation of energy selected single isomer in the isoprene oxidation pathway, enables the study of important channels that

are difficult to unravel in non isomer specific experiments. The major addition channel in OH isoprene oxidation has been studied following the isomeric selective approach and using Laser Photolysis-Laser Induced Fluorescence (LP-LIF) as the primary experimental technique. The study reveals important information about the oxidative chemistry of the δ-peroxy radicals, accounting for about 20% of missing carbon balance in isoprene oxidation, and isomeric specific rate constants.

A similar approach was applied to study the oxidation of 1,3-butadiene, and the photolytic precursor for the dominant hydroxy alkyl isomer in the OH initiated oxidation of 1,3-butadiene was synthesized. The subsequent experiments and analysis revealed detailed information about the oxidative chemistry accounting for approximately 26% of the missing chemistry.

Finally, non isomeric selective OH cycling experiments were carried out on the1,3-butadiene system. By analyzing the OH cycling data with the combined information obtained from the isomeric specific studies of the two isomeric channels of 1,3-butadiene oxidation, the relative branching between the two isomeric channels of OH-1,3-butadiene oxidation was determined.

To my wife

ACKNOWLEDGMENTS

I am grateful to my wife Leema for her love and support, and to my family members and friends back in India and UK. I am especially thankful to my advisor Simon North who has always been very supportive, and understanding. It's highly advantageous to have a smart and helpful advisor like him. I am thankful to my committee members, Dr. Yi-Qin Gao, Dr. Dong H. Son, and Dr. Sarah Brooks for coming up with thought provoking and critical questions and comments regarding my research, that helped me to view my work from different perspectives. I am especially thankful to Dr. Don Collins, for agreeing to substitute in my defense in a very short notice. I am also thankful to Dr. Marian Hyman, who was the professor of the CHEM 320 course that I taught for over three years. She was very nice and helpful, and she also wrote recommendation letters for me. I owe my thanks to Alejandro Bugarin and Dr. Brian Connell for helping me with organic synthesis. Without their help, it would have been much more difficult to do this work. I am also thankful to my group members, Michael and Qingnan who have been true friends. They are two extremely useful people in the laboratory as Michael knows everything about programming and Qingnan knows everything about everything! I'll miss you guys! Last but not least, I am thankful to my former and current group members: Hahkjoon, Erin, Kate, Kristin, Justine, Rodrigo, Michelle and Doyoung. Most of them have been very helpful and friendly for all these time.

TABLE OF CONTENTS

CHAPTER Page

LIST OF FIGURES

FIGURE Page

FIGURE Page

FIGURE Page

LIST OF TABLES

CHAPTER I

INTRODUCTION

The envelope of gas surrounding Earth is called the atmosphere. It has a mass of about 5×10^{21} g, which is primarily composed of N_2(78%), O_2 (21%), Ar (0.9%) and a varying amount of other gases including water vapor, CO_2, methane, and ozone. The atmospheric density decreases exponentially with altitude in a continuous way with four distinct layers identified in terms of temperature behavior. The lowest layer starting at the earth surface and extending up to 8-15 km is called the troposphere. The troposphere contains approximately 75% of the total atmospheric mass, and it is the place where all the life exists. Thus the tropospheric chemistry has the most intense effect on human life and is also influenced by human activity. This makes tropospheric chemistry the most widely studied field within atmospheric chemistry.

The majority of the chemical constituents of troposphere are chemically non reactive and it is the trace gases that are primarily responsible for the bulk of the chemistry taking place in the troposphere. Therefore the troposphere behaves like a complex chemical reactor. These trace species include various hydrocarbons emitted into the atmosphere from different biogenic and anthropogenic sources, NOx and other nitrogen compounds, sulfur compounds, oxides of carbon, ozone, and aerosols. Chemical reactions generally require activation energy and tropospheric temperatures are too low for thermal activation. As a consequence, tropospheric reactions are often initiated by

---

This dissertation follows the format of the *Journal of Physical Chemistry A*.

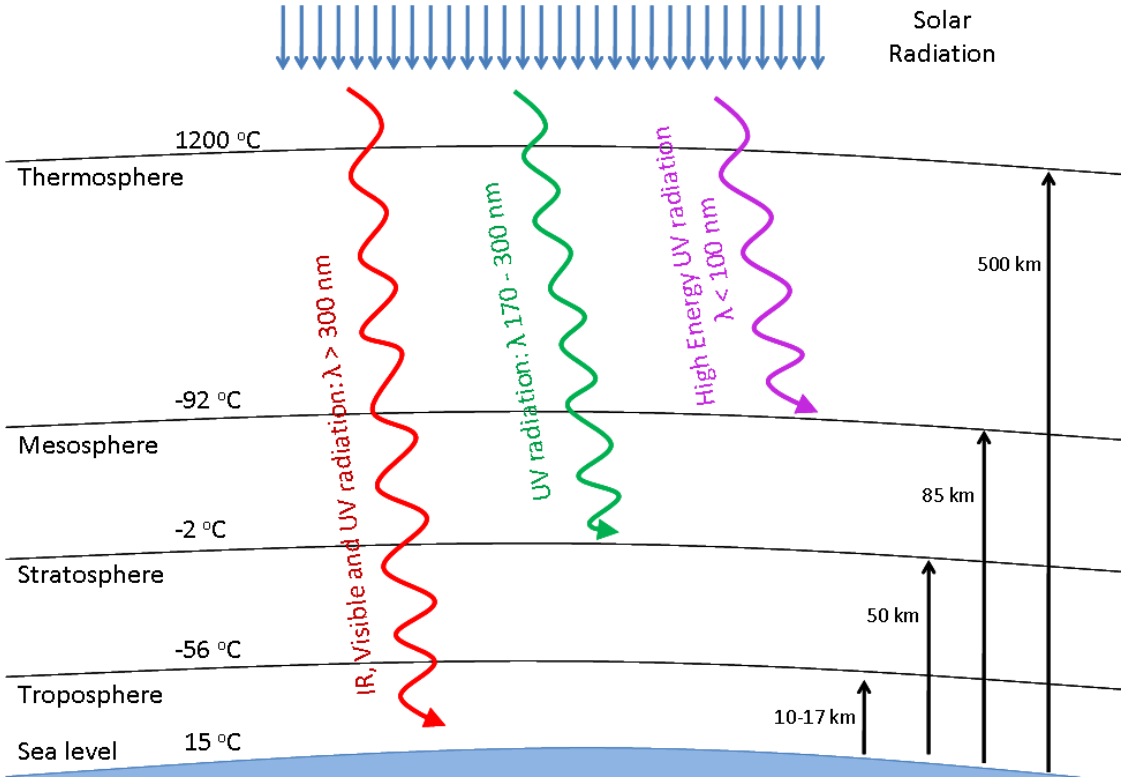

Figure I-I. Schematic description of the different layers of atmosphere.

radicals, as radical reactions typically feature low activation barriers. The primary radicals are often generated by photochemical dissociation caused by sunlight, and their subsequent reactions generate secondary radicals. The nature of photochemical processes at different parts of the atmosphere largely depends on the range of the wavelengths from solar radiation (Figure I-I). The lower wavelength limit of solar radiation entering the stratosphere is 170 nm and entering the troposphere is 300 nm. This influences the photochemical properties of these two layers of atmosphere and the major photochemical process in the stratosphere is the photodissociation of O_2 in the wavelength region of 170-240 nm and photodissociation of O_3 in the wavelength region 210-300 nm. These processes, along with a series of oxygen reactions maintain the stratospheric ozone equilibrium. About 1% of the stratospheric ozone is transported to the troposphere, where the O_3 molecule is photodissociated in the wavelength region 290-330 nm to produce excited state oxygen atom that results in the production of hydroxyl radical.

$$O_3 + h\nu \rightarrow O(^1D) + O_2 \qquad (290 < \lambda < 320 \text{ nm})$$

$$O\ (^1D) + M \rightarrow O(^3P) + M \qquad (M: N_2, O_2)$$

$$O\ (^1D) + H_2O \rightarrow 2OH$$

Photodissociation of ozone is the primary source of tropospheric OH radical, and about 25% of O (^{1}D) ultimately produces OH radicals. The tropospheric OH concentration shows a strong diurnal variation, with a peak around mid-day, due to the variation in the solar flux. Other sources of OH radical include photodissociation of HCHO and HONO as well as reaction of ozone with alkenes, and its primary decay processes are reactions with methane and carbon monoxide. Hydroxyl radical has a global average concentration of $(8\pm2) \times 10^5$ molecule cm^{-3} and a high reactivity towards many of the atmospheric trace

gases. Its reaction is the primary tropospheric decay process for CO, methane and most of the volatile organic compounds (VOC) in the troposphere. These VOCs are emitted into the atmosphere from both biogenic and anthropogenic sources, with a global emission rate of 1×10^{14} g carbon per year and 1.2×10^{15} g carbon per year respectively from the two types of sources. In the atmosphere they primarily react with OH radical, followed by a series of radical chain propagating reactions. In the urban atmosphere with high NOx concentration, VOC oxidation leads to the formation of ground level ozone, secondary organic aerosols and photochemical smog.

Approximately 5% to 30% of tropospheric ozone comes from stratosphere due to vertical mixing,[1] and the rest is photochemically produced in the troposphere during the daytime. Tropospheric ozone production is primarily initiated by reaction of NO and peroxy radicals producing NO_2, whose photolysis leads to the formation of ozone. Unlike the VOC, the NOx is primarily emitted from anthropogenic sources.

$$RO_2 + NO \rightarrow RO + NO_2 \qquad \text{(R: H, Alkyl group)}$$

$$NO_2 + h\nu \rightarrow NO + O(^3P) \qquad (\lambda < 430 \text{ nm})$$

$$O + O_2 + M \rightarrow O_3 + M \qquad \text{(M: } N_2, O_2\text{)}$$

Although tropospheric ozone constitutes only 10% of the total ozone in the atmosphere, it plays a central role in atmospheric chemistry as it is an important greenhouse gas and a toxic pollutant. Tropospheric ozone has adverse effect on both human health as well as vegetation and it is also the main constituent of photochemical smog. It results in destruction of chlorophyll in plant levees and leads to lung disease and respiratory infections in human due to its strong oxidizing power. Besides being an oxidant itself, it

is the precursor for other important tropospheric oxidants, *i.e.* OH radical and NO_3 radical.

Photochemical smog develops when primary pollutants like VOC, NOx, react photochemically to produce a mixture of hazardous secondary pollutants. It primarily consists of ground level ozone as well as peroxyacetyl nitrate (PAN), nitric acid, aldehydes, particulate nitrate and sulfate. Photochemical smog has strong oxidizing power that causes respiratory problems in animal, damages plant membrane, and it also leads to reduced visibility.

Our research is aimed at studying the OH radical initiated photochemical oxidation of VOCs by studying the rate constants of the intermediate radical reactions. A general oxidation mechanism for VOCs is described in figure I-II. In the atmosphere, these hydrocarbons primarily react with OH radical to form alkyl radical, which react with molecular oxygen to produce peroxy radicals. The peroxy radical may undergo a number of competing reactions including reactions with NO, HO_2, and self/cross reactions with peroxy radicals. In the pristine environment of Amazonian rain forest, the concentration of NO is low, and the peroxy-NO reaction is slow. In such a "low NOx" situation, the peroxy radicals react with HO_2 or other peroxy radicals to form either ROOH or carbonyl and alcohols respectively. These carbonyl compounds are one of the building blocks of the secondary organic aerosol. However, in most parts of the continental US and globally, the atmosphere contain relatively high concentration of NO. In these "high NOx" conditions associated with the polluted atmosphere, the NO-peroxy reaction dominates, and the peroxy radical produces alkoxy radical and NO_2. The alkoxy radicals can either react with molecular oxygen or fall apart to form different products

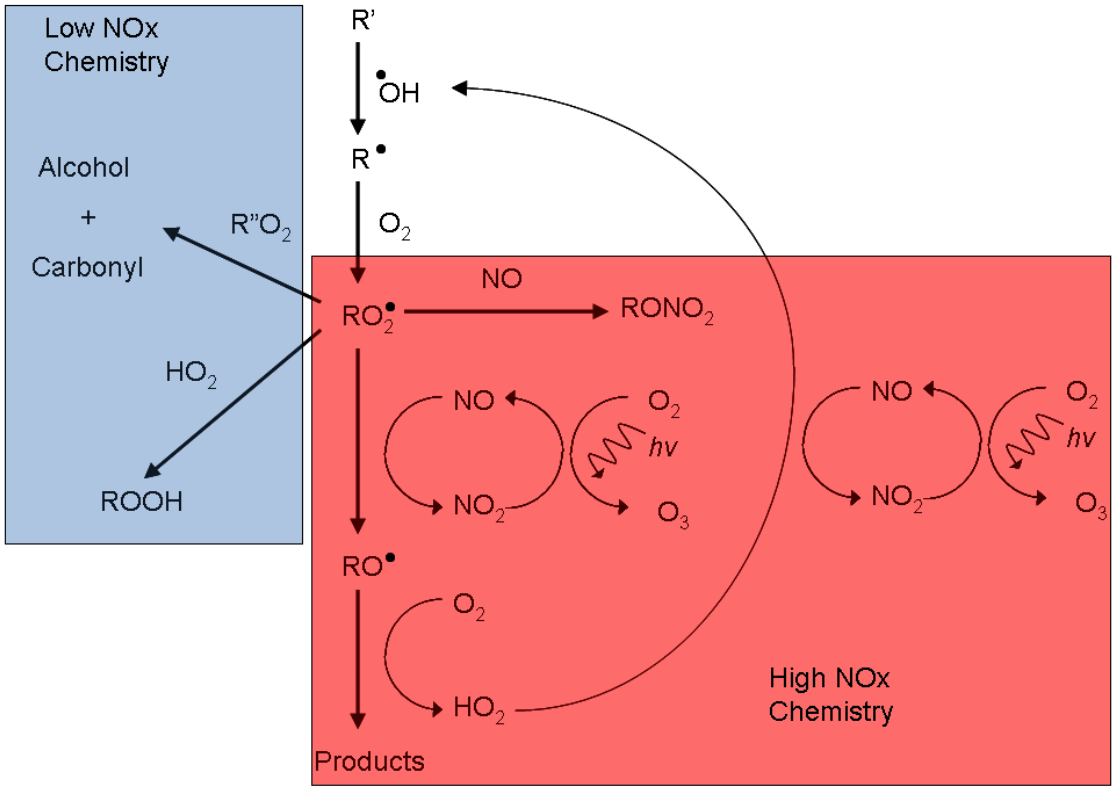

Figure I-II. General description for OH radical initiated photochemical oxidation of VOC in atmosphere.

and HO_2. HO_2 can further react with NO to recycle OH radical back, along with the production of NO_2. Thus, OH is not consumed in reaction with trace gases, rather it is regenerated in catalytic cycles of chain reactions. This helps to maintain a non-negligible steady concentration of OH ($5\text{-}10\times10^5$ molecule cm^{-3}) in the troposphere, in spite of its high reactivity towards most trace gases. It is the moderate concentration of OH, coupled with its high reactivity and ability to initiate chain reaction, that make OH radical the most powerful oxidizing agent in the troposphere. The NO_2 that is formed during the oxidation process photolyzes to form NO and O (^3P), which reacts with molecular oxygen to produce ozone. Thus, it is the photodissociation of NO_2 that drives the formation of tropospheric ozone, which is also the major component of photochemical smog. So, the broader goal of the research is to understand the formation of tropospheric ozone, photochemical smog and secondary organic aerosols by studying VOC oxidation. A clear understanding of VOC oxidation mechanism will help in improving the atmospheric model for regional and global air quality modeling.

Air Quality Models (AQMs) are mathematical representation of the atmospheric processes which attempt to simulate, by varying degree of detail, the formation, transport, transformation, and deposition of different atmospheric pollutants. AQMs are used in analyzing the behavior and effects of different secondary pollutants like tropospheric ozone, secondary organic aerosols (SOA), particulate matter (PM), acid deposition, regional haze, and photochemical smog. AQMs are essential tools in evaluating the effects of possible control strategies placed on the emission sources aimed at reducing pollution to meet air quality goals. In order to simulate the atmosphere, an AQM must consist of components describing the emission sources of different chemicals, the

meteorological input such as sunlight, wind and temperature, vertical and horizontal transportation and diffusion, aerosol chemistry, clouds and aqueous chemistry, photolysis rates of different chemical species and gas phase chemical mechanism of different compounds. The gas phase chemical mechanism is an important component of AQM describing the chemical reactions, product distribution and kinetic data necessary to simulate the photochemical decay of the primary pollutants and the formation of the secondary pollutants. Due the involvement of large number of compounds in atmosphere, and the large number of reactions these compounds (and their reaction products) undergo, considerable effort is spent approximating and condensing the chemical mechanism. In early modeling, one factor restricting the level of detail in chemical mechanism was the computational cost, as much of the computational effort in AQM is used up in numerically solving the chemical mechanism. However, with the advancement of powerful computational techniques, more recently, the main factor limiting the level of detail of chemical mechanism is our lack of clear understanding of major chemical processes. Carbon Bond[2] mechanism (CB4), SAPRC[3] mechanism and their respective updated versions CB05[4] and SAPRC-99[5] are the most commonly used chemical mechanisms to describe atmospheric chemistry, especially tropospheric ozone formation. However, serious discrepancies are observed among these models in ozone prediction and the largest differences often occur in areas with high biogenic emission (central and southern US) and urban areas with high NOx emission.[6] The maximum difference in predicted ozone concentrations between SAPRC-99 and CB4 can be as high as 44.6 ppb.[7] Thus, while one model predicts ozone concentrations below the EPA regulated value; on other model may predict an ozone concentration above the regulated value. A major

reason for the discrepancy is believed to be the uncertainty in biogenic alkene oxidation mechanism under high NOx conditions, due to their high reactivity and large emission. A better understanding of alkene oxidation will help to create better atmospheric chemistry models which will help in making proper regulatory policies to control the amounts of the atmospheric pollutants. We have used different experimental approach to study the atmospheric oxidation of different unsaturated hydrocarbons, namely isoprene and 1,3-butadiene under high NOx conditions, as high NOx conditions are more relevant air quality in the United States.

The OH radical acts as an electrophile towards alkenes, and adds to the double bond to form hydroxyl alkyl radicals, which undergo further reactions (Figure I-II). In case of asymmetric alkenes, the OH radical can add to two possible carbons of the double bond, leading to two different hydroxyl alkyl radicals. Different hydroxyl alkyl radicals, in general, exhibit different reactivity and lead to different end products through diverse chemistry. Until recently, studies of alkene oxidation chemistry have been non-isomer specific, *i.e*. an alkene is reacted with OH radicals in presence of other reactant gases and the resulting chemistry is studied using various spectroscopic, separation, and mass spectrometric methods. The main drawback of such an approach is that the results reflect the reactivity of the combined isomeric pathways and are often insensitive to specific details of the individual pathways. Thus, minor channels are very difficult to study as they can be obscured by the major channels. We have developed an *Isomeric Selective Approach* where a hydroxyl group and an iodine atom are added across a C=C double bond in an alkene through proper organic synthesis to produce an iodohydrin precursor. The C-I bond in the iodohydrin can be photolyzed *in situ* using a laser pulse to produce

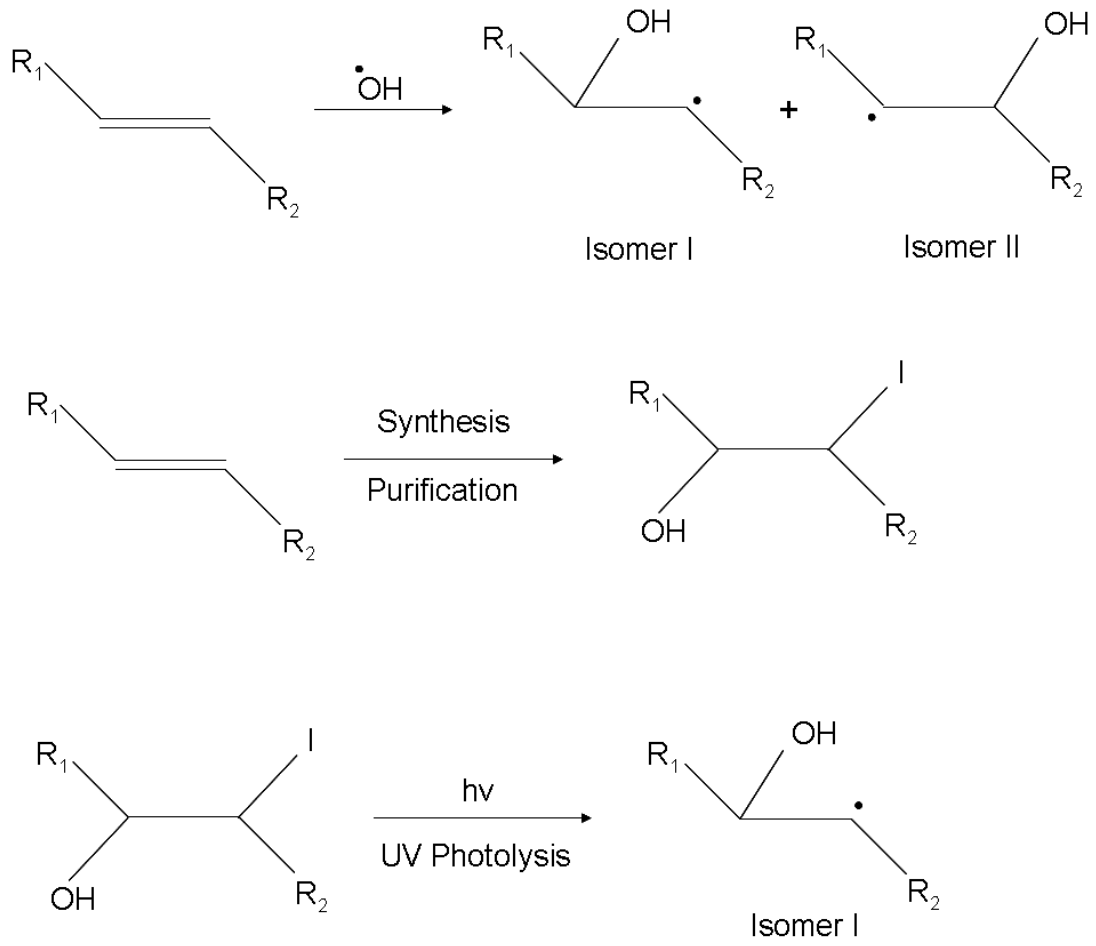

Figure I-III. Schematic description of Isomeric Selective Approach.

one specific hydroxyl alkyl isomer, out of the two possible isomers that would be produced by OH radical addition to the alkene (Figure I-III). In this way, we can isolate a single OH-alkene adduct isomer and study its reactivity exclusively, without any interference from the other isomeric channels. In our previous studies, we demonstrated that isomer selective kinetic experiments permit the investigation of minor important channels in alkene oxidation that are obscured by the major channel kinetics.[8-9] In the present study, we focused on the dominant channels of the isoprene and 1,3-butadiene oxidation, and to this end, we have synthesized the photolytic precursors 2-iodo-2-methyl-but-3-en-1-ol and 2-iodo-but-3-en-1-ol respectively. In doing so, we reduce the complex chemistry of isoprene and 1,3-butadiene oxidation to the chemistry of a single isomeric pathway permitting determination of isomer specific kinetic rate constants. The chemistry is discussed in more detail in the respective chapters.

Isoprene (2-methyl-1,3-butadiene) is the dominant non methane organic compound (NMOC) emitted into the atmosphere by vegetation with an annual global emission rate of ~ 500 Tg.[10] It represents almost 50% of all biogenic non-methane hydrocarbons on a global scale[11] with an atmospheric concentration between 1-30 ppb.[12-13] In the atmosphere, isoprene reacts with the OH radical, NO_3 radical, Cl radical and O_3,[14] although a strong diurnal emission rate and high reactivity towards the OH radical results in chemistry dominated by OH initiated oxidation (90 %) with an atmospheric lifetime with respect to the OH radical of approximately 1.5 hours.[15] The OH initiated oxidation of isoprene is a central issue in atmospheric chemistry and is responsible for 50-100% of ozone production attributed to VOC oxidation in the continental US[13] which has adverse effect on vegetation[16-17] and human health.[17] Isoprene oxidation also leads to

the formation of organic nitrates which are responsible for removal of as much as 7% of the NO emitted in North America in the summer time[15] accounting for 4% of nitrogen oxide transported from North America.[18] Isoprene is responsible for a 10% increase in the half-life of methane.[19] Finally, the oxidation of isoprene leads to US and global biogenic SOA formation of 50% and 58%, respectively.[20-22] The accuracy of air quality modeling depends on a detailed understanding of the mechanism of OH initiated isoprene oxidation. We have used laser based experimental techniques to study the dominant addition channel of isoprene oxidation that accounts for 55-70% of its oxidation chemistry. We have experimentally identified and quantified the δ-hydroxy alkyl peroxy radical channel that accounts for about 20% of the missing carbon balance and the results have been discussed in Chapter III.

1,3-butadiene is an anthropogenic hydrocarbon, emitted into the atmosphere primarily as a combustion by-product with automobile exhaust contributing ~ 80% to the total 1,3-butadiene emission in USA.[23] Other sources of 1,3-butadiene include open burning (~15% contribution),[23] and industrial emissions[23] resulting in atmospheric concentrations ranging from 0.1 to 15.0 ppb.[24-25] 1,3-butadiene is one of the most important bulk chemicals with an annual production rate of 6 million tons.[26] It is also a significant toxic pollutant,[23] recognized as a known human carcinogen,[27-28] with a 30 times higher unit risk factor than that of benzene,[24] and a known mutagen.[29] In the troposphere, removal of 1,3-butadiene is initiated by its reaction with OH, Cl, NO_3 and O_3 although the dominant removal process is the reaction with OH.[30-33] Developing a detailed tropospheric oxidation mechanism for 1,3-butadiene is vital in improving air quality model for toxic chemicals which guide regulatory policies. We have used an

isomeric selective approach to study the dominant addition channel of OH initiated oxidation of 1,3-butadiene. Our studies lead to an understanding of the chemistry of the *δ*-peroxy channel, which provides a mechanistic pathway for the formation of 26% of first generation end products and the results have been discussed in the Chapter IV. We have performed OH cycling experiments on OH-1,3-butadiene oxidation to unravel the initial branching in between the two addition channel. The two addition channels shows distinctly different oxidation chemistry and have very different end product formation as well as consequence on ozone production. The results are discussed in the Chapter V. Finally some concluding remarks and future direction for the research has been discussed in the Chapter VI.

CHAPTER II

EXPERIMENTAL TECHNIQUES

A. OH Cycling Experiments

We have used Laser Induced Fluorescence (LIF) technique to probe OH radical concentration over reaction time scale. OH radicals add to 1,3-butadiene or isoprene to form hydroxyl alkyl radicals. The hydroxyl alkyl radicals undergo further reaction with molecular oxygen to form peroxy radicals which then react with NO to form alkoxy radicals and NO_2. Alkoxy radical dissociates and/or reacts with O_2 to produce HO_2 which further reacts with NO to regenerate OH radicals. Thus, OH acts as a catalyst in the oxidation of isoprene/1,3-butadiene and is cycled through the reaction sequence. The time dependent kinetics of OH in the presence of NO and O_2 is a sensitive probe of the detailed mechanism of the oxidation process and this constitutes the basis of OH cycling experiments. We have performed primarily two different types of experiments to study the oxidative chemistry of isoprene and 1,3-butadiene systems; the isomeric selective experiments that are described in chapter III and IV and the non isomeric OH cycling experiments. In isomeric selective experiments, a precursor iodohydrin class of compound is photolyzed to selectively produce the hydroxyl alkyl radical of choice directly, without the addition of either the alkene or the OH radicals. The hydroxyl alkyl radical then undergoes the reaction sequence to produce OH radicals characterized by an initial rise in OH signal followed by long range decay due to radical termination processes. In these experiments, OH radicals are not strictly “cycled” through the reaction sequence, but rather are formed from the oxidation of the precursor. Thus, although the

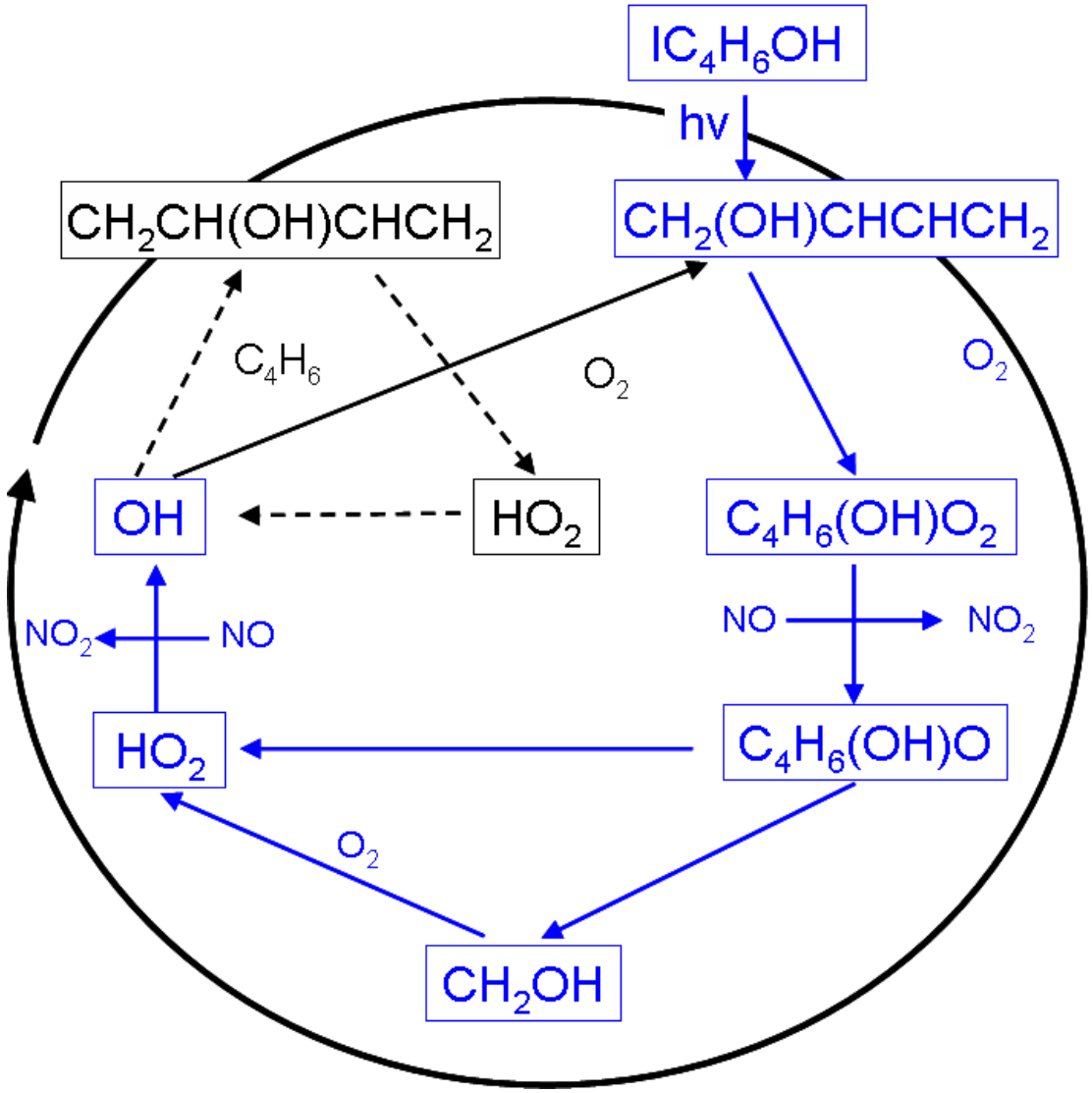

Figure II-I. The mechanism of non isomeric OH cycling and isomeric selective OH cycling chemistry is shown in the case of 1,3-butadiene. While both the □hydroxyl alkyl radicals are formed in non isomeric experiments, only certain □hydroxyl alkyl radicals are generated in situ in isomeric selective experiments, to study their chemistry exclusively (shown in blue).

process should not be called OH cycling but OH formation, we retain the notation since the experiments are similar to common cycling experiments. In the non isomeric OH cycling experiments, however, the alkene is introduced in the experiment along with H_2O_2. The laser photolysis of H_2O_2 produces the OH radical, which then reacts with the alkene to produce the mixture of all the possible hydroxyl alkyl radicals. The hydroxyl alkyl radicals then undergo the series of reaction, finally resulting in OH formation. These experiments, unlike the isomeric selective experiments, reflect OH cycling. The two types of experiments are depicted in the case of 1,3-butadiene in Figure II-I.

B. Laser Photolysis-Laser Induced Fluorescence (LP-LIF)

A detailed description of LP/LIF experiment is presented here. A 248 nm beam (8 mm × 2 mm, 15 mJ/pulse) from an EX10 Excimer laser (GAM laser) was used to photolyze the precursor iodohydrin to produce specific hydroxyl alkyl radical or H_2O_2 to produce OH radical. The concentration of the OH/OD radical that were generated, were monitored by measuring the OH/ OD fluorescence by exciting at the Q_1 (1) and Q_1 (2) transitions of the A ← X (1, 0) band at 282 nm or 287 nm for OH or OD, respectively. The probe beam was generated by doubling the output from a dye laser (Quantel TDL-51) running Rhodamine 590 dye or a mixture of Rhodamine 590 and Rhodamine 610 dye pumped by a 532 nm beam (5/16” diameter, 175 mJ/pulse) from an Nd YAG laser (Spectra Physics Quanta Ray INDI). The LP-LIF setup is schematically described in Figure II-II. The experiment cell was a stainless steel hollow cube, vacuum sealed by 4.5” stainless steel flanges at the six surfaces using copper gaskets. A cross section view of the LP-LIF experiment cell is given in Figure II-III and a digital picture is provided in

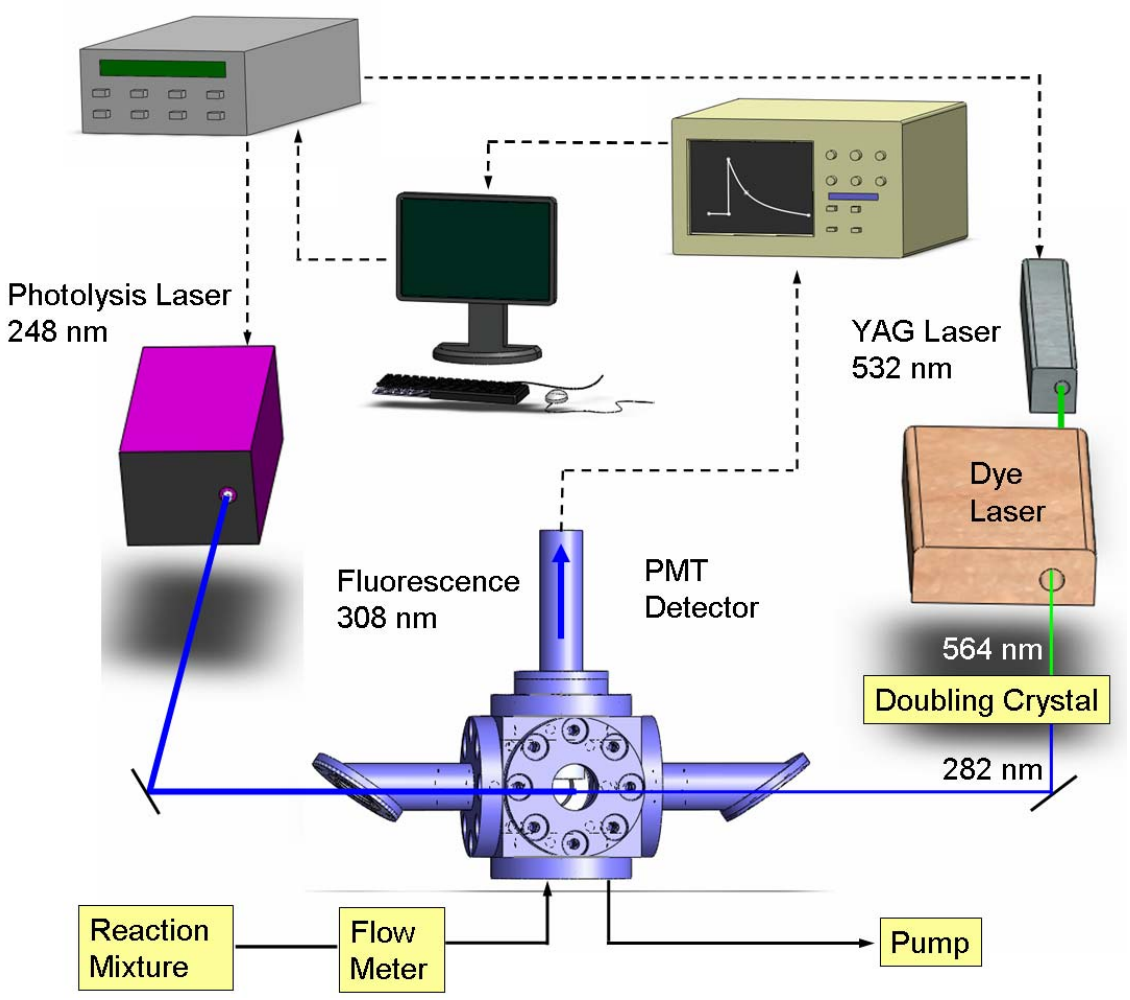

Figure II-II. Laser Photolysis-Laser Induced Fluorescence (LP-LIF) set up.

Figure II-IV. Two quartz windows were mounted at the two opposite ends of the reaction cell through two side arms. The pump and the probe laser beams were introduced to the reaction cell through these windows and were collinearly aligned. The windows were kept at Brewsters angle to reduce beam reflection. A set of conical skimmers were installed in the beam path inside both the side arms, to reduce the scattering of light as well as to maintain a pump beam size ten time large compared to the probe beam to reduces the fly out effect. Keeping a larger probe beam compared to pump beam also reduces the fly out effect, however a larger probe beam at 282/287 nm results in more noise at the photomultiplier tube (PMT) installed to detect 308 nm signal, compared to a large pump beam at 248 nm. The PMT was housed in cylindrical holder mounted on a flange and vacuum sealed by a BK7 window to reduce the scattering from the pump or probe beam. A visible filter was also placed in front of the PMT, providing a band-pass filter near 300 nm that significantly decreased the contribution from scattered light. The resulting fluorescence was collected by a lens assembly. An 1" diverging lense was used to collimate the beam which was passed through an 1" converging lense to focus the beam onto the PMT after passing through the optical filter setup. The signal was integrated by a using a digital oscilloscope (Lecroy 9310A) and the time delay between the two lasers was controlled by a digital delay generator (SRS DG-535). The kinetic experiments were performed by changing the delay between the two lasers and monitoring the fluorescence signal, being averaged over 50-100 laser pulses. A Labview program was used to control the experiments. The precursor iodohydrin compounds were introduced into the reaction cell using an MKS flow meter by flowing Argon through a bubbler that contained the sample at room temperature. When running 1,3-butadiene, the

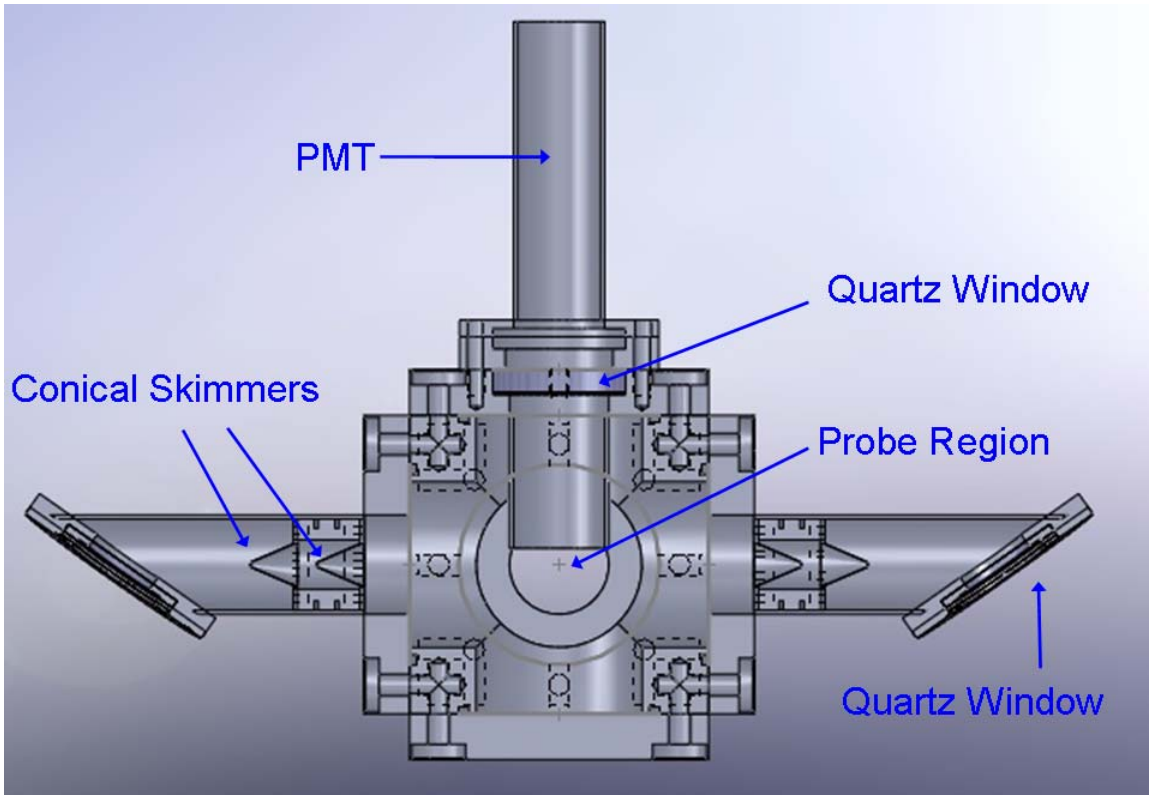

Figure II-III. A close up cross-section view of LP-LIF reaction cell.

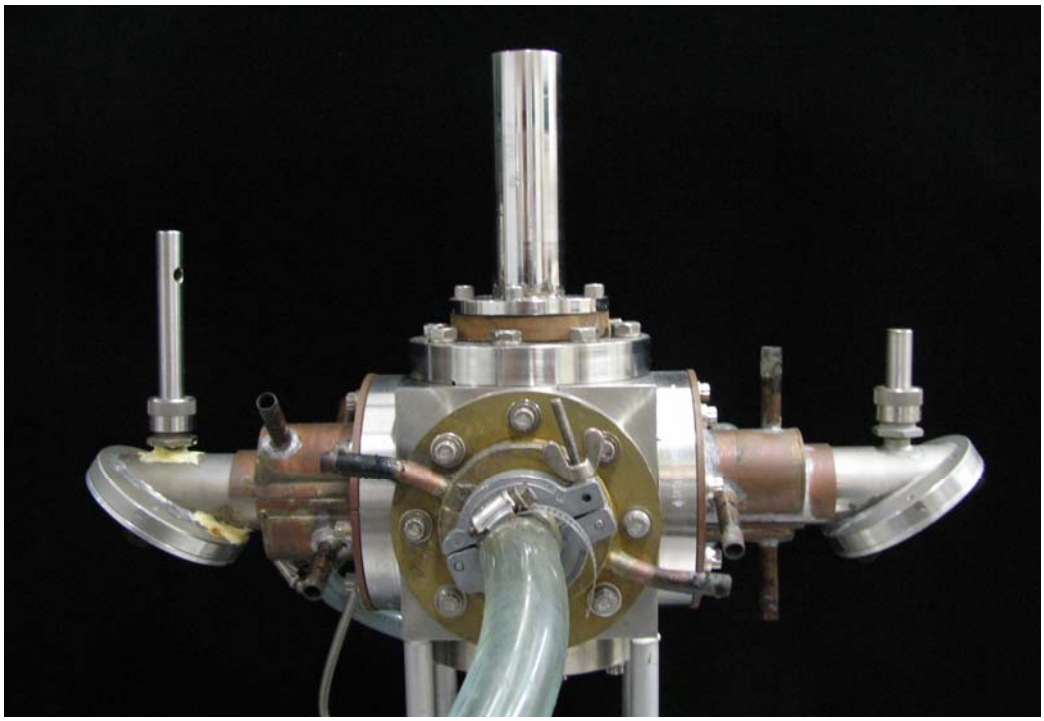

Figure II-IV. A close up digital picture of LP-LIF reaction cell.

sample was buffered with argon and introduced into the reaction cell though an MKS flow meter. NO (Sigma Aldrich, 98.5%) was purified to remove HONO and NO_2 by using an ascarite trap before buffering it with argon in a 5L bulb and was introduced into the chamber through an MKS flow meter. O_2 (BOTCO, 99.995%) was also buffered with argon (BOTCO) to make a known concentration and introduced into the cell through flow meters. The cell was evacuated through a dry ice trap by a mechanical pump to maintain a slow flow state, such that the reactant molecules were replenished in between every shot while the lasers were operated at 10 Hz. Experiments were typically run at fixed concentration of iodohydrin/1,3-butadiene, while varying the concentration of NO and O_2. The temperature of the reaction cell was maintained at room temperature (297 ± 3 K) and an MKS baratron was used to monitor the total pressure inside the cell.

The probe laser beam was calibrated using a separate LIF wavelength calibration cell. A prism mounted on a rotatable mount was used to direct the probe laser beam alternatively through the LP-LIF experiment cell or the LIF wavelength calibration cell. A rough calibration of wavelength was performed by collecting an optogalvanic (OG) spectrum using a copper neon hollow cathode lamp (Figure II-V); however the fine tuning of the wavelength for the LIF detection of OH or OD was carried out by using the LIF calibration cell. A schematic of the calibration cell is given in the Figure II-VI. A quartz tube is connected to the aluminum made calibration cell through a stainless steel ultra torr connection. Argon is bubbled through H_2O or D_2O through the quartz tube into the calibration cell which is pumped down to a pressure of few torr through dry ice trap by using a vacuum pump. An Evenson cavity (Opthos) connected to a microwave generator (Opthos) is installed on the quartz tube. The microwave generator

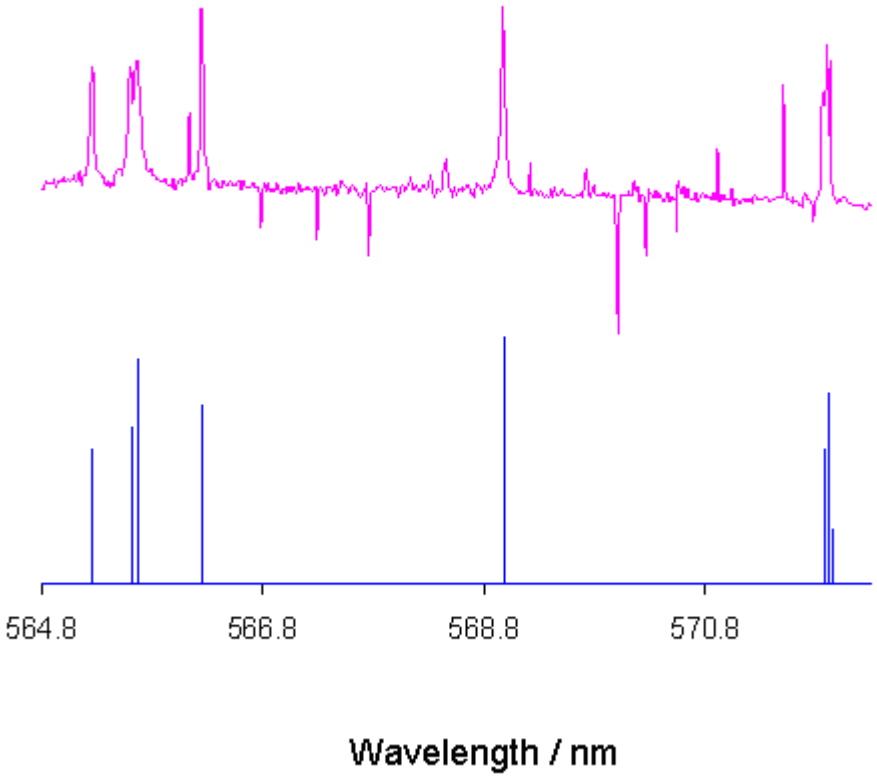

Figure II-V. Experimental (pink) and literature (blue) optogalvanic (OG) spectrum (Copper hollow cathode lamp) in the region of 564 nm.

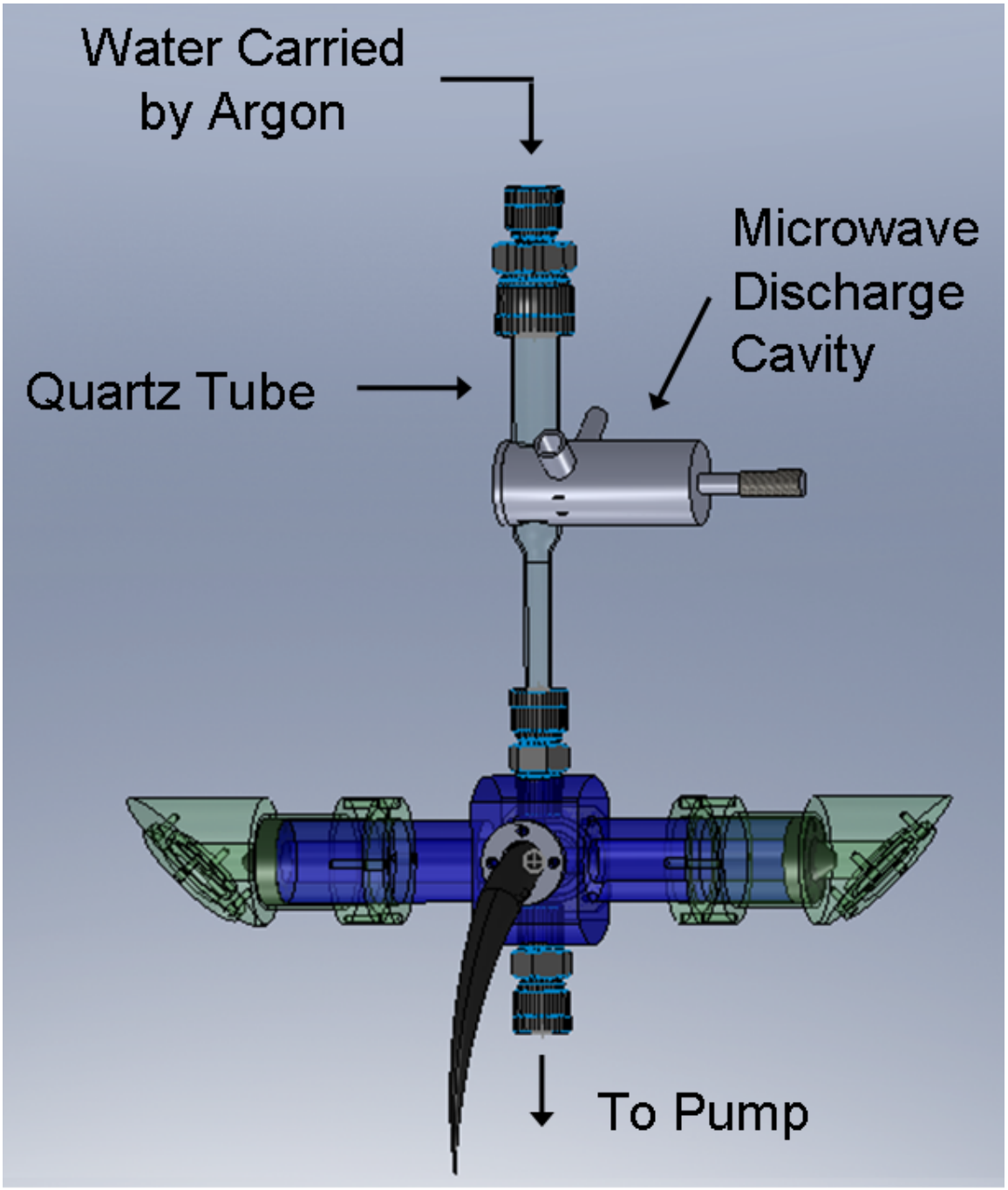

Figure II-VI. OH/OD LIF calibration cell.

produces radiation in the microwave range (2.4 GHz) and the cavity transfers the power from the microwave radiation to the water vapor flowing through the quartz tube.[34] This produces plasma, which was initiated using a tesla coil. A digital picture of the plasma is provided in Figure II-VII. A fraction of the water molecules are dissociated in the plasma, producing detectable yields of OH/OD radicals. The probe beam was used to excite the OH/OD radicals via A ← X (1, 0) transition and the fluorescence originating from the excited OH/OD radicals were detected by a sideways mounted PMT. The signal is integrated using a digital oscilloscope. The laser is scanned over the rotational lines of the A ← X (1, 0) transition to generate the LIF spectrum. The experimentally obtained LIF spectrum is compared with the simulated LIF spectrum to find out the strongest peak in the spectrum and the experiments are performed at this particular wavelength. A set of experimental and simulated LIF scans for OH and OD are shown in the Figure II-VIII and Figure II-IX.

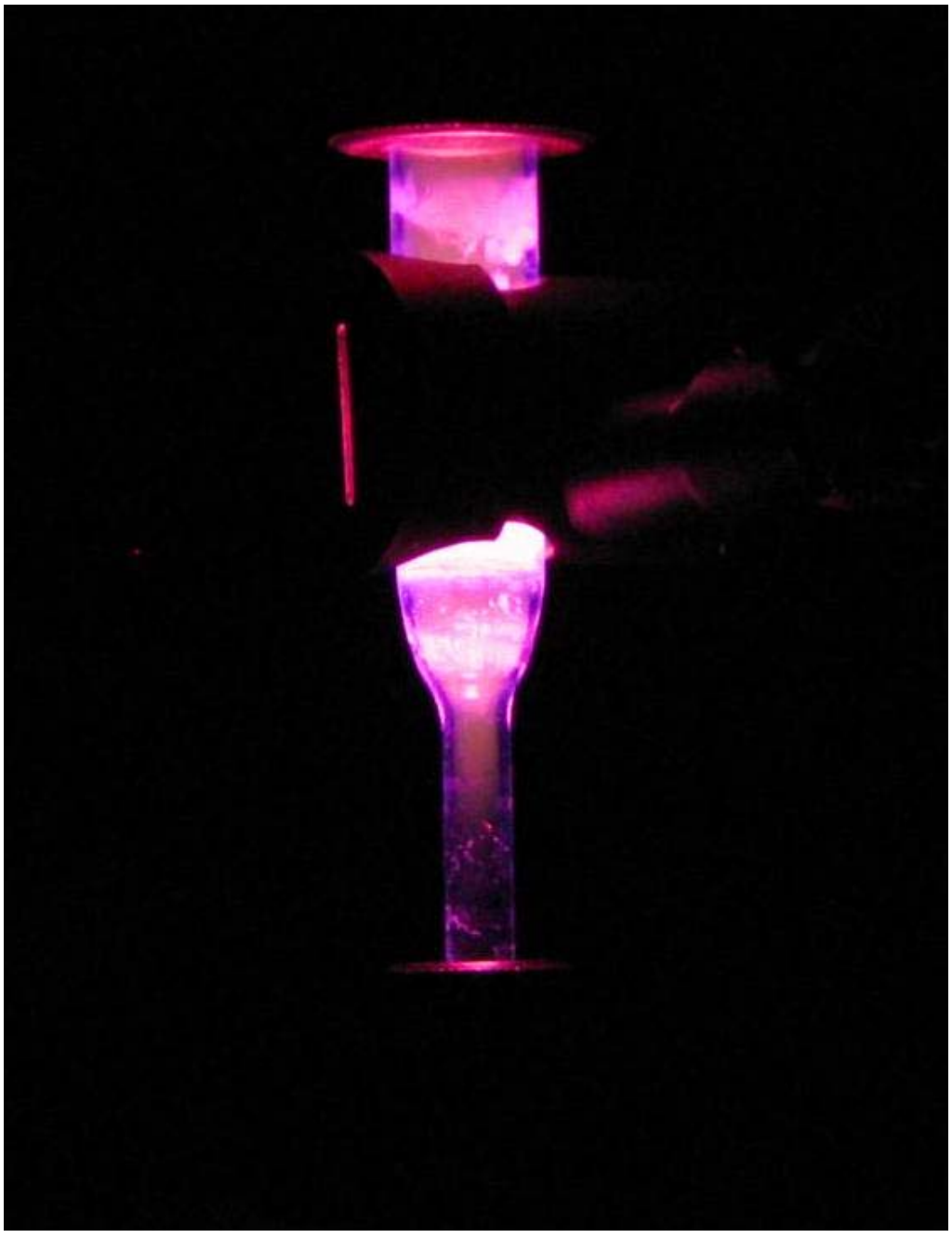

Figure II-VII. Digital picture of the plasma used to generate OH/OD radicals.

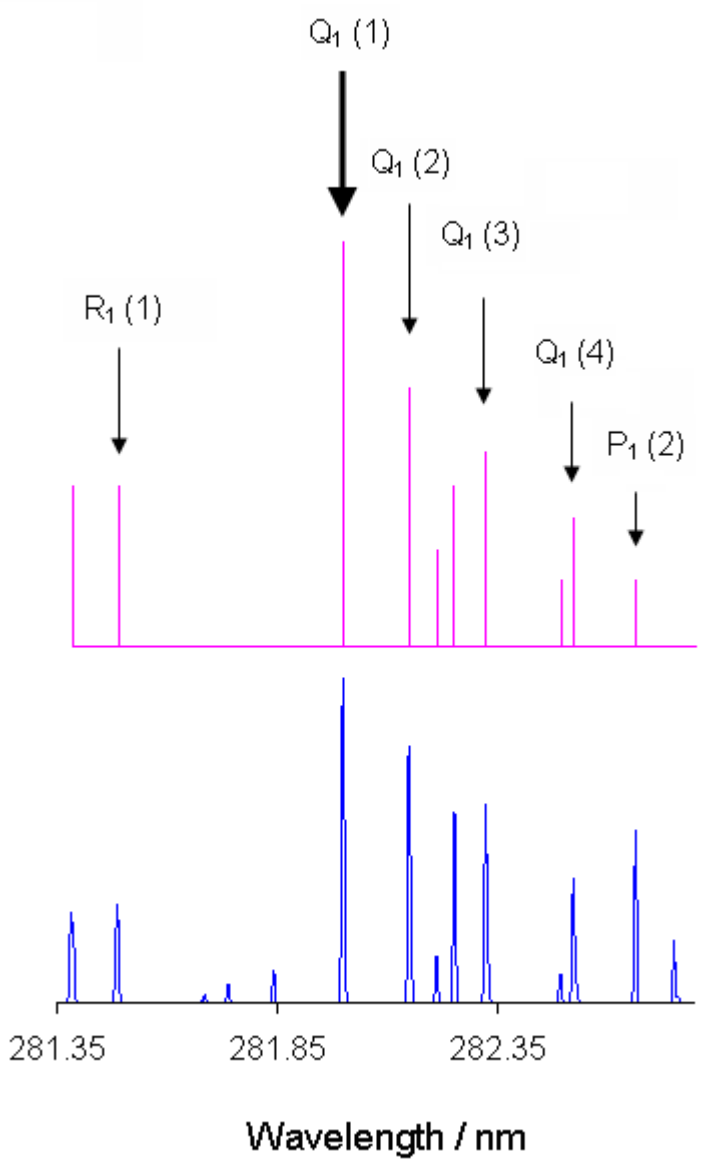

Figure II-VIII. Experimental (pink) and simulated (blue) LIF scan for OH radical on the A← X (1,0) vibrational band.

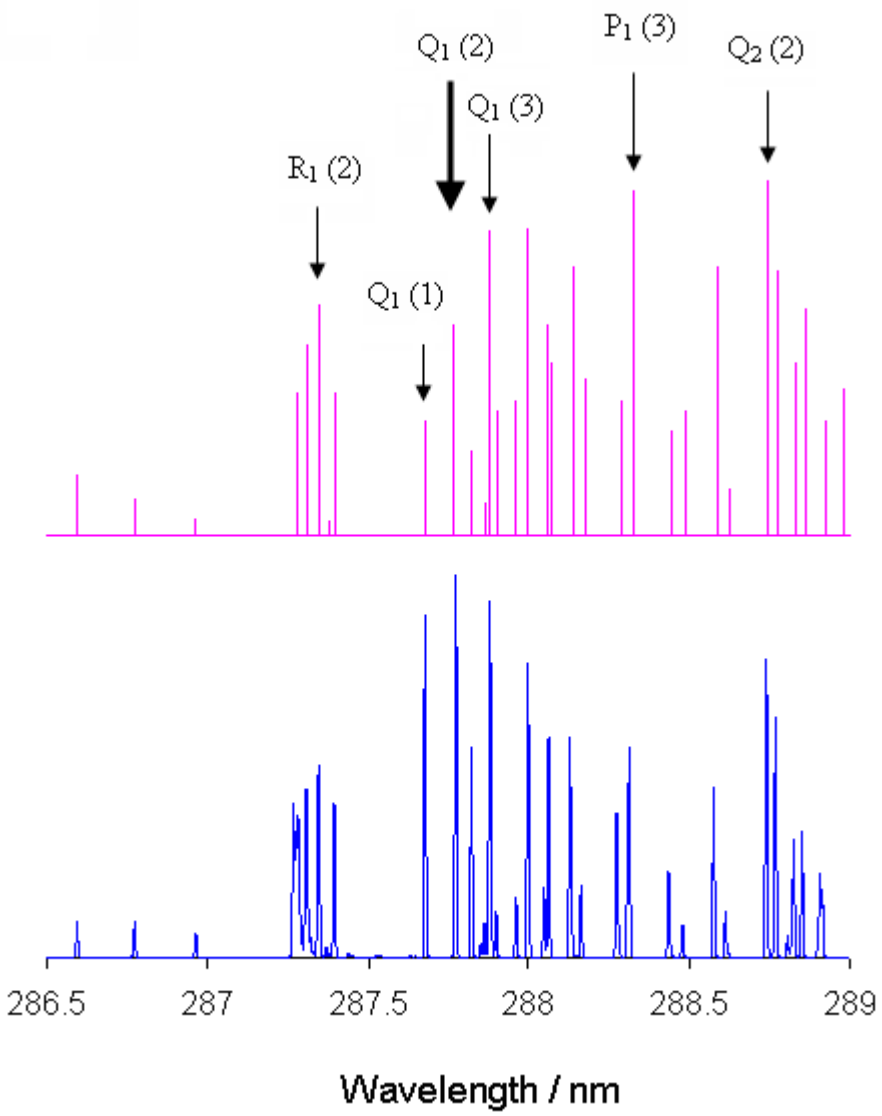

Figure II-IX. Experimental (pink) and simulated (blue) LIF scan for OD radical on the A← X (1, 0) vibrational band.

CHAPTER III

ISOMERIC SELECTIVE STUDIES OF THE HYDROXYL RADICAL INITIATED OXIDATION OF ISOPRENE: THE MAJOR ADDITION CHANNEL*

A. Introduction

Isoprene (2-methyl-1,3-butadiene) is emitted into the atmosphere from vegetation. Isoprene emission typically accounts for about 2% of total photosynthesized carbon from trees, but can be as high as 7-8%.[35] The reason why trees and plants emit isoprene is related to the possible involvement of isoprene emission in thermal tolerance.[19] Isoprene can be rapidly produced in the leaf and it protects trees from thermal damage under rapid temperature increase.[36] The exact mechanism by which isoprene provides thermal tolerance is still not clear,[19] however it is believed that isoprene dissolves in the membrane to alter their properties to increase thermotolerance.[36] Isoprene also protects plants against damage caused by ozone or other reactive oxygen species (ROS).[37] However it is unlikely that the ground level ozone concentration was significant over the evolutionary timescale and hence isoprene emission is not likely to be a response to ozone damage.

The addition of OH to isoprene results in four distinct hydroxyl alkyl isomers (Figure III-I), each of which ultimately leads to different first generation end products. Although, there has been no direct experimental determination of the branching between

---

* Parts of this chapter are preprinted with permission from "Isomeric Study of the OH-Initiated Oxidation of Isoprene in the Presence of O_2 and NO: 2. The Major OH Addition Channel" Ghosh, B.; Bugarin, A.; Connell, B.; North, S. W. *J. Phys. Chem. A* **2010**, *114*, 2553.

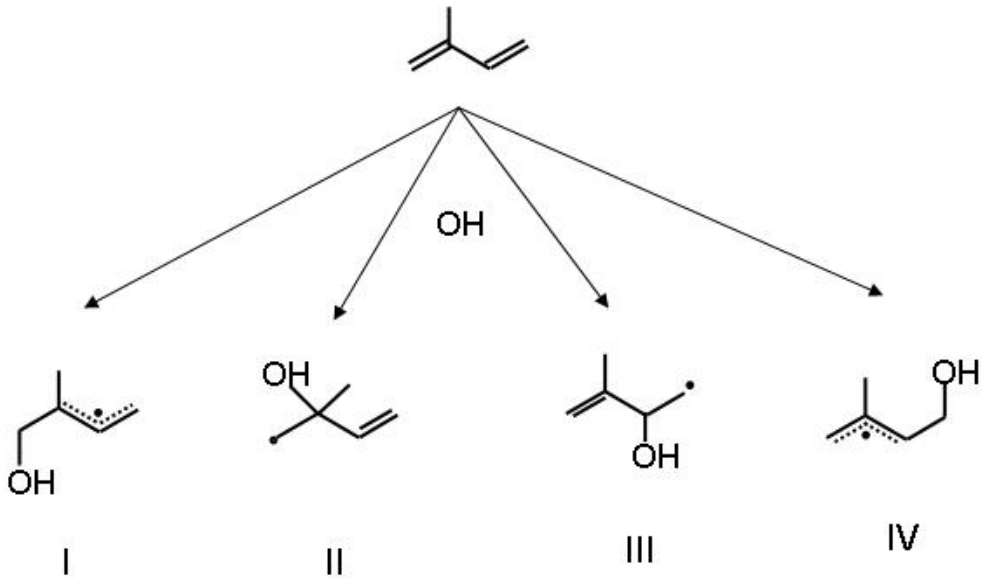

Figure III-I. Initial branching of □hydroxyl alkyl radicals followed by the reaction of OH radical with isoprene

channels, theoretical work has predicted branching of 0.67, 0.02, 0.02 and 0.29 respectively for isomers I, II, III, IV,[38] with an overall rate of $(1.0\pm0.1) \times 10^{-10}$ molecule^{-1} cm^3 s^{-1}.[38-42] End product analysis studies also suggest that OH addition occurs preferentially at the terminal carbons.[43-44]

The radicals formed from OH addition to the terminal carbons react with molecular oxygen under atmospheric conditions to form peroxy radicals, which subsequently react with NO to form alkoxy radicals. This contrasts with the dominant pathway for the radicals formed from OH addition to the inner carbons. For these radicals recent studies have demonstrated prompt isomerization to form α–hydroxyl alkyl radicals occurs followed by reaction with oxygen to form C_5 carbonyl compounds and HO_2.[8-9,45]

Theoretical studies suggest that decomposition is the sole fate for the *β*-hydroxyalkoxy radicals[46-48] leading to the formation of methyl vinyl ketone, methacrolein, and formaldehyde as first generation end products.[49-55] The *δ*-hydroxyalkoxy radicals, however, undergo prompt 1,5 hydrogen shift[56-57] followed by hydrogen abstraction or reaction with O_2 to form C_5 or C_4 hydroxy carbonyl compounds.[58] Hydrogen abstraction by O_2 during the oxidation process generates HO_2 which reacts with NO to regenerate OH radicals (Figure III-II). Thus, the time dependent kinetics of OH in the presence of NO and O_2 is a sensitive probe of the detailed mechanism of the oxidation process.

Until recently, studies of isoprene chemistry have been non-isomer specific, *i.e.* they reflect the reactivity of the combined pathways and are often insensitive to specific details of the isomeric pathways. In a previous study, we demonstrated that isomer selective kinetic experiments permit the investigation of minor important channels in

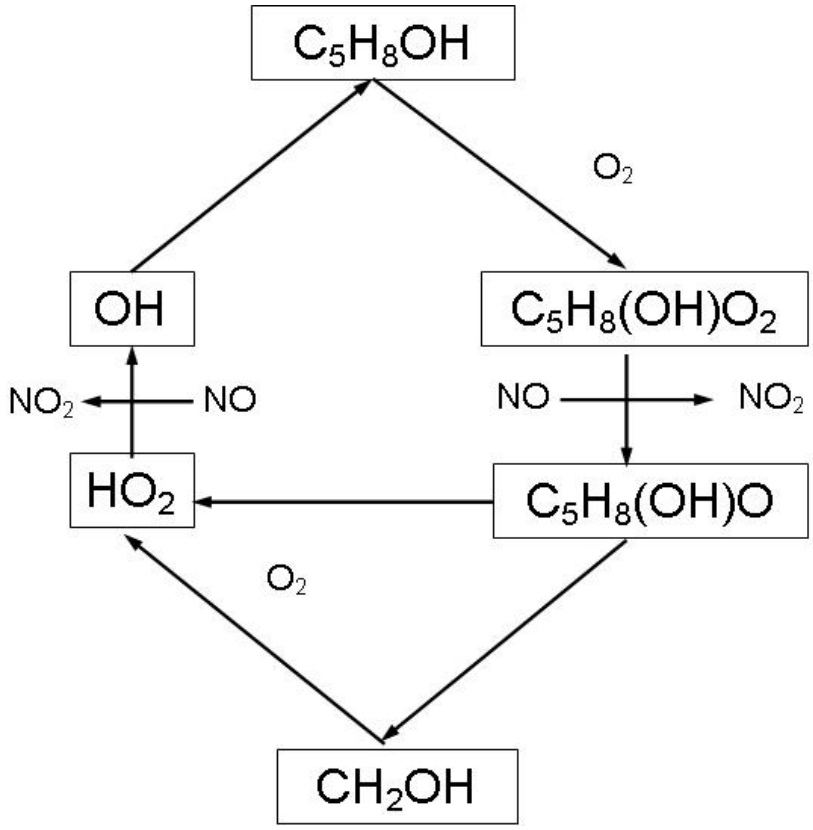

Figure III-II. Schematic diagram of OH cycling in isoprene oxidation.

isoprene oxidation that are obscured by the major channel kinetics.[8-9] The photodissociation of a suitable iodohydrin precursor provides a route to the formation of a single OH-isoprene adduct isomer enabling such studies. In the present study, we focus on the major channel of the isoprene oxidation, and to this end, we have synthesized the photolytic precursor 2-iodo-2-methyl-but-3-en-1-ol. In doing so, we reduce the complex chemistry of isoprene oxidation to the chemistry of a single pathway (species I in Figure III-I) permitting determination of isomer specific kinetic rate constants.

Product studies on the isoprene oxidation account for only 60-70% carbon balance (MVK+ formaldehyde ~30%, MACR+ formaldehyde ~27%, organic nitrate ~ 10%, furan derivative ~ 3%),[53] while predicting that carbonyl compounds may account for the remaining 30%.[55] Theory suggests that the major channel for isoprene oxidation may lead to ~20% carbonyl compounds through *δ*-hydroxyalkoxy radicals.[58] *Isomeric selective studies would be valuable in assessing the chemistry that gives rise to the production of hydroxyl carbonyls.* The *δ*-hydroxyalkoxy radical can exist in either (*E*-) or the (*Z*-) form. The yield of the (*E*-)*δ*-hydroxyalkoxy channel, although predicted from theoretical calculations,[53,56] is yet to be measured experimentally since the complexity of the reaction systems has precluded a direct experimental confirmation. Isomer selective isotopically labeled OH-cycling experiments may provide quantification of this channel by measuring the relative formation of OD (*Z*) to OH formation (*E*).

The accuracy of regional air quality modeling depends on a detailed understanding of the mechanism of OH initiated isoprene oxidation. The goal of our current study is to elucidate the mechanism of the dominant isomeric pathway of OH-

isoprene oxidation and consequently assess the validity of condensed chemical oxidation models.

B. Synthesis of Photolytic Precursor

The photolytic precursor, 2-iodo-2-methyl-but-3-en-1-ol, was synthesized following the methodology reported by Snider *et al*.[59] In a 100 Ml round bottom flask, 2.54 g of iodine (10 mmol) was dissolved in 15 Ml of acetonitrile. 2.36 g of silver oxide (10 mmol) was added to it followed by 15 Ml of water. After that, 2 Ml of isoprene (20 mmol, 1.362 g) was added to it slowly .The resulting mixture was stirred for 2.5 h at room temperature. After 2.5 h, the reaction resulted in a product mixture containing the product isomers primary and tertiary alcohols in 1:3 ratio. The primary alcohol, which was the desired product, was always the minor product of the synthesis, as it represents the unfavorable anti-Markovnikov product. The product mixture was first filtered and then extracted in diethylether and the remaining aqueous layer was extracted in ethyl acetate. The ethyl acetate layer mainly contained the primary alcohol, along with some of the tertiary alcohol, whereas the diethylether layer contained bulk of the tertiary alcohol along with some primary alcohol. Ethyl acetate layer was dried by anhydrous sodium sulphate and rotorvapped to concentrate the product mixture. The two product isomers were then separated by column chromatography, using a solvent system of 60% ethyl acetate/hexane. The overall yield was 15%. The synthesis scheme is shown schematically in Figure III-III. The compound was identified by ^{1}H NMR, ^{13}C NMR, (Figure III-IV and III-V) mass spectrometry and IR spectroscopy. The O-H stretching and C=C stretching frequencies were identified in IR spectroscopy (3385.5 cm^{-1}: O-H stretching), 3088.3 cm^{-}

[1]: C=C stretching). In high resolution mass spectrometry, (chemical ionization, CH_4) the $(M+H)^+$ peak for the C_5H_9IO molecule (*mlz* 211.97) was obtained at *mlz* 213.1.

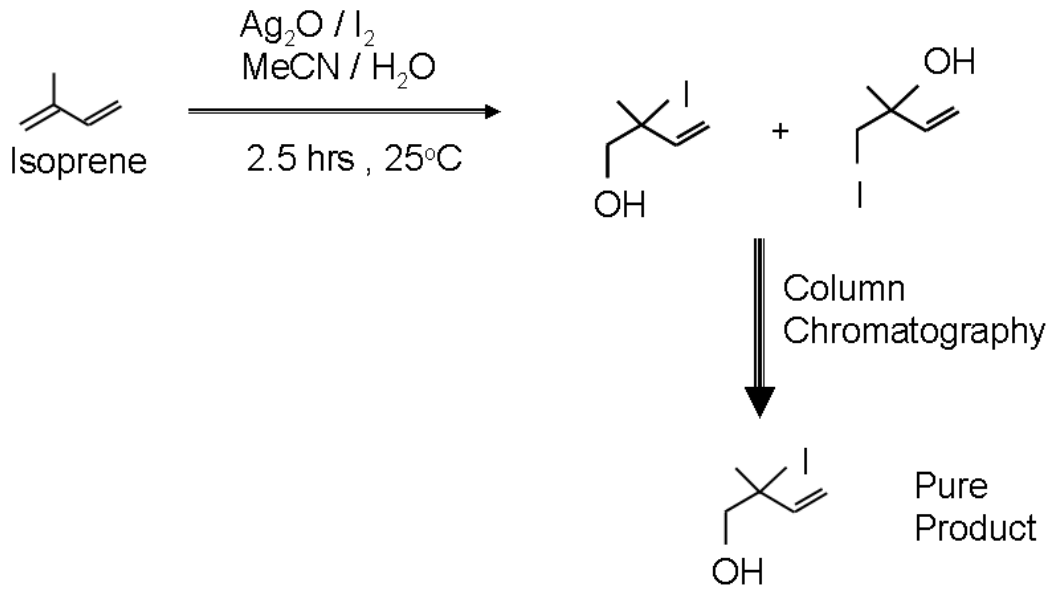

Figure III-III. Synthetic scheme for the precursor 2-iodo-2-methyl-but-3-en-1-ol.

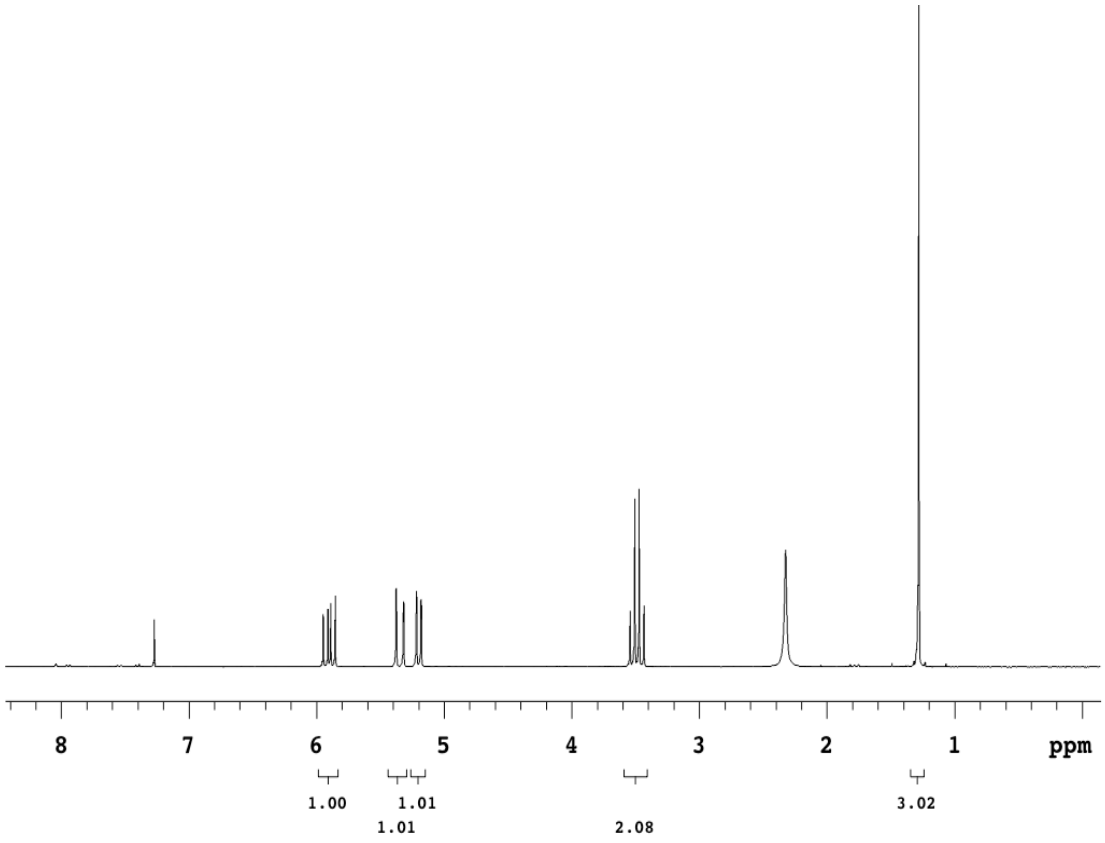

Figure III-IV. ^{1}H NMR (300MHz, $CDCl_3$) spectrum of 2-iodo-2-methyl-but-3-en-1-ol: δ 5.84-5.93 (q, 1H, J = 9 Hz), 5.34 (d, 1H, J = 6), 5.16 (d, 1H, J = 4), 3.49 (q, 2H, J = 10), 2.32 (b, 1H), 1.26 (s, 3H).

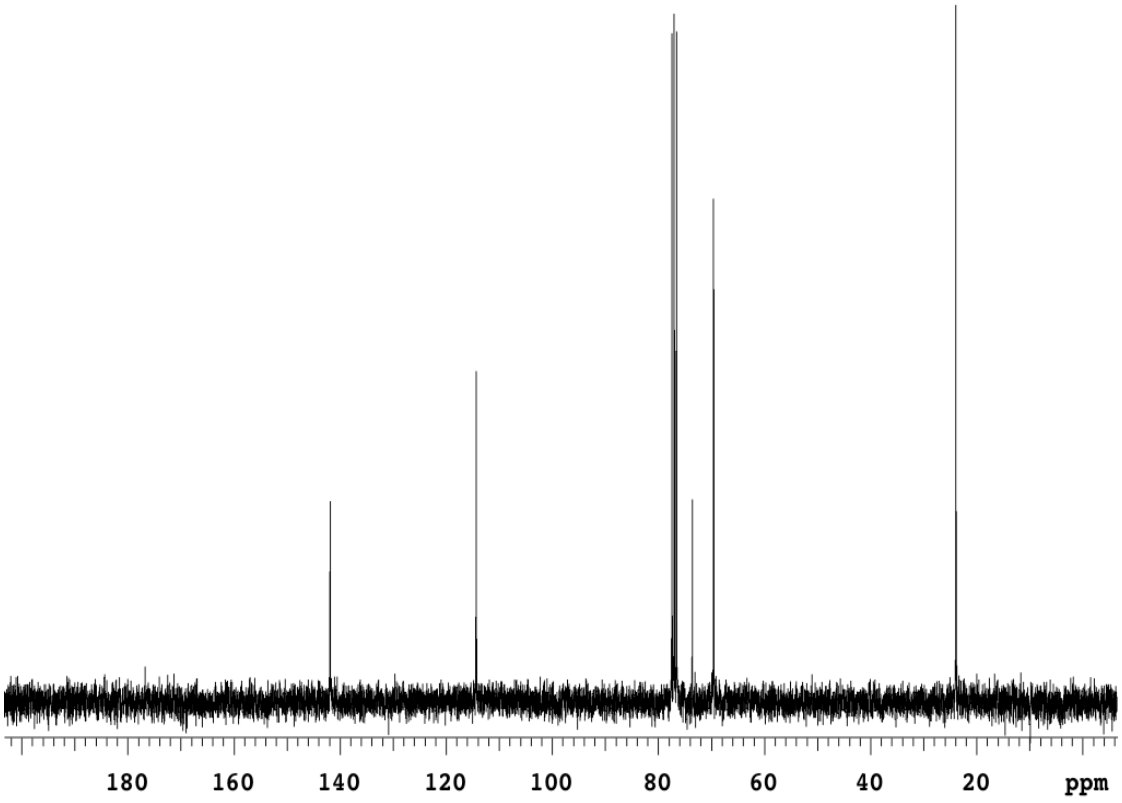

Figure III-V. ^{13}C NMR (75MHz, $CDCl_3$) spectrum of 2-iodo-2-methyl-but-3-en-1-ol: δ 141.91, 114.15, 73.56, 69.53, 23.84.

C. Results and Discussion

In this section we present the results obtained from OH-cycling experiments and the related analysis of the data. We first describe OH-cycling experiments using a non-deuterated precursor molecule, including a discussion on sensitivity analysis of the derived rate constants. Next, we describe kinetic experiments using a deuterated precursor molecule and the determination of branching between β- and δ-hydroxyalkoxy radicals.

I. OH cycling from the non-deuterated precursor. In these experiments, the precursor molecule, 2-iodo-2-methyl-but-3-en-1-ol, was dissociated by a 248 nm laser pulse to form the radical (I) of the four possible isomers of hydroxyl isoprene radical (Figure III-I). A simplified mechanism of OH cycling is described schematically in Figure III-II. The kinetics experiments rely on the time-dependent formation of OH as a function of O_2 and NO concentrations to provide information about rate constants of intermediate reactions and can be effective with judicious choice of experimental conditions guided by sensitivity analysis. These experiments were performed in moderate to high NO concentration to ensure OH cycling and the O_2 concentrations were maintained at a higher value, to ensure a higher rate of OH formation, than loss (see text below). A summary of the concentrations of reacting species is tabulated in Table III-I below.

Table III-I. Summary of the experimental conditions applied in the isomeric selective studies of isoprene oxidation

[Precursor] 10^{13} molecules/cc	[NO] 10^{14} molecules/cc	[O_2] 10^{15} molecules/cc
OH cycling experiments from IC_5H_8OH		
2.1	28.0	7.8
2.1	28.0	13.0
2.1	28.0	15.0
3.8	6.1	9.8
3.8	8.0	9.8
1.5	9.7	40.2
1.5	13.8	26.2
OH cycling experiments from IC_5H_8OD		
1.4	28.0	29.4
1.4	28.0	31.4
1.4	28.0	36.0
1.4	28.0	60.0
OD cycling experiments from IC_5H_8OD		
1.4	35.0	54.0
1.4	35.0	75.0

Figure III-VI shows a typical set of experimental data from OH-cycling experiments where the concentration of the precursor molecule was 2.1×10^{13} molecules cm^{-3}, [NO] = 2.8×10^{15} molecules cm^{-3}, and the O_2 concentrations have been varied from 7.8×10^{15} molecules cm^{-3} to 1.5×10^{16} molecules cm^{-3}. The prompt rise in OH signal following precursor photolysis is due to the fraction (25%-30%) of nascent hydroxyl alkyl radicals produced with energy exceeding the threshold to decomposition to form OH and isoprene prior to collisional stabilization. In the absence of O_2 and NO, this OH

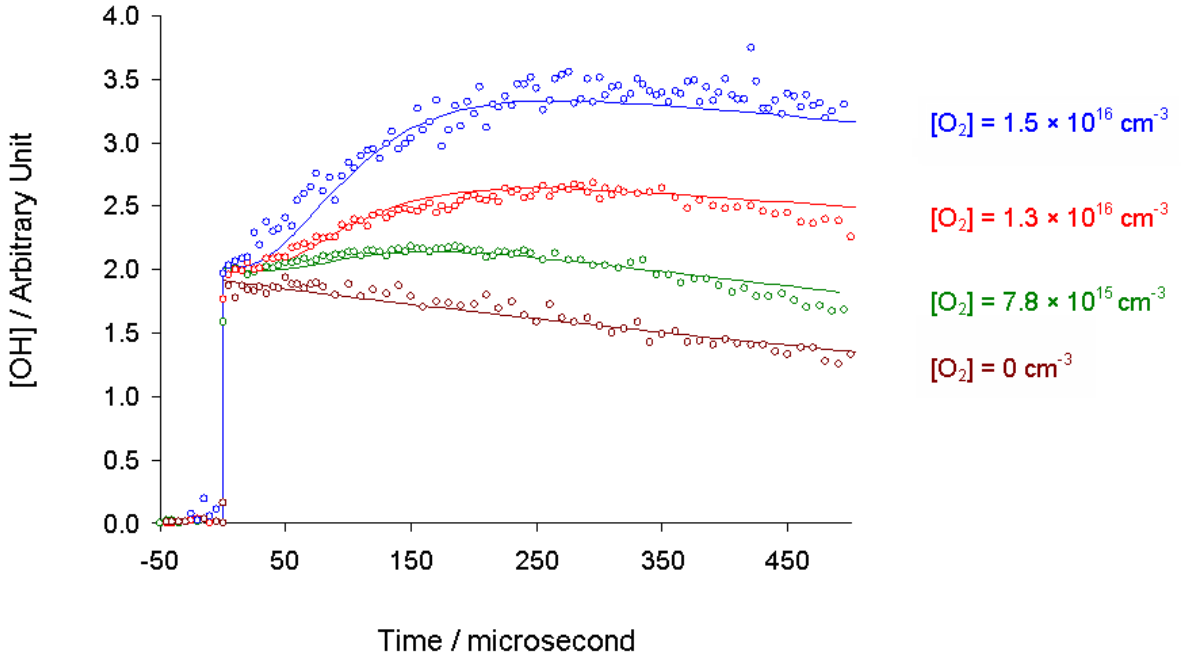

Figure III-VI. OH fluorescence intensity plotted against reaction time at multiple O_2 concentrations. Symbols represent experimental data and solid lines represent the fits using the reaction mechanism and rate constants in Table III-II. $[IC_5H_8OH] = 2.1 \times 10^{13}$ molecules cm^{-3}, $[NO] = 2.8 \times 10^{15}$ molecules cm^{-3}. The last plot was taken in the absence of O_2.

signal exhibits an exponential decay due to reaction with the precursor with a rate constant of $k_{23} = 1.3 \times 10^{-11}$ molecules^{-1} cm^3 s^{-1}. This value is similar to values measured for the rate of OH addition to similar compounds[8-9] presumably via OH addition to the iodohydrin double bond. In the presence of O_2 and NO, photolysis of the iodohydrin precursor and subsequent chemistry results in an OH signal that exhibits an initial rise over 150 μs to 300 μs due to the cycling mechanism shown in Figure III-II followed by decay due to termination reactions.

The numerical program KINTECUS[60] was used to simulate the experimental data as well as to perform sensitivity analysis. The 25 reactions that were used to simulate the OH cycling data are provided in Table III-II along with the corresponding rate constants. A more detailed 30 reaction mechanism which includes the OH cycling arising from the reaction of OH radical with the precursor molecule IC_5H_8OH was also used to simulate the data. The fits using the extended model are virtually indistinguishable from those using the concise model, as the OH cycling from the precursor molecule has little effect in the current experimental conditions. So we have used a simpler and more concise model to fit our data. The best fit to the data are shown as the solid lines in Figure III-VI. The reaction mechanism given in Table III-II is shown in Figure III-VII. One of the goals of current study is to determine the rate constants for the intermediate reactions based on time-dependent hydroxyl radical measurements as a function of O_2 and NO concentrations. In order to assess the viability of extracting intermediate rate constants in this way, we rely on sensitivity analysis which describes the dependence of the data to

Table III-II. Kinetics mechanism employed in modeling the time-dependent OH signals. Rate constants are in molecule^{-1} cm^3 s^{-1} unless otherwise stated.

	Reaction			Rate Constant	Ref	Comment
k_1	HOC_5H_8	→	$OH+C_5H_8$	Prompt (30%)	a	
k_2	HOC_5H_8	→	HOC_5H_8	Prompt (70%)	a	
k_3	$HOC_5H_8 + NO$	→	HOC_5H_8NO	1.2×10^{-11}	a	
k_4	$HOC_5H_8 + O_2$	→	β-$HOC_5H_8O_2$	8.0×10^{-13}	a	β- branching
k_5	$HOC_5H_8 + O_2$	→	Z-$HOC_5H_8O_2$	1.0×10^{-13}	a	Z-δ branching
k_6	$HOC_5H_8 + O_2$	→	E-$HOC_5H_8O_2$	1.0×10^{-13}	a	E-δ branching
k_7	β-$HOC_5H_8O_2 + NO$	→	β-$HOC_5H_8O + NO_2$	7.0×10^{-12}	a	
k_8	β-$HOC_5H_8O_2 + NO$	→	β-$HOC_5H_8ONO_2$	1.1×10^{-12}	61-62	Peroxy radicals reacting with NO to form alkoxy radicals
k_9	Z-$HOC_5H_8O_2 + NO$	→	Z-$OHC_5H_7OH + NO_2$	7.0×10^{-12}	a	
k_{10}	Z-$HOC_5H_8O_2 + NO$	→	Z-$HOC_5H_8ONO_2$	1.1×10^{-12}	61-62	
k_{11}	E-$HOC_5H_8O_2 + NO$	→	E-$OHC_5H_7OH + NO_2$	7.0×10^{-12}	a	
k_{12}	E-$HOC_5H_8O_2 + NO$	→	E-$HOC_5H_8ONO_2$	1.1×10^{-12}	61-62	
k_{13}	β-HOC_5H_8O	→	$CH_2OH + OC_4H_6$	Prompt	46-48	
k_{14}	Z-$OHC_5H_7OH + O_2$	→	$HO_2 + OC_5H_7OH$	1.0×10^{-11}	39	Chemistry of Z-δ channel
k_{15}	Z-OHC_5H_7OH+NO	→	Z-OHC_5H_7OHNO	3.0×10^{-11}	63-66	
k_{16}	E-OHC_5H_7OH+NO	→	E-OHC_5H_7OHNO	1.2×10^{-11}	a	
k_{17}	E-$OHC_5H_7OH+O_2$	→	E-$OHC_5H_7OHO_2$	1.0×10^{-12}	a,56	
k_{18}	E-$OHC_5H_7OHO_2 + NO$	→	E-$OHC_5H_7OHO+NO_2$	7.0×10^{-12}	a,56	Chemistry of E-δ channel
k_{19}	E-$OHC_5H_7OHO_2 + NO$	→	E-$OHC_5H_7OHONO_2$	1.1×10^{-12}	61-62	
k_{20}	E-OHC_5H_7OHO	→	$OHC_4H_5O + CH_2OH$	Prompt	66	
k_{21}	$CH_2OH + O_2$	→	$CH_2O + HO_2$	1.0×10^{-11}	39	
k_{22}	$CH_2OH + NO$	→	CH_2OHNO	1.2×10^{-11}	67	
k_{23}	$OH + IHOC_5H_8$	→	$IHOC_5H_8OH$	1.3×10^{-11}	a	
k_{24}	$HO_2 + NO$	→	$OH + NO_2$	8.8×10^{-12}	68	
k_{25}	$OH + NO$	→	$HONO$	9.4×10^{-13}	69-70	

[a] This work

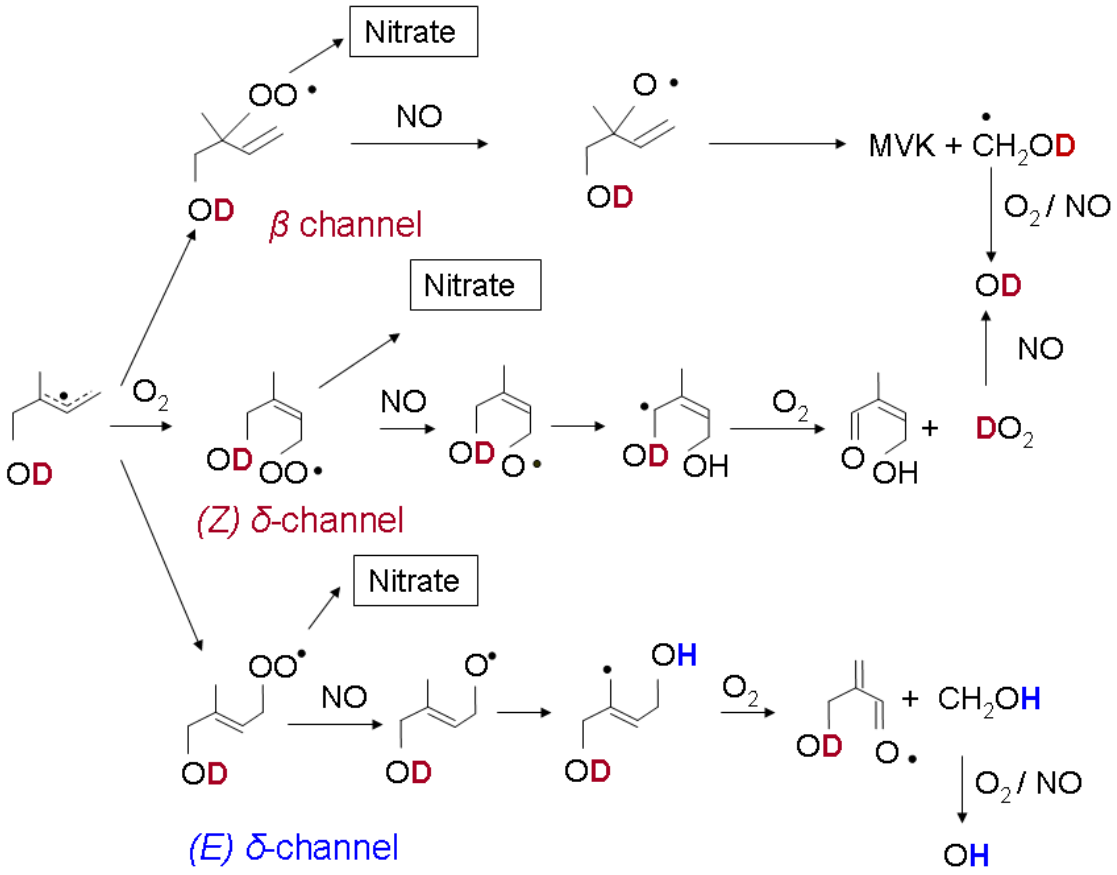

Figure III-VII. Oxidation mechanism of isomer I.

specific rate constants in the reaction mechanism.[71] The normalized sensitivity coefficient (NSC) is defined as,

$$\mathrm{NSC} = \left[\frac{\delta \ln [\mathrm{OH}]}{\delta \ln k_i}\right]_{j \neq i}$$

where k_i represents the rate constant of the i^{th} reaction in the reaction mechanism and [OH] represents the concentration of the hydroxyl radical at a specific time. An NSC of 1.0, for example, indicates that a 20% change in the rate constant *I* results in a 20% change in the OH concentration at a given time.

Figure III-VIII shows NSC's for all the rate constants in the reaction mechanism evaluated at an NO concentration of 2.8×10^{15} molecules cm^{-3} and two different O_2 concentrations of 1.5×10^{16} molecules cm^{-3} and 7.9×10^{15} molecules cm^{-3}, respectively at a reaction time of 171 μs. It is clear from inspection of Figure III-VIII that the OH concentration profile depends sensitively on a limited number of rate constants, specifically, the branching between metastable hydroxyalkyl radicals which decompose and thermalized hydroxyalkyl radicals (k_1 and k_2), the rate constant for the reaction of NO and hydroxyalkyl radical (k_3), the reaction of O_2 and hydroxyalkyl radicals (k_4), and the reaction of NO and hydroxyalkyl peroxy radical (k_7). Although the NSC for the NO + HO_2 rate constant (k_{24}) is comparable with that of the peroxy radical reaction with NO, it is a well studied reaction and we have adopted the reported room temperature values.[70]

At moderate to high NO concentrations, the radical chain termination steps arising from the addition of NO to radical species become important as it affects the overall decay of the signal. The mechanism needs to incorporate these steps since the NO concentrations employed in this study are relatively high to ensure rapid cycling. We

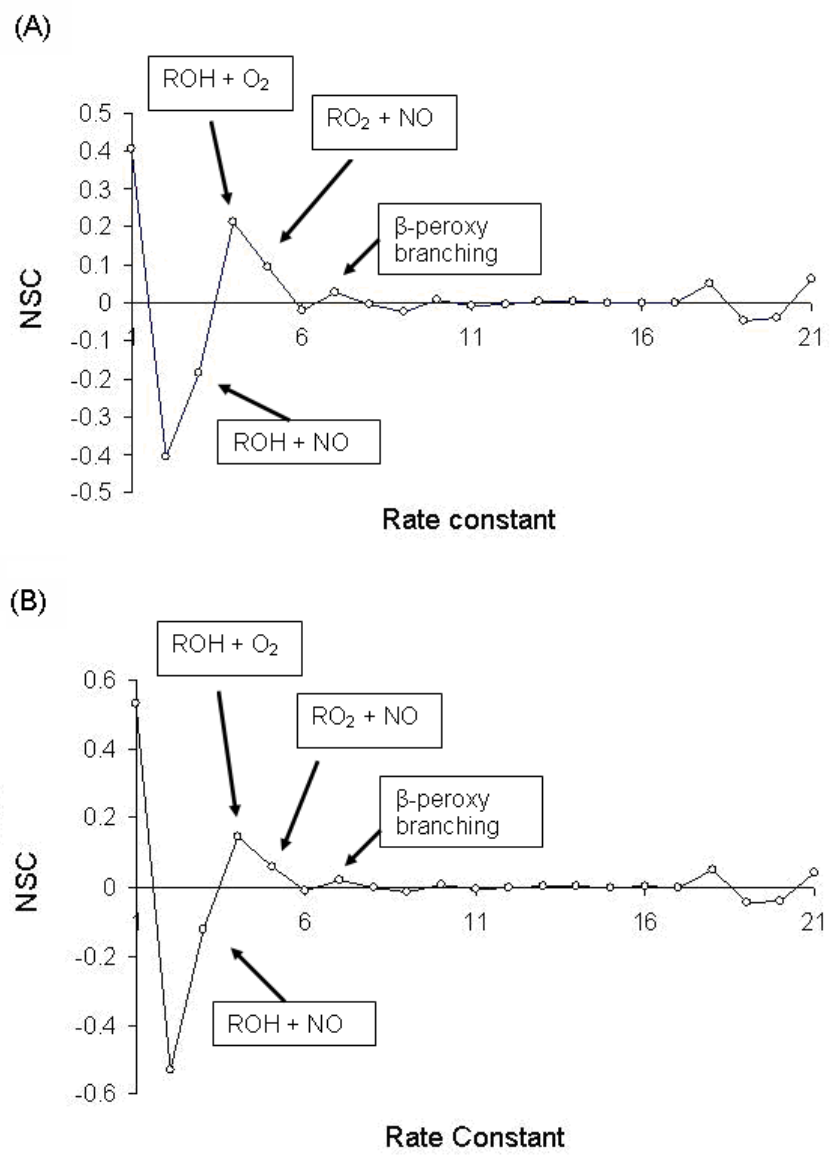

Figure III-VIII. A: Sensitivity analysis at time 171 μs for $[IC_5H_8OH] = 2.1 \times 10^{13}$ molecules cm^{-3}, $[NO] = 2.8 \times 10^{15}$ molecules cm^{-3}, $[O_2] = 1.5 \times 10^{16}$ molecules cm^{-3}

B: Sensitivity analysis at time 170 μs for $[IC_5H_8OH] = 2.1 \times 10^{13}$ molecules cm^{-3}, $[NO] = 2.8 \times 10^{15}$ molecules cm^{-3}, $[O_2] = 7.9 \times 10^{15}$ molecules cm^{-3}

have used a rate constant of $k_{15} = 3.0 \times 10^{-11}$ cm^3 molecule^{-1} s^{-1}, for the reaction of hydroxyl alkoxy radical and NO, which is based on the value reported by Park *et. al*[66] and the recommendation made by Atkinson for similar reactions.[63] It is also similar to the rate constant of $3.9 \pm 0.3 \times 10^{-11}$ cm^3 molecule^{-1} s^{-1} reported by Lotz and Zellner for the reaction of the 2-butoxyl radical with NO.[72] Work by Deng *et al*.[65] and Blitz *et al*.[64] also support adopting a pressure independent rate constant of 3.0×10^{-11} cm^3 molecule^{-1} s^{-1} for this reaction. The NO addition to CH_2OH has been assigned a rate of $k_{22} = 1.2 \times 10^{-11}$ cm^3 molecule^{-1} s^{-1} based on recommendations from other studies.[67]

At moderate to high concentrations of O_2, sensitivity analysis predicts a moderate NSC for the rate constant of O_2 addition to the hydroxyl alkyl radical. We have calculated the dependence of the NSC for ($k_4 + k_5 + k_6$) as a function of time delay and O_2 concentration (Figure III-IX). The NSC reaches a maximum value for O_2 concentrations near 1.5×10^{16} molecules cm^{-3}. As a result, we have employed similar oxygen concentrations in our experiments to ensure maximum sensitivity to this rate constant in our simulations.

The addition of either O_2 or NO to the hydroxyl alkyl radical represents a competition between radical chain propagation ($k_4 + k_5 + k_6$) and chain termination *(k_3)* and it is the relative magnitude of these two rates *i.e.* k_3[NO] and ($k_4 + k_5 + k_6$)[O_2] that controls the shape of the simulated curve. As a consequence, both rate constants are strongly coupled. Thus, the value of k_3 will have an effect on the value of ($k_4 + k_5 + k_6$) and the range of k_3 will help to determine the range for ($k_4 + k_5 + k_6$). However, according to previous studies, the value of the NO addition rate constant has a relatively narrow

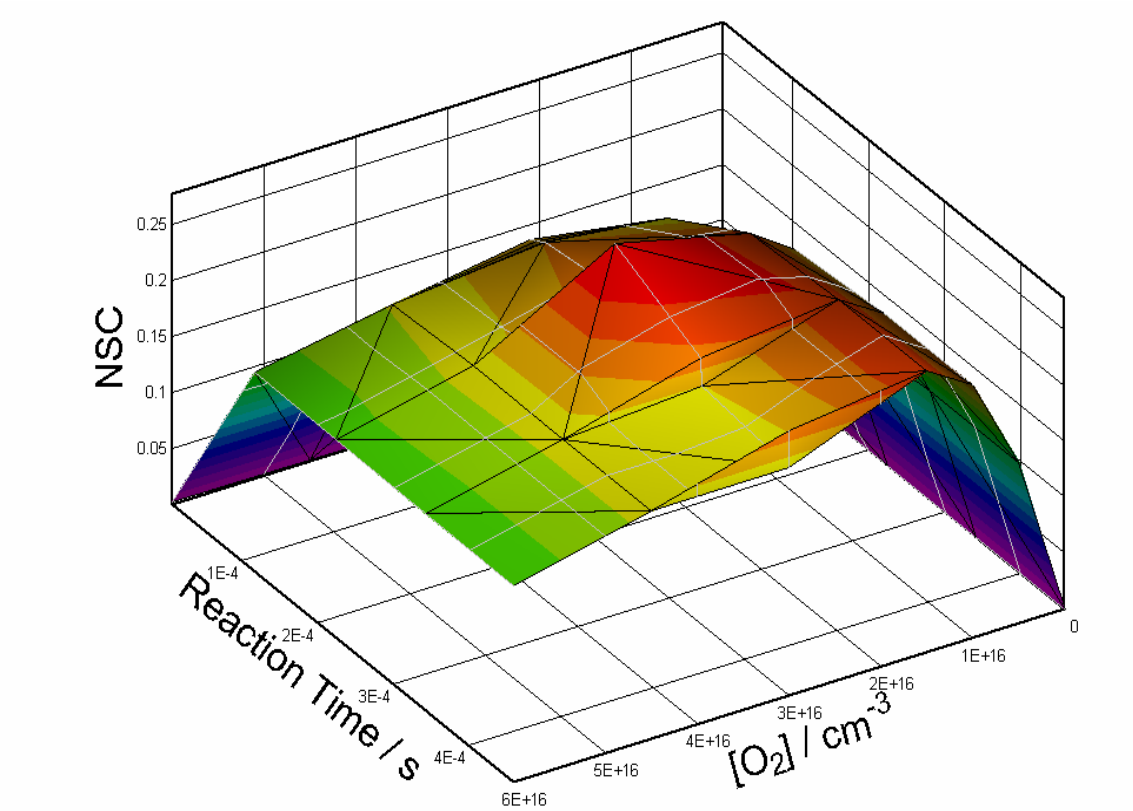

Figure III-IX. 3-Dimensional plot of normalized sensitivity coefficient (NSC) for the reaction of hydroxyl alkyl radical with O_2 ($k_4 + k_5 + k_6$) in Table III-II) as a function of reaction time and O_2 concentrations for $[C_5H_8] = 2.13 \times 10^{13}$ molecules cm^{-3} and $[NO] = 2.83 \times 10^{15}$ molecules cm^{-3}.

range,[8-9,66] and we have adopted values ranging from 7.0×10^{-12} molecule^{-1} cm^3 s^{-1} to 2.0×10^{-11} molecule^{-1} cm^3 s^{-1} (Figure III-X). We were unable to achieve satisfactory fits to our experimental data with values for k_3 outside this range. We have chosen a value of 1.2×10^{-11} molecule^{-1} cm^3 s^{-1} for k_3 since this value provides the best fit to the experimental data and agrees well with values used in previous studies.[9,66] Using this fixed value of 1.2×10^{-11} molecule^{-1} cm^3 s^{-1} for the rate of hydroxyl radical reaction with NO (k_3), we find the best fit for the O_2 addition rate to the hydroxyl radical of 1.0×10^{-12} molecule^{-1} cm^3 s^{-1} with an upper limit of 1.8×10^{-12} molecule^{-1} cm^3 s^{-1} and a lower limit of 6.0×10^{-13} molecule^{-1} cm^3 s^{-1}. When we include the range of k_3, the error bars on ($k_4 + k_5 + k_6$) reflect the inter dependence of these rate constants. For this range of the NO addition rate constant *(k_3)*, we find the upper and lower limits of O_2 addition rate change to 2.7×10^{-12} molecule^{-1} cm^3 s^{-1} and 5.0×10^{-13} molecule^{-1} cm^3 s^{-1} respectively (Figure III-XI). Thus, the uncertainty in the value of k_3 results in a higher uncertainty in the value of ($k_4 + k_5 + k_6$) and we report a value of $1.0^{+1.7}_{-0.5} \times 10^{-12}$ cm^3 s^{-1} for the O_2 addition to hydroxyl alkyl radical.

Although the exact value of this rate constant is unimportant under atmospheric conditions due to the high O_2 concentration, the value is necessary for accurate modeling of laboratory kinetics studies. Rate constants for O_2 addition to hydroxyl alkyl radical have been calculated theoretically and the rate constant for isomer I was reported to be 2.7×10^{-12} molecule^{-1} cm^3 s^{-1},[73] in the range of our observed value. The rate constant we have determined lies within the range of $(7.0 \pm 3.0) \times 10^{-13}$ molecule^{-1} cm^3 s^{-1} determined from non isomer selective experimental studies performed by Zhang *et al.*[74] It is also within the range of 6.0×10^{-13} molecule^{-1}cm^{3}s^{-1} and 2.0×10^{-12} molecule^{-1} cm^3 s^{-1}

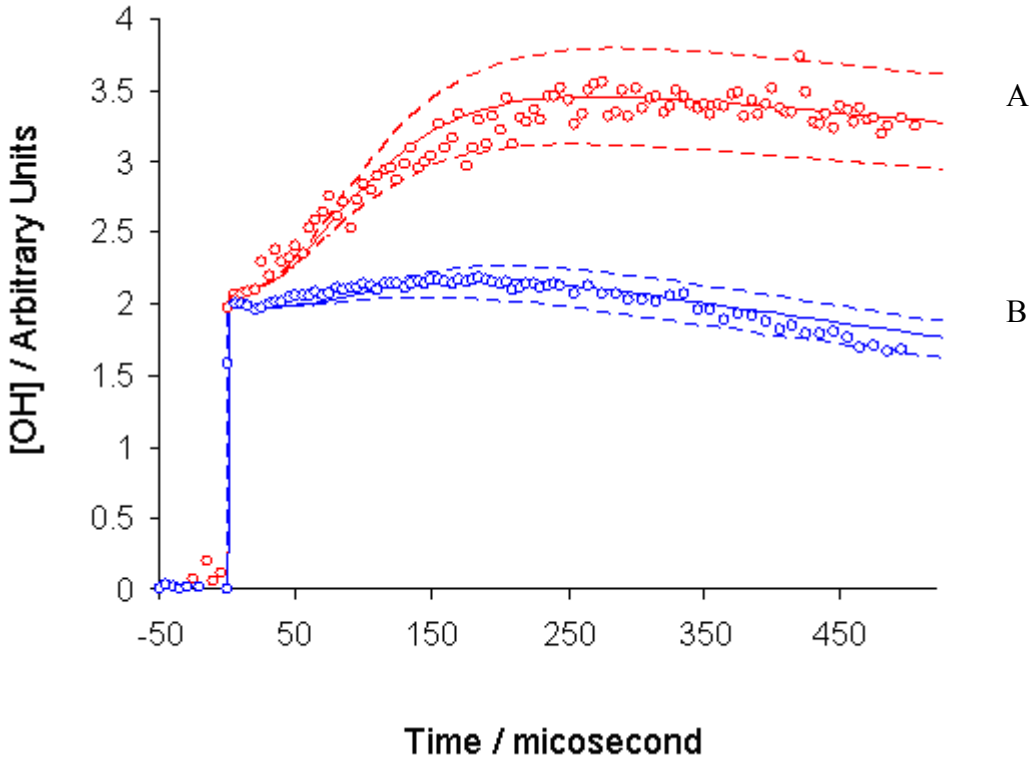

Figure III-X. Dashed lines indicate the rate constants for the estimated error range for NO addition to hydroxyl alkyl radical rate (k_3).

A: $[IC_5H_8OH] = 2.1 \times 10^{13}$ molecules cm^{-3}, $[NO] = 2.8 \times 10^{15}$ molecules cm^{-3}, $[O_2] = 1.5 \times 10^{16}$ molecules cm^{-3}
Upper limit = 20.0×10^{-12} $molecule^{-1}$ cm^3 s^{-1}, lower limit = 7.0×10^{-12} $molecule^{-1}$ cm^3 s^{-1}

B: $[IC_5H_8OH] = 2.1 \times 10^{13}$ molecules cm^{-3}, $[NO] = 2.8 \times 10^{15}$ molecules cm^{-3}, $[O_2] = 7.8 \times 10^{15}$ molecules cm^{-3}
Upper limit = 20.0×10^{-12} $molecule^{-1}$ cm^3 s^{-1}, lower limit = 7.0×10^{-12} $molecule^{-1}$ cm^3 s^{-1}.

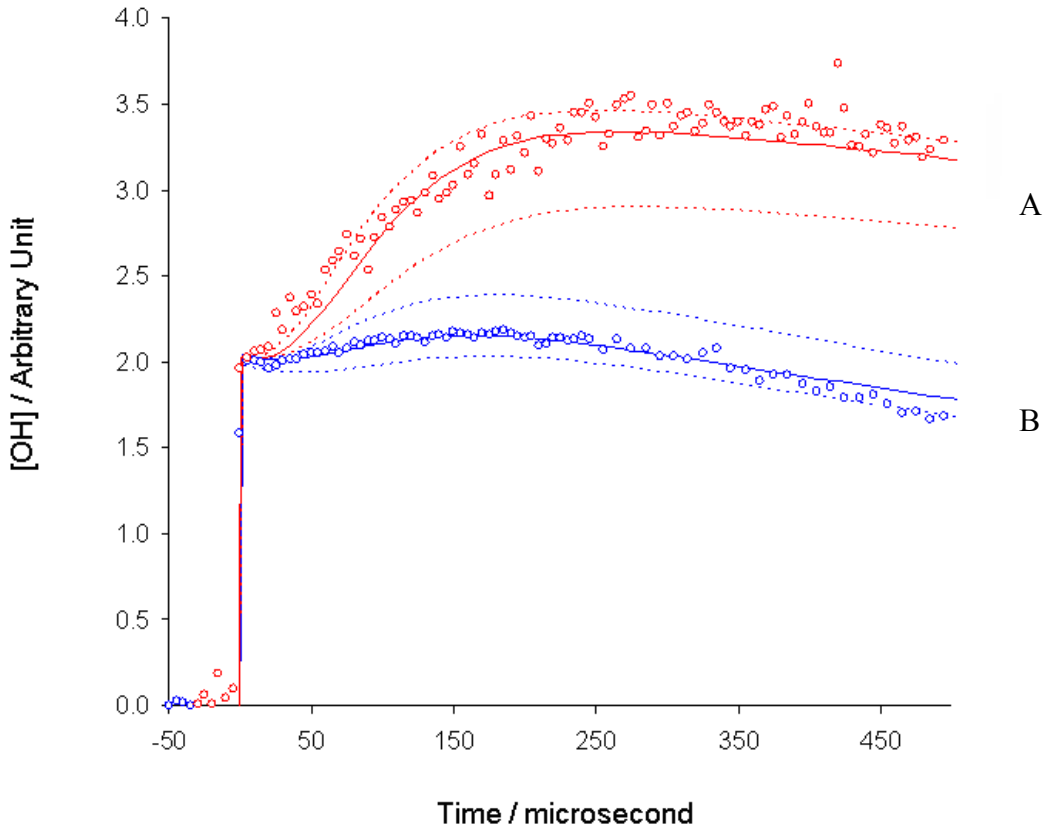

Figure III-XI. Dashed lines indicate the rate constants for estimated error range for O_2 addition to hydroxyl alkyl radical ($k_4 + k_5 + k_6$).

A: $[IC_5H_8OH] = 2.1 \times 10^{13}$ molecules cm^{-3}, $[NO] = 2.8 \times 10^{15}$ molecules cm^{-3}, $[O_2] = 1.5 \times 10^{16}$ molecules cm^{-3}
Upper limit = 2.7×10^{-12} molecule^{-1} cm^3 s^{-1}, lower limit = 5.0×10^{-13} molecule^{-1} cm^3 s^{-1}

B: $[IC_5H_8OH] = 2.1 \times 10^{13}$ molecules cm^{-3}, $[NO] = 2.8 \times 10^{15}$ molecules cm^{-3}, $[O_2] = 7.8 \times 10^{15}$ molecules cm^{-3}
Upper limit = 2.7×10^{-12} molecule^{-1} cm^3 s^{-1}, lower limit = 5.0×10^{-13} molecule^{-1} cm^3 s^{-1}.

determined by Koch *et al*.[75] at 345 and 300 K, respectively and is consistent with the range of $(2.3 \pm 2.0) \times 10^{-12}$ molecule^{-1} cm^3 s^{-1} determined by Park *et al*.,[66] both based on non isomer selective cycling experiments. The rate agrees with the rates on the order of 10^{-12} molecule^{-1} cm^3 s^{-1} reported by Atkinson for alkyl radicals.[63]

The hydroxyl peroxy radical reacts with NO under atmospheric conditions to form an activated nitrite species which promptly decomposes to form a hydroxyl alkoxy radical and NO_2 with a minor fraction isomerizing to form the stable nitrate.[76] Previous laboratory measurements of the rate constant for hydroxyl peroxy radical + NO reaction involved direct monitoring of the reactant hydroxyl peroxy radical, *i.e*. measurement of the overall loss rate via the pseudo first order decay of the hydroxyl peroxy radical.[61-62] In the present study, sensitivity analysis predicts a moderate NSC for NO to NO_2 conversion but a small NSC for the minor nitrate formation reaction. Thus, we are sensitive only to the rate constant k_7 and based on previous reports have adopted a nitrate yield of 15% to assign a value for k_8.[61-62] The 15% nitrate yield represents the higher end of the predicted nitrate yield,[58,66] which ranges from 4% to 15%. We have calculated the NSC for the hydroxyalkyl peroxy radical + NO rate constant as a function of both reaction time and O_2 concentration. The sensitivity of the data to the rate constant increases with time to a maximum value near the observed onset of cycling (180 μs). The NSC also increases with increasing concentration of oxygen reflecting the higher formation rate for the hydroxyalkyl peroxy radical. We find that the NSC levels off at higher O_2 concentrations since the yield of hydroxyalkyl peroxy radical becomes invariant. On the basis of such analysis, we have determined a rate constant for the

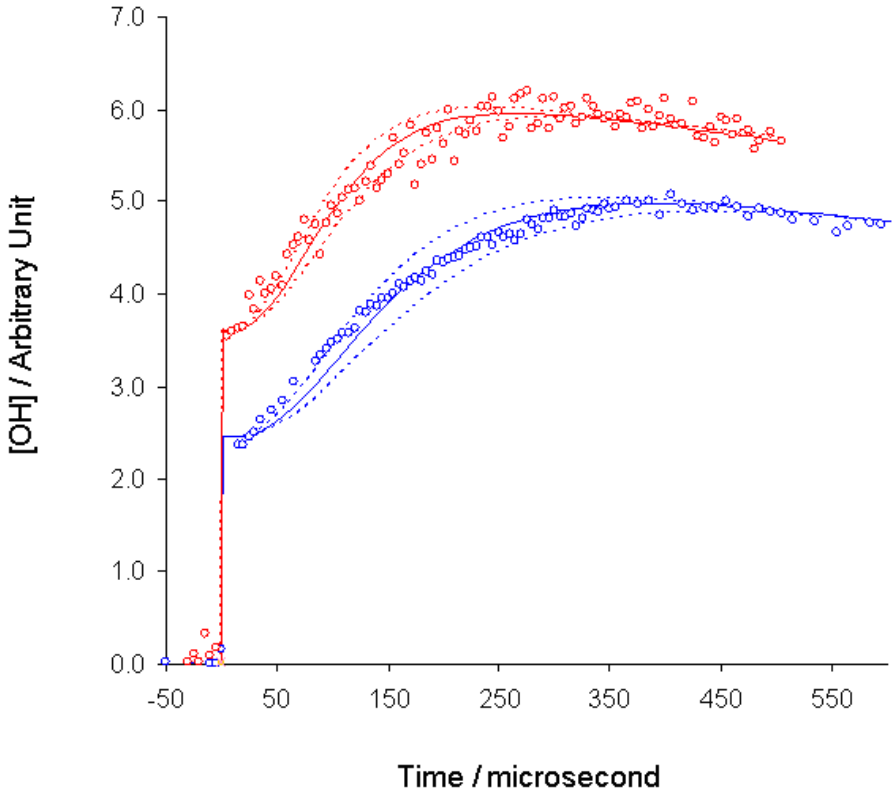

Figure III-XII. Dashed lines indicate the rate constants for estimated error range for NO reaction with hydroxyl alkyl peroxy radical rate ($k_7 + k_8$).

A: $[IC_5H_8OH] = 2.1 \times 10^{13}$ molecules cm^{-3}, $[NO] = 2.8 \times 10^{15}$ molecules cm^{-3}, $[O_2] = 1.5 \times 10^{16}$ molecules cm^{-3}
Upper limit = 11.5×10^{-12} $molecule^{-1}$ cm^3 s^{-1}, lower limit = 5.8×10^{-12} $molecule^{-1}$ cm^3 s^{-1}

B: $[IC_5H_8OH] = 2.5 \times 10^{13}$ molecules cm^{-3}, $[NO] = 1.7 \times 10^{15}$ molecules cm^{-3}, $[O_2] = 2.3 \times 10^{16}$ molecules cm^{-3}
Upper limit = 11.5×10^{-12} $molecule^{-1}$ cm^3 s^{-1}, lower limit = 5.8×10^{-12} $molecule^{-1}$ cm^3 s^{-1}.

overall reaction of NO with hydroxyl alkyl peroxy radical of $8.1^{+3.4}_{-2.3} \times 10^{-12}$ molecule^{-1} cm^3 s^{-1} which agrees with other reported values.[63] Figure III-XII shows the best fit (solid line) to the data obtained by using the above mentioned value for the NO reaction rate with hydroxyl alkyl peroxy radical and the dashed lines represent upper and lower error bounds of 11.5×10^{-12} molecule^{-1} cm^3 s^{-1} and 5.8×10^{-12} molecule^{-1} cm^3 s^{-1} respectively. The value for this rate constant lies in the range of $(9.0 \pm 3.0) \times 10^{-12}$ molecule^{-1} cm^3 s^{-1} reported by the cycling study[66] by Park *et al*. and the value determined from direct measurement[62] of the rate constant by Zhang *et al*. This value is also in good agreement with the overall rate constant of $(8.8 \pm 1.2) \times 10^{-12}$ molecule^{-1} cm^3 s^{-1} reported for this reaction by Miller *et al*.[61] and is close to the value of 7.6×10^{-12} molecule^{-1} cm^3 s^{-1} recommended by Paulson *et al*. for atmospheric modeling.[53]

Unimolecular reactions in the oxidation mechanism that arise from activated, nonthermal species have rate constants that exceed or are comparable to the collision frequency and are treated as instantaneous on the time scale of the overall kinetics. We have denoted these reactions (k_{13} and k_{20}) as *prompt* in Table III-II and the simulations are insensitive to the value utilized provided the rate constants are $>1.0 \times 10^6$ s^{-1}. The absolute values for these rate constants are not determinable in current study, and we have used recommended rates from previous studies.[66]

The reaction rate constants k_4, k_5 and k_6 in Table III-II correspond to relative branching ratios of different peroxy radicals. Reaction 4 corresponds to the branching ratio of β-hydroxy peroxy radicals, which subsequently reacts with NO to form β-hydroxy alkoxy radicals that undergo prompt decomposition. Reaction 5 corresponds to the branching of the *Z*-δ-hydroxy peroxy radicals which react with NO to form the

corresponding alkoxy radicals and reaction 6 refers to the branching ratio of the *E*-*δ*-hydroxy alkoxy radicals which reacts with NO to form its corresponding alkoxy radical. The *E*- and *Z*- forms of the *δ*-hydroxy alkoxy radicals undergo 1-5 hydrogen shifts to form dihydroxy radicals (Figure III-IV). The *Z* form of the dihydroxy radical reacts with molecular oxygen by H-abstraction mechanism to form a C_5 hydroxy carbonyl; whereas the *E* form of the dihydroxy radical reacts with O_2 and NO and subsequently decomposes to form a C_4 hydroxy carbonyl.[46] Dibble has reported another potential pathway for the (*E*)-OHC_5H_7OH isomer from theoretical studies, which leads to the formation of a C_5-di hydroxyl carbonyl compound.[46] However, no product study has observed this species,[50] and have concluded that the yield of this channel would be negligible;[77] hence we have not included this channel in our model. Dibble has also reported another potential fate of the *Z*-*δ*-hydroxy alkyl alkoxy radical where it reacts with another oxygen molecule following electron delocalization.[78] However, the same author also suggests that the fractional yield of the above mentioned channel would be very small (1-2%),[78] hence we have not included this chemistry in our model. We find that an 80:20 relative branching between the *β*- and *δ*-peroxy radicals provides the best fit to all the data. Since theoretical calculations predict equivalent branching between the *E*- and *Z*- forms due to the low barrier associated with E/Z isomerization compared to the initial activation energy,[56] a 20% branching for *δ*- peroxy radicals corresponds to a branching of 10% for both *E*- and *Z*- channels. Error analysis provides a large error bar of (80^{+19}_{-30}) % on the branching of *β*-peroxy radicals (Figure III-XIII). The source for the large error bas is the fact that the current experiment is only moderately sensitive to the branching between the *β*- and the

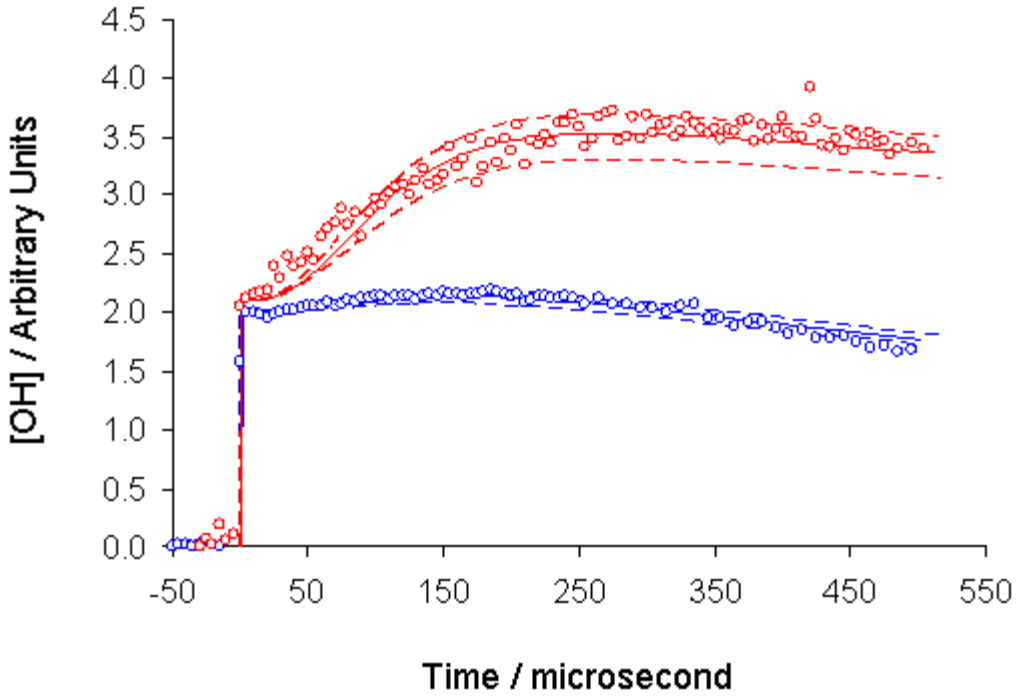

Figure III-XIII. Dashed lines indicate the rate constants for estimated error range for the branching between the β- and the δ- hydroxyl peroxy channels.

A: $[IC_5H_8OH] = 2.1 \times 10^{13}$ molecules cm^{-3}, $[NO] = 2.8 \times 10^{15}$ molecules cm^{-3}, $[O_2] = 1.5 \times 10^{16}$ molecules cm^{-3}
Upper limit to β- branching = 99.0%, lower limit = 50.0%

B: $[IC_5H_8OH] = 2.1 \times 10^{13}$ molecules cm^{-3}, $[NO] = 2.8 \times 10^{15}$ molecules cm^{-3}, $[O_2] = 7.8 \times 10^{15}$ molecules cm^{-3}
Upper limit to β- branching = 99.0%, lower limit = 50.0%.

δ-hydroxyalkoxy radical channels, as concluded by the sensitivity analyses. This motivates our study of isotopically labeled OH/OD cycling.

II. Isotopically labeled OH/OD cycling experiments. The use of a precursor molecule where OH has been replaced by OD can provide additional insight into the role of the *E*-*δ*-hydroxy alkoxy radical. As illustrated in Figure III-VII, in an isotopically labeled experiment, both the *β*-hydroxy alkoxy radicals channel and the (*Z*) form of the *δ*-hydroxy alkoxy radical channel lead to the formation of OD. In contrast, the (*E*) form of the *δ*-hydroxy alkoxy radical will lead to the formation of OH. Thus the observation of OH formation from a deuterated precursor is a signature of the production of the (*E*) form of the *δ*-hydroxyalkoxy radical channel. To pursue these studies, the precursor molecule was deuterated by dissolution in D_2O for 30 minutes followed by extraction from the aqueous solution. The reaction cell was passivated with D_2O to reduce H/D exchange from the hydrogen adsorbed in the kinetic cell and inlet lines. Figure III-XIV shows the OH signal observed from cycling experiment using the photolysis of the deuterated precursor. This observation provides the first direct evidence for the role of the (*E*) – *δ*-hydroxyalkoxy channel in isoprene oxidation. The lower signal to noise ratio in this data is consisted with the low branching ratio (0.1) for this channel. It is clear from the data shown in Figure III-XIV that there appears to be a small contribution from prompt OH formation even though a purely deuterated precursor should only give rise to prompt OD signal. This suggests that there is a small fraction of deuterated precursor that undergoes H/D exchange prior to photolysis despite efforts to minimize exchange. The photolysis of this non deuterated precursor should result in a similar fraction (25%-30%) of prompt OH and isoprene prior to collisional stabilization. The dashed line shown in Figure III-XIV is

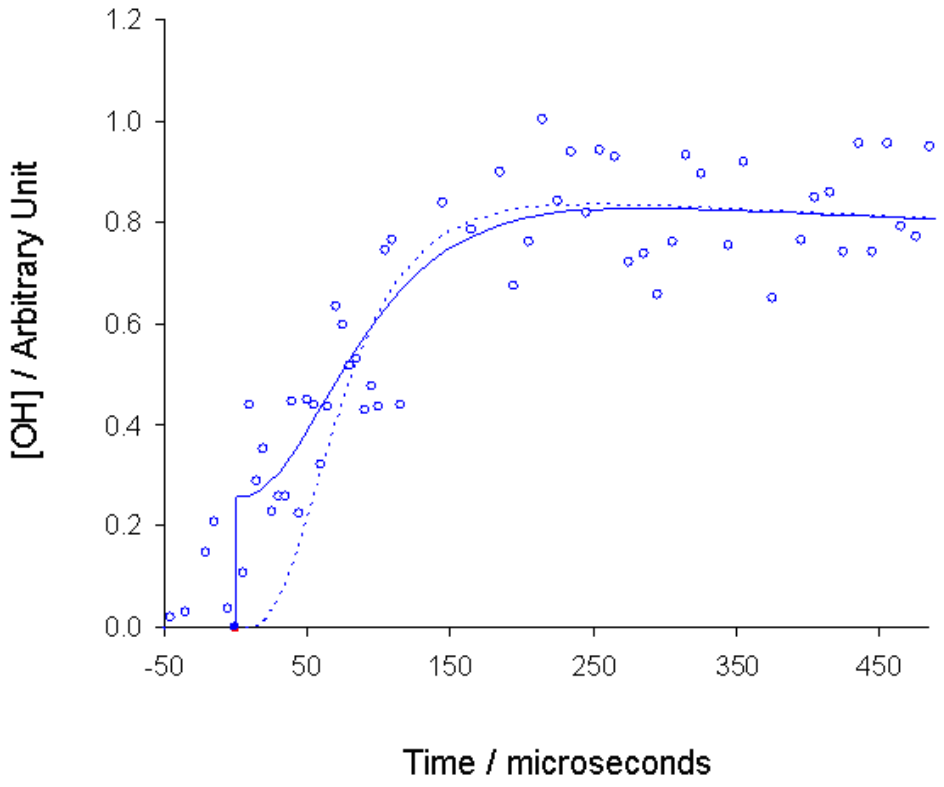

Figure III-XIV. OH cycling from deuterated precursor.
$[IC_5H_8OD] = 1.4 \times 10^{13}$ molecules cm^{-3}, $[NO] = 2.8 \times 10^{15}$ molecules cm^{-3}, $[O_2] = 3.3 \times 10^{16}$ molecules cm^{-3}
The dashed line assumes no H/D exchange while the solid line assumes 6% H/D exchange (see text for details).

a simulation assuming no exchange in the mechanism while the solid line is a simulation assuming that only 6% of the deuterated precursor molecule undergoes H/D exchange prior to photolysis. This small contribution from H/D exchange provides a better fit to the experimental data. A significant fraction of H/D exchange would result in a much larger prompt signal which is not observed. Although including minor contribution of H/D exchange in the model improves the fit, the experimental results are still consistent with the presence of (*E*) – *δ*-hydroxyalkoxy channel.

Figure III-XV shows the OD signal obtained from the OD cycling experiments using the deuterated precursor. In OD cycling using a deuterated precursor, a clear prompt rise in signal is seen followed by a gradual change of signal over time similar to the data shown in the non deuterated studies in Figure III-VI. Since the (*E*) – *δ*-hydroxyalkoxy channel results in OH from a deuterated precursor; this channel decreases the amount of OD production due to cycling relative to the prompt OD signal. In this data, it is therefore the decrease in the ratio of the cycling signal to the prompt rise which provides an additional constraint in quantifying the yield of the (*E*) – *δ*-hydroxyalkoxy channel. The best fit to this data, as shown by the solid line, corresponds to a (*E*) – *δ*-hydroxyalkoxy channel branching of 10% whereas the dashed line corresponds to no *δ*-hydroxyalkoxy channel (Figure III-XV). It is worth noting here, that alternate chemistry reported by Paulot and co workers[79] suggests that the (*Z*) – *δ*-di-hydroxy radical may also undergo a second O_2 addition, as opposed to undergoing H abstraction, to form a di-hydroxy peroxy radical, which undergoes further reactions to finally form HO_2; a route to produce OH via the (*Z*) – *δ*-di-hydroxy radical channel starting from a deuterated

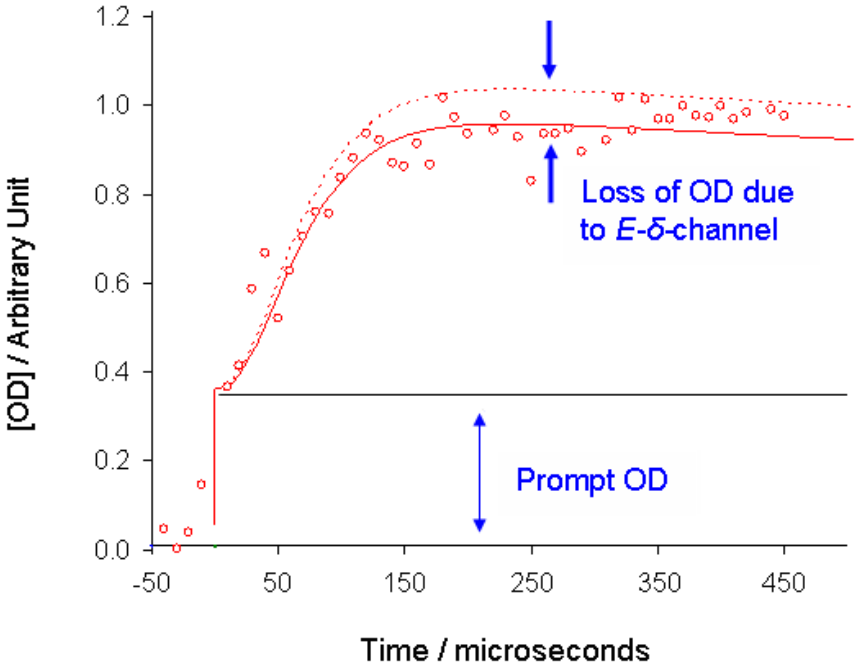

Figure III-XV. OD cycling from deuterated precursor.
$[IC_5H_8OD] = 1.4 \times 10^{13}$ molecules cm^{-3}, $[NO] = 3.5 \times 10^{15}$ molecules cm^{-3}, $[O_2] = 5.4 \times 10^{16}$ molecules cm^{-3}
The solid line assumes a branching of 0.2 for the δ-hydroxyalkoxy channel while the dashed line assumes a branching of 0.0 for the δ-hydroxyalkoxy channel (see text for details).

precursor, in contrast to our model. The authors reported a branching of 0.35 for this di-hydroxy peroxy channel within the *(Z)*-*δ*-peroxy channel and a branching of 0.65 for the traditional (*Z*) – *δ*-di-hydroxy radical chemistry where the radical reacts with oxygen via hydrogen abstraction to form a hydroxyl carbonyl and thus not leading to OH formation from a deuterated precursor. However, a fraction of the *Z*- di-hydroxy peroxy radical channel which leads to methyl glyoxal and glycolaldehyde will lead to the formation of OD from a deuterated precursor and hence this model, with these reported branching ratios will however result in only half of OH signal from a deuterated precursor compared to what is observed in our isotopically labeled experiments. The branching of 0.35 for the O_2 addition channel seems to be an over-estimate as previous studies suggest that α-hydroxy radicals react with O_2 almost exclusively by H abstraction.[80-82] The authors have also suggested that the E/Z branching would not be 1:1, but rather is 0.15/0.85. Also, previous computational work[56] and modeling studies[53,58] have estimated a nearly equivalent branching for the *E*- and the *Z*- isomers of *δ*-hydroxy peroxy radical channels. Furthermore, the chemistry proposed by Paulot et al.[79] predicts formation of 3%-4% of methyl glyoxal and glycolaldehyde as first generation end products which is contradictory to previous end product analysis studies.[49,80] Thus, although this chemistry will reproduce our experimental results, we have not included this chemistry in our model as we think it will have a very small contribution. A chi-square analysis of the simulation fit to the data indicates that the error in this branching ratio is ± 3% resulting in a final branching for the *E*- channel of (10±3)%, which will provide an upper limit to the branching of the *(E)*-*δ*-peroxy channel in case any other chemistry is capable of producing OH from a deuterated precursor. Assuming an equal yield of the *E*- and the *Z*-

isomers of *δ*-hydroxy peroxy radical channels, this corresponds to a yield of (20±6)% for the *δ*-hydroxyalkoxy channel, consistent with our non-isotopic results but with better error limits.

D. Predicted First Generation End Product Distribution

This study has determined a branching ratio of (10±3) % for the *E*- form of the δ-hydroxyalkoxy radical channel, and predicts an overall (20±6) % yield for the δ-hydroxyalkoxy radical. Since the rate constants obtained in this study of the major channel are very similar to those obtained for isoprene-OH oxidation as a whole,[66] we predict that the other terminal OH addition channel (channel IV in Figure III-I) will exhibit similar chemistry. Based on this assumption, we have predicted the end product distribution for two different initial hydroxyl alkyl radical branching of 0.67:0.02:0.02:0.29[38] and 0.56:0.023:0.046:0.37[42] for the channel I: II: III: IV and assuming two limiting values for the nitrate yield of 5% and 15%. The results are shown in the Table III-III.

Table III-III. Summary of end product distributions (in percentage yield) predicted by the branching ratios determined in this study. Included are the end product distributions used in several other chemical models.

End Product	Current Study				MIM2[83]	Zhao[55]	Jenkin[84]	Atkinson[49]
OH-Isoprene adduct ratio	I: II: III: IV 67:2:2:29		I: II: III: IV 56:2.3:4.6:37					
Nitrate yield	5	15	5	15	10	55	10	12
MVK	51	46	43	38	45.6		33.1	29
MACR	22	20	28	25	22.1		22.2	21
OH carbonyl	18	16	17	15	22.3	22.6	20.2	25

The yields of MVK, MACR and hydroxyl carbonyls vary from 38% to 51%, from 20% to 28% and from 15% to 18% respectively. These predicted yields are close to those found in other studies and used in chemical models. The predicted MVK yields probably represent the upper limit, but it depends largely on the initial branching of hydroxyl alkyl radicals I, II, II and IV (Figure III-I). We did not measure that branching in this study, and we have used reported value from literature. There are other conflicting values in the literature for that initial branching, and they lead to different final product yields. The hydroxyl carbonyl yield from currents study is within the margin of error of other studies, but is lower. Our current results for the terminal OH addition to isoprene, coupled with previous studies on the OH addition to inner carbons of isoprene,[8] enables us to express

the OH initiated oxidation of isoprene under high NOx condition using a condensed, lumped mechanism (assuming an initial branching of I:II:III:IV = 67:2:2:29).

Isoprene + OH = 0.10 $RONO_2$ + 0.90 HO_2 + 0.48 MVK+ 0.21 MACR+ 0.21 ISPD + 0.92 NO_2 + 0.75 HCHO

where,

$RONO_2$ = Organic nitrate (assuming 10% nitrate yield)

ISPD = First generation products other than MVK, MACR, hydroxyl Carbonyls, C_5 carbonyls

NO_2 = Total NO_2 formed from NO

E. Conclusions

The current study is the first isomeric selective study on the major channel of isoprene oxidation. The results of the OH cycling experiment provide insight into channel branching and yield isomeric selective rate constants. Sensitivity analysis has been employed to ensure that experimental conditions are suitable for determination of the rate constant for O_2 addition to the hydroxyl alkyl radical, and for NO reaction with the hydroxyl peroxy radicals and we have determined the rate constants of $1.0^{+1.7}_{-0.5} \times 10^{-12}$ molecule^{-1} cm^3 s^{-1} and $8.1^{+3.4}_{-2.3} \times 10^{-12}$ molecule^{-1} cm^3 s^{-1} respectively. Isotopically labeled studies have provided the first experimental evidence of the *δ*-hydroxyalkoxy channel and we have determined an upper limit of (10±3) % on the branching of the *E*- form of *δ*-hydroxyalkoxy radical channel. Since the values of the intermediate rate constants for this major channel are similar to the values obtained for isoprene as a whole, we surmise that the other major channel (isomer IV in Figure III-I) must have similar kinetic

parameters associated with the OH initiated oxidation. Hence, a lumped model including the chemistry of the δ-peroxy channel should provide an accurate enough description of isoprene-OH chemistry at high NOx condition.

CHAPTER IV

HYDROXYL RADICAL INITIATED OXIDATION OF 1,3-BUTADIENE: ISOMERIC SELECTIVE STUDIES OF THE DOMINANT ADDITION CHANNEL*

A. Introduction

1,3-butadiene is an anthropogenic hydrocarbon and its primary atmospheric decay process is reaction with OH radical. The addition of OH to either the terminal or the inner carbons in 1,3-butadiene results in two distinct □hydroxyl alkyl isomers (Figure IV-I) with an overall rate constant of $(7.0\pm0.5)\times10^{-11}$ molecule^{-1} cm^3 s^{-1}.[30] Based on their study of the peroxy radical kinetics resulting from OH initiated 1,3-butadiene oxidation, Jenkin et al. recommended a branching ratio between isomers I and II of 0.87 to 0.13.[84] The subsequent chemistry of each □hydroxyl alkyl isomer is distinct and leads to unique first generation end products. The differences in the chemistry of isomer I and II originates from their reaction with molecular oxygen. The hydroxyalkyl radical generated by OH addition to a terminal carbon (isomer I) reacts with oxygen to form a peroxy radical.[84] Under high NOx conditions, the peroxy radical formed from isomer I reacts with NO to form an alkoxy radical, with a minor channel leading to the formation of organic nitrate.[33] The alkoxy radicals ultimately form carbonyl/hydroxyl carbonyl compounds as the first generation end products, as observed in end product analysis studies.[33] In contrast, the minor hydroxyalkyl radical (isomer II) isomerizes to an α-

---

* Parts of this chapter are preprinted with permission from "OH radical Initiated Oxidation of 1,3-Butadiene: Isomeric Selective Study of the Dominant Addition Channel" Ghosh, B.; Bugarin, A.; Connel, B.; North, S. W. *J. Phys. Chem. A* **2010**, *114,* 5299

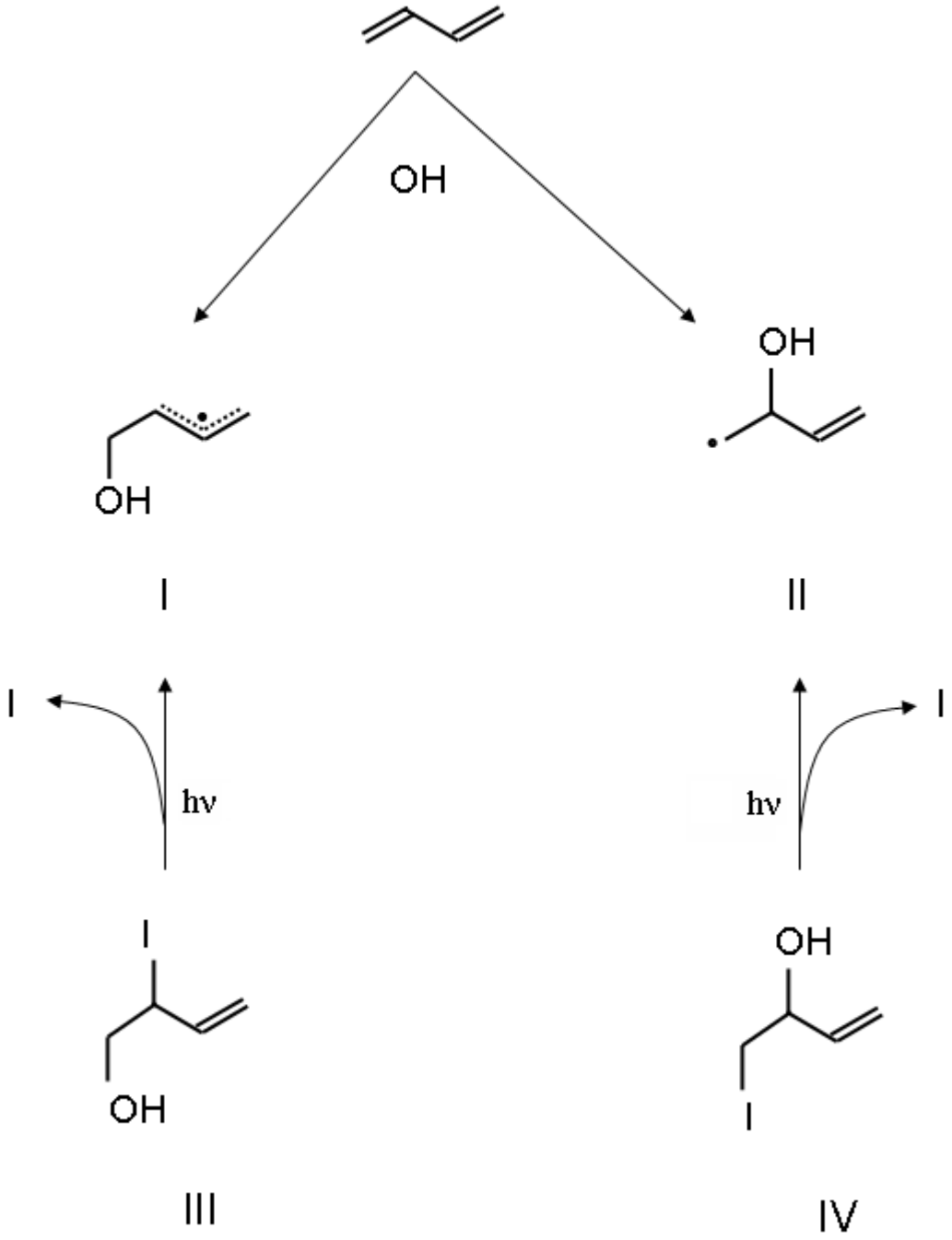

Figure IV-I. Initial branching of □hydroxyl alkyl radicals followed by the reaction of OH radical with 1,3-butadiene.

hydroxyalkyl radical via a cyclic intermediate and subsequently reacts with oxygen via H abstraction to form a C4 carbonyl compound.[9]

In spite of the importance of 1,3-butadiene oxidation in atmospheric chemistry modeling, there have been few detailed studies of the oxidation mechanism. In the case of isoprene, theoretical studies have demonstrated that the *β*-hydroxy alkoxy radicals undergo decomposition to form carbonyl compounds and HCHO.[46-48] The *δ*-hydroxy alkyl isomers, however, undergo a prompt 1,5 H shift followed by H abstraction by oxygen to form hydroxyl carbonyl compounds.[56-58] Since isoprene is structurally similar to 1,3 butadiene, it is reasonable to assume that 1,3-butadiene will exhibit similar chemistry and that the associated *β*-hydroxy alkoxy radicals lead to the formation of acrolein. Unlike isoprene, in 1,3-butadiene oxidation only the *Z*- form of hydroxyl alkoxy radicals undergo a 1,5 H shift, leading to the formation of 4-hydroxy-2-butenal. Although the *E*- isomer does not undergo a 1,5 H shift due to the absence of the methyl group, it still leads to the formation of 4-hydroxy-2-butenal. Hydrogen abstraction by O_2 during the oxidation process results in HO_2 radicals which, under high NO conditions, react with NO to regenerate OH radicals. Thus, the time-dependent kinetics of OH in the presence of known concentrations of NO and O_2 can be a sensitive probe of the detailed mechanism of the oxidation process.

In our recent study of the OH initiated oxidation of isoprene, we demonstrated that isomeric selective studies can provide considerable mechanistic insight.[8,85] Photodissociation of a suitable precursors enable routes to the formation of energy selected single isomers, enabling the study of important channels that are often difficult to unravel in non isomer specific experiments. Previously, Greenwald et al. have reported

isomeric selective studies of isomer II in 1,3-butadiene oxidation.[9] Here, we focus on the major channel of the 1,3-butadiene oxidation using the photolysis of the precursor 1-hydroxy-2-iodo-3-butene. In doing so, we reduce the complex chemistry of 1,3-butadiene oxidation to a single isomeric pathway permitting determination of isomeric selective rate constants and insight into the mechanism.

Although end product studies have observed acrolein[33,86] and 4-hydroxy-2-butenal[26] the associated isomeric specific rate constants of different reactions and the branching between the β- and the δ-hydroxyl alkoxy radicals have only been inferred. The *E*- and *Z*- isomers of the δ-hydroxy alkoxy radical both lead to the identical first generation end products, but there has been no direct measurement of the branching between these isomers due to the complex nature of chemistry. We find that isotopically labeled cycling experiments can be used to estimate the branching ratio of the *E*- channel.

B. Synthesis of Photolytic Precursor

The precursor 1-hydroxy-2-iodo-3-butene was synthesized by reacting hydroiodic acid with butadiene monoxide in H_2O. To a 0°C solution of butadiene monoxide (1 Ml, 870 mg, 12.42 mmol) in 20 Ml of H_2O, protected from light using aluminum foil, was added 57% HI (1.72 Ml, 1.67 g, 13.04 mmol) slowly over a 5-min period. The resulting mixture was stirred for an additional 5 min at 0°C.

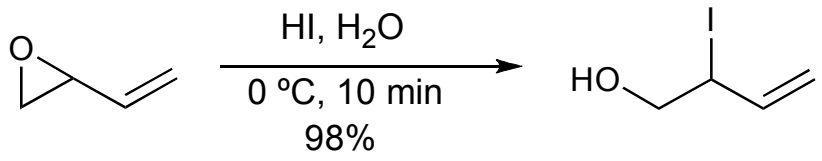

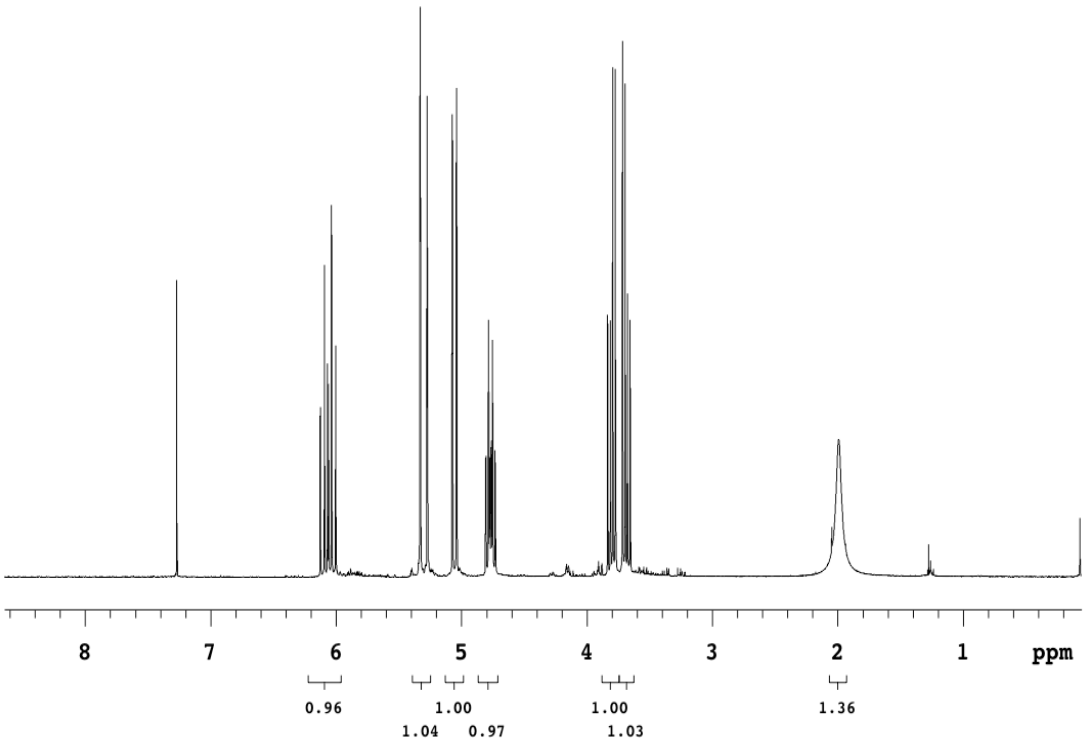

Figure IV-II. ^{1}H NMR (300MHz, $CDCl_3$) spectrum of 1-hydroxy-2-iodo-3-butene: δ 6.12-6.00 (dt, 1H, J = 9.92 Hz, J = 16.90 Hz), 5.32 (dt, 1H, J = 1.01 Hz, J = 17.05 Hz), 5.03 (dt, 1H, J = 0.46 Hz, J = 9.85 Hz), 4.77 (m, 1H), 3.79 (dd, 1H, 6.23 Hz, J = 5.12 Hz), 3.67 (dd, 1H, 6.45 Hz, J = 5.56 Hz), 1.98 (bs, 1OH).

The reaction mixture was quenched with saturated $Na_2S_2O_7$ (50 Ml), and the aqueous layer was extracted with ethyl acetate (50 Ml, 2X). The organic layers were dried with Na_2SO_4, and concentrated under reduced pressure to give the desired pure primary alcohol as colorless oil (2.404 g). The overall yield of the reaction was 98%. The compound was identified by ^{1}H NMR, ^{13}C NMR, (Figure IV-II and IV-III) mass spectrometry and IR spectroscopy. The O-H stretching and C=C stretching frequencies were identified in IR spectroscopy (3350.2 cm^{-1}: O-H stretching), 3084.1 cm^{-1}: C=C stretching). In high resolution mass spectrometry, (chemical ionization, CH_4) the $(M+H)^+$ peak for the C_4H_7IO molecule (*mlz* 197.95) was obtained at *mlz* 198.94.

C. Results and Discussion

We first discuss the results obtained from OH cycling experiments involving the non-deuterated precursor molecule and the corresponding modeling of data including sensitivity analysis of the rate constants. Next we present OD cycling experiments using a deuterated precursor molecule and determination of the branching of the *E*-δ-hydroxy peroxy radical channel.

I. OH cycling from a non deuterated precursor. In these experiments, the non deuterated precursor molecule was photolyzed by the 248 nm laser pulse to generate the hydroxyl alkyl radical I (Figure IV-I) which, in the presence of O_2 and NO produces OH radical, monitored by LIF, through a series of reactions. All experiments were performed under moderate to high NO concentration conditions to ensure rapid OH cycling. In addition, oxygen concentrations higher than the NO concentrations were employed to guarantee higher production rates for OH than loss rates due to

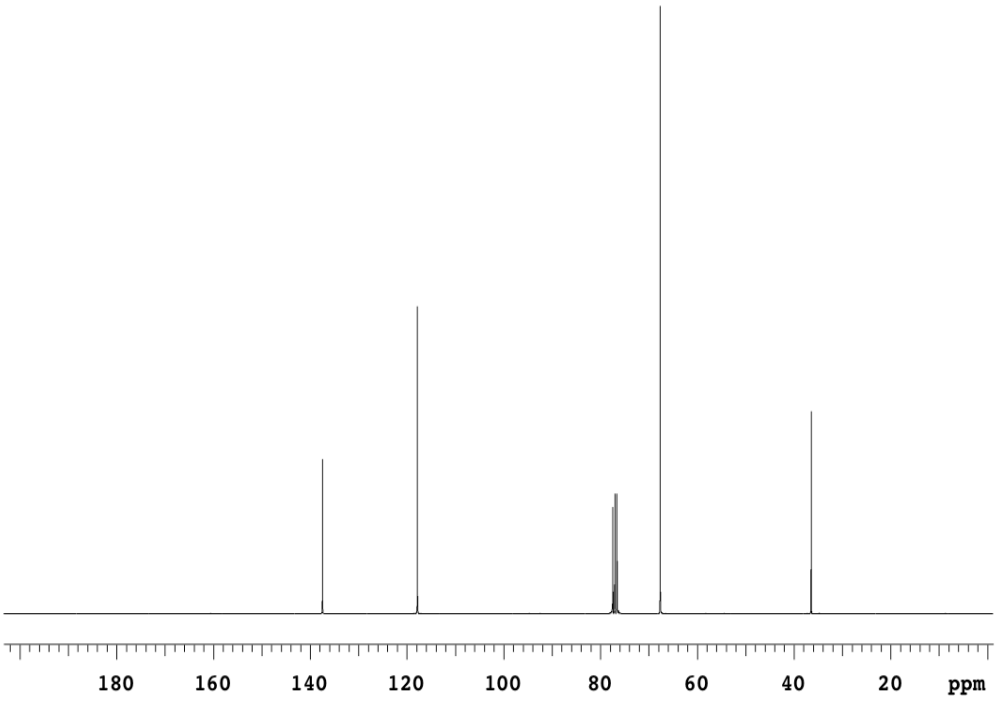

Figure IV-III. ^{13}C NMR (75MHz, $CDCl_3$) spectrum of 1-hydroxy-2-iodo-3-butene: δ 137.44, 117.82, 67.63, 36.43.

Table IV-I. Summary of the experimental conditions employed in the isomeric selective studies of 1,3-butadiene oxidation.

[Precursor] 10^{13} molecules/cc	[NO] 10^{14} molecules/cc	[O_2] 10^{15} molecules/cc
OH cycling experiments from IC_4H_6OH		
3.0	5.0	6.5
3.0	5.0	13.1
3.0	3.2	49.1
3.0	3.2	65.5
3.0	6.4	65.5
3.0	9.6	65.5
3.0	12.8	65.5
3.0	17.0	65.5
3.0	19.0	65.5
OD Cycling experiments from IC_4H_6OD		
1.5	11.5	32.8
1.4	13.9	32.8
4.0	19.3	32.8

radical termination. A summary of the species concentrations for these experiments is tabulated in Table IV-I. A simplified mechanism for OH cycling is shown in Figure IV-IV.

Figure IV-V shows a representative data set obtained from OH cycling experiments where the concentration of the precursor molecule was 3.0×10^{13} molecules cm^{-3}, $[O_2] = 6.5 \times 10^{16}$ molecules cm^{-3}, and the [NO] was varied from 9.6×10^{14} molecules cm^{-3} to 1.9×10^{15} molecules cm^{-3}. The circles represent the data points and the solid lines represent the best fit simulation to the data using the mechanism described in Figure IV-VI and tabulated in Table IV-II. The prompt rise in the signal following the photolysis laser pulse is due to the fraction (25%) of the nascent hydroxyl alkyl radical which are formed with energy exceeding the OH + 1,3-butadiene reaction threshold. In the absence of NO or O_2, the signal decays exponentially as the prompt OH radicals reacts with the precursor molecule with a rate constant of $k_{20} = 3.0 \times 10^{-11}$ cm^3 s^{-1}. Similar values for this rate constant were observed for analogous iodohydrins.[8-9] In the presence of O_2 and NO, the □hydroxyl alkyl radical undergoes a series of reactions to form OH. Under these conditions, the OH signal increases to maxima at times ranging from 100 to 200 μs and decreases at long times.

The analysis program KINTECUS[60] was used to simulate the time dependent OH concentrations and perform the associated sensitivity analysis. A set of 22 reactions was used to simulate the data and is provided in Table IV-II. A more detailed oxidation mechanism for isomer I is shown schematically in Figure IV-VI.

One objective of the study was determination of rate constants for intermediate reaction steps by modeling the OH cycling data. The comprehensive mechanism

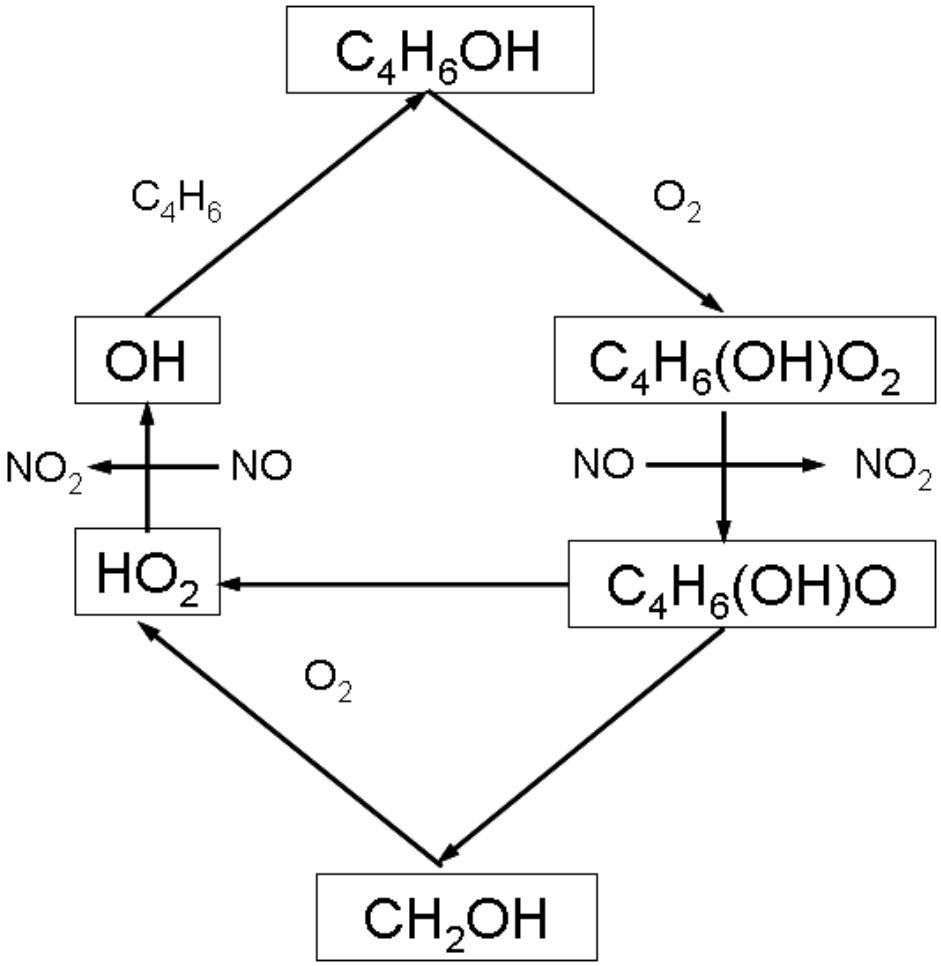

Figure IV-IV. Schematic diagram of OH cycling in 1,3 butadiene oxidation.

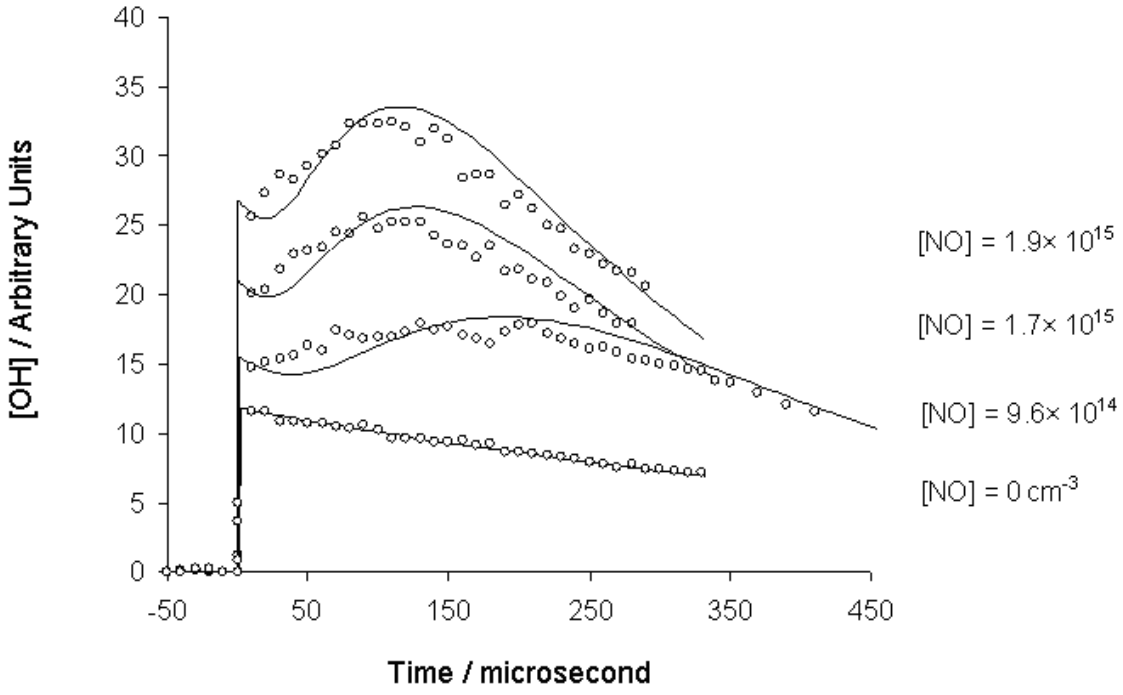

Figure IV-V. OH fluorescence intensity plotted against reaction time at multiple NO concentrations. Symbols represent experimental data and solid lines represent the fits using the reaction mechanism and rate constants in Table IV-II. The individual plots have been shifted vertically for clarity. $[IC_4H_6OH] = 3.0 \times 10^{13}$ molecules cm^{-3}, $[O_2] = 6.5 \times 10^{16}$ molecules cm^{-3}. The lowest plot was taken in the absence of NO.

employed in the fitting procedure includes all the intermediate reactions. Despite the large number of reactions, the simulations are sensitive to a limited number of the rate constants and several of the rate constants are well known.[87] In order to assess which reactions have significant effect on the simulations and to guide the choice of experimental conditions, we have used sensitivity analysis.[66] The Normalized Sensitivity Coefficients (NSC) describe the fractional change of the simulations, in this case the OH concentration, at a specific reaction time given a fractional change of each rate constant keeping all other rate constants fixed.

Figure IV-VII shows the sensitivity analysis calculated at a reaction time of 80 μs, an O_2 concentration of 6.5×10^{16} cm^{-3}, and at two different NO concentrations of 9.6×10^{14} cm^{-3} and [NO] = 1.9×10^{15} cm^{-3}. It is clear from the plots that the OH simulations depend sensitively only on few rate constants, specifically the initial branching between the dissociating hydroxyl alkyl radical and the collisionally stabilized hydroxyl alkyl radical (k_1 and k_2), the NO addition to the hydroxyl alkyl radical (k_3), the O_2 addition to the same (k_4), the NO reaction to the hydroxyl peroxy radical (k_7), and the reaction of NO and HO_2 radical (k_{21}). Of these rate constants, the NO reaction rate with HO_2 has been well studied and we have used the recommended literature value.[88] The absolute values of k_1 and k_2 are unimportant since both are instantaneous on the time scale of the experiments and only their *relative* magnitudes is important. We have assumed a value of 75% for the thermalized hydroxyl alkyl radicals, which is close to the value used in the study of the dominant channel of OH-isoprene oxidation.[85] The remaining three rate constants with high NSC (k_3, k_4 and k_7) are the focus of the analysis, and we seek to extract their values.

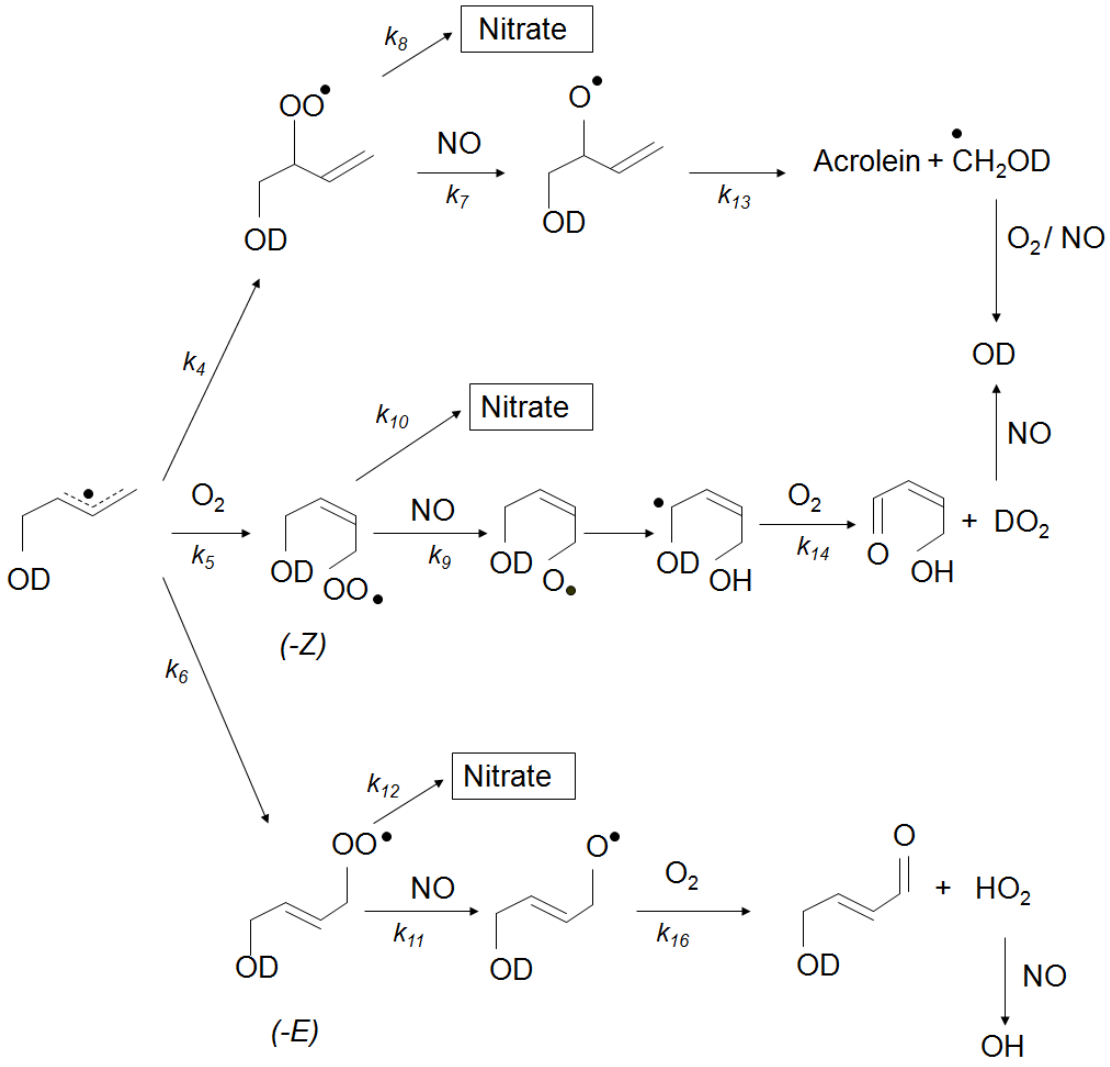

Figure IV-VI. Oxidation mechanism of isomer I.

TABLE IV-II. Reaction mechanism and corresponding rate constants (298 K) used for simulation of the experimental data.[a]

	Reaction		Rate Constant	Ref	Comment
k_1	HOC_4H_6 →	$OH+C_4H_6$	Prompt (25%)	[b]	"Prompt" OH
k_2	HOC_4H_6 →	HOC_4H_6	Prompt (75%)	[b]	OH cycling
k_3	HOC_4H_6+NO →	HOC_4H_6NO	2.0×10^{-11}	[b]	
k_4	$HOC_4H_6 + O_2$ →	β-$HOCH_2CH(O_2)CH=CH_2$	5.25×10^{-13}	[b]	β- branching
k_5	$HOC_4H_6 + O_2$ →	Z-$HOCH_2CH=CHCH_2O_2$	8.75×10^{-14}	[b]	Z-δ branching
k_6	$HOC_4H_6 + O_2$ →	E-$HOCH_2CH=CHCH_2O_2$	8.75×10^{-14}	[b]	E-δ branching
k_7	β-$HOCH_2CH(O_2)CH=CH_2$ +NO →	β-$HOCH_2CH(O)CH=CH_2$+NO_2	1.4×10^{-11}	[b]	Peroxy radicals
k_8	β-$HOCH_2CH(O_2)CH=CH_2$ + NO→	β-$HOCH_2CH(ONO_2)CH=CH_2$	1.0×10^{-12}	33	reacting with
k_9	Z-$HOCH_2CH=CHCH_2O_2$ + NO →	Z-$HOCHCH=CHCH_2OH$+ NO_2	1.4×10^{-11}	[b, c]	NO to form
k_{10}	Z-$HOCH_2CH=CHCH_2O_2$ + NO →	Z-$HOCH_2CH=CHCH_2ONO_2$	1.0×10^{-12}	33	alkoxy radicals
k_{11}	E-$HOCH_2CH=CHCH_2O_2$ + NO →	E-$HOCH_2CH=CHCH_2O$ + NO_2	1.4×10^{-11}	[b]	along with
k_{12}	E-$HOCH_2CH=CHCH_2O_2$ + NO →	E-$HOCH_2CH=CHCH_2ONO_2$	1.0×10^{-12}	33	nitrates
k_{13}	β-$HOCH_2CH(O)CH=CH_2$ →	CH_2OH+CH_2CHCHO	Prompt	66	
k_{14}	Z-$HOCHCH=CHCH_2OH$ + O_2 →	HO_2+$OCHCH=CHCH_2OH$	1.0×10^{-11}	66	Chemistry of Z-
k_{15}	Z-$HOCHCH=CHCH_2OH$ +NO →	Z-$HOCH(NO)CH=CHCH_2OH$	3.0×10^{-11}	63-66	δ channel
k_{16}	E-$HOCH_2CH=CHCH_2O$ + O_2 →	E-$HOCH_2CH=CHCHO$ + HO_2	1.0×10^{-11}	66	Chemistry of E-
k_{17}	E-$HOCH_2CH=CHCH_2O$ + NO →	E-$HOCH_2CH=CHCH_2ONO$	3.0×10^{-11}	63-66	δ channel
k_{18}	$CH_2OH + O_2$ →	$HCHO + HO_2$	9.8×10^{-12}	88	
k_{19}	CH_2OH + NO →	CH_2OHNO	1.2×10^{-11}	66	
k_{20}	$OH+IHOC_4H_6$ →	$IHOC_4H_6OH$	3.0×10^{-11}	[b]	
k_{21}	HO_2+NO →	$OH+NO_2$	1.2×10^{-11}	66	
k_{22}	OH + NO →	HONO	9.4×10^{-13}	70	

[a] Rate constants are in molecule^{-1} cm^3 s^{-1} unless otherwise stated. [b] This work.
[c] The formation of the Z-δ-hydroxy alkoxy radical and the subsequent isomerization to the Z-δ-di- □hydroxyl alkyl radical have been incorporated into one rate constant k_9 as the isomerization reaction is "prompt" in experimental time scale.

The termination reactions by NO with alkyl and alkoxy radicals (k_{15} and k_{17} respectively) are important at the moderate to high NO concentrations employed in the study to ensure fast cycling. However, the cycling experiments are not particularly sensitive to the precise values of these rate constants, as evident from the sensitivity analysis, and we have used a value of 3.0×10^{-11} cm^3 s^{-1} based on our previous cycling study.[85] We note that this value is close to the other values reported for similar systems.[63-65] The NO addition to hydroxyl 1,3-butadiene (k_3), however, has an appreciable NSC and we have determined a best fit value of $2.0\times10^{-11}cm^3$ s^{-1} for this reaction. This value is very similar to the value of 2.2×10^{-11} cm^3 s^{-1} reported for NO addition to the other hydroxyl alkyl isomer generated by OH addition to the inner carbon of 1,3-butadiene[9] and agrees well with the rate constant of 1.2×10^{-11} cm^3 s^{-1} reported for NO addition to the hydroxyl alkyl radical generated from OH addition to the outer carbon of isoprene.[85] The simulations are not sensitive to the rate constant for NO addition to CH_2OH and we have adopted a slightly smaller value for this rate constant, i.e. $k_{19} = 1.2\times 10^{-11}$ cm^3 s^{-1}, which was reported previously.[66]

The O_2 addition to the hydroxyl alkyl radical plays an important role in atmospheric hydrocarbon oxidation as a chain propagation step leading to ozone formation. Although the very high ambient oxygen concentration in troposphere renders accurate determination of this rate constant unnecessary for atmospheric modeling, an accurate value is needed for proper modeling of laboratory kinetic data. Given the sensitivity of the simulations to k_4 we can determine its value with moderate error limits. The rate constants k_3 and ($k_4 + k_5 + k_6$) represent a set of parallel reactions leading towards chain termination and chain propagation respectively. It is the competition between these

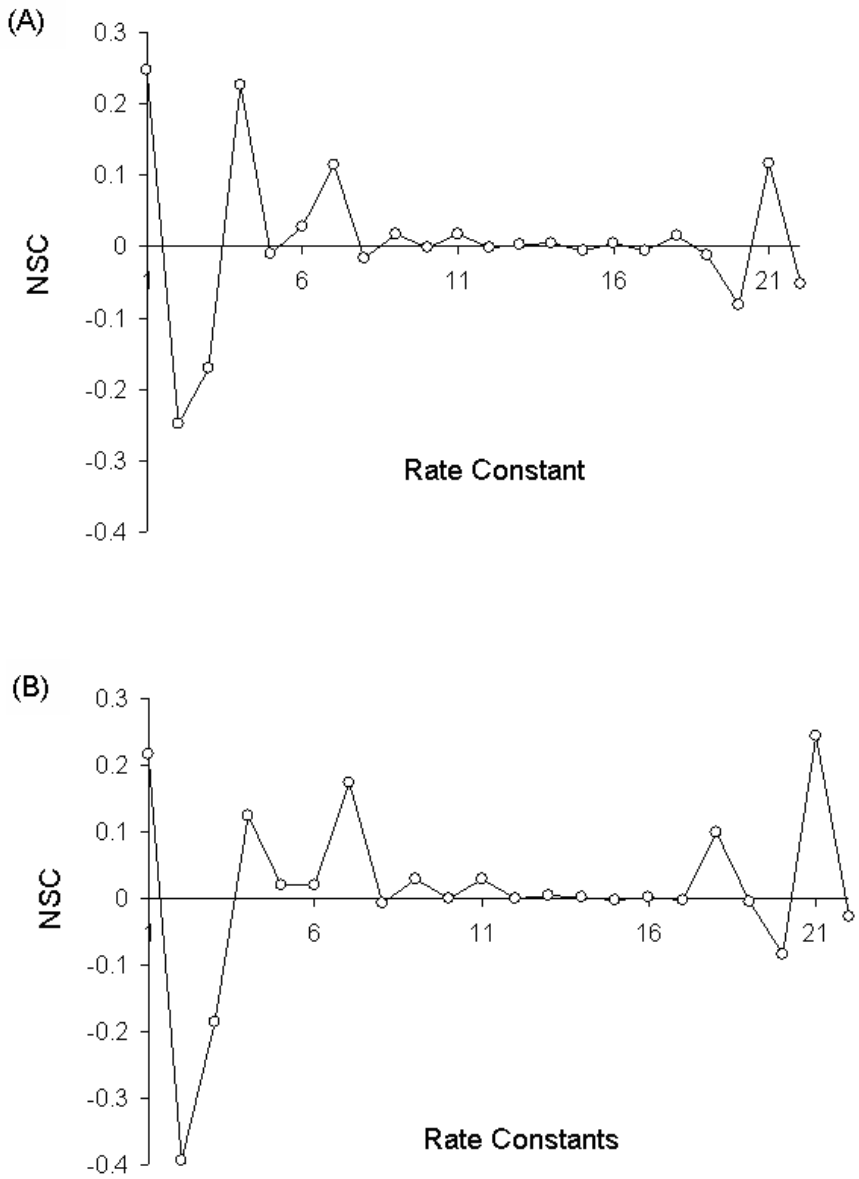

Figure IV-VII. A: Sensitivity analysis at time 80 μs for $[IC_4H_6OH] = 3.0 \times 10^{13}$ molecules cm^{-3}, $[NO] = 1.9 \times 10^{15}$ molecules cm^{-3}, $[O_2] = 6.5 \times 10^{16}$ molecules cm^{-3}

B: Sensitivity analysis at time 80 μs for $[IC_4H_6OH] = 3.0 \times 10^{13}$ molecules cm^{-3}, $[NO] = 9.6 \times 10^{14}$ molecules cm^{-3}, $[O_2] = 6.5 \times 10^{16}$ molecules cm^{-3}.

two reactions, *i.e.* k_3 [NO] and ($k_4 + k_5 + k_6$) [O_2], that largely controls the shape of the OH profile. Thus, the value of k_3 affects determination of ($k_4 + k_5 + k_6$) and the error in the determination of k_3 will be reflected in the error range of ($k_4 + k_5 + k_6$). However, we rely on the numerous studies on the addition of NO to alkyl radicals which report rate constant values within a relatively narrow range.[9,66,85] A reasonable fit to our data can be obtained by using values ranging from 1.5×10^{-11} molecule^{-1} cm^3 s^{-1} to 3.0×10^{-11} molecule^{-1} cm^3 s^{-1} for the NO addition rate constant (k_3) (Figure IV-VIII), and the best fit to the data is achieved for a value of 2.0×10^{-11} molecule^{-1} cm^3 s^{-1} for k_3. Using this value of 2.0×10^{-11} molecule^{-1} cm^3 s^{-1} for k_3, we find that the best fit to data is obtained by using the value of 7.0×10^{-13} molecule^{-1} cm^3 s^{-1} for the O_2 addition rate constant to the hydroxyl radical ($k_4 + k_5 + k_6$) with an upper limit of 1.3×10^{-12} molecule^{-1} cm^3 s^{-1} and a lower limit of 5.0×10^{-13} molecule^{-1} cm^3 s^{-1}. However, including the range of k_3 results in larger upper and lower limits for ($k_4 + k_5 + k_6$) of 1.4×10^{-12} molecule^{-1} cm^3 s^{-1} and 4.0×10^{-13} molecule^{-1} cm^3 s^{-1}, respectively (Figure IV-IX).

To our knowledge, there have been no detailed kinetics studies on the major addition channel of OH initiated butadiene oxidation. However, there have been extensive studies on isoprene oxidation and given the similarity between isoprene and butadiene, the mechanism of oxidation is expected to be similar. According to the theoretical study by Lei et al.,[73] the O_2 addition rate constant to the different hydroxyl-isoprene isomers lie in the range of 1.0×10^{-13} cm^3 s^{-1} and 3.0×10^{-12} cm^3 s^{-1}, and our rate constant of $7^{+7.0}_{-3.0} \times 10^{-13}$ cm^3 s^{-1} lies within this range. Our rate constant is similar to the value of $(7.0 \pm 3.0) \times 10^{-13}$ cm^3 s^{-1} obtained from experimental studies by Zhang et al.[74] for O_2 addition rate constant to hydroxyl alkyl isoprene and within the mutual error limits of

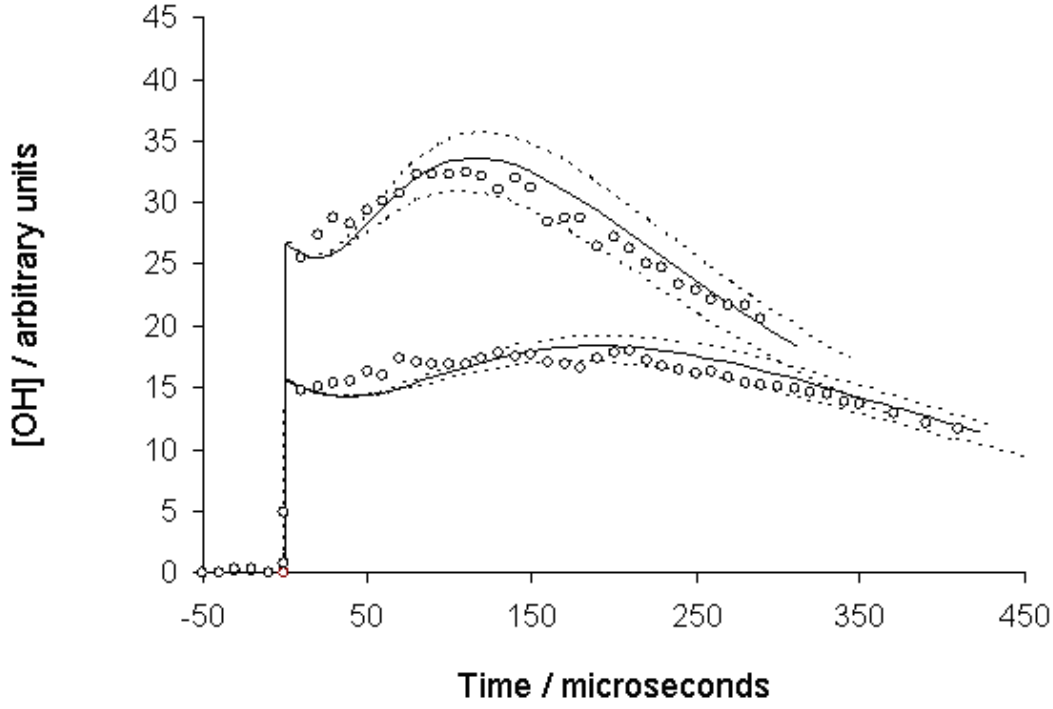

Figure IV-VIII. Dashed lines indicate the rate constants for the estimated error range for NO addition to hydroxyl alkyl radical rate (k_3).

A: $[IC_4H_6OH] = 2.1 \times 10^{13}$ molecules cm^{-3}, $[NO] = 1.9 \times 10^{15}$ molecules cm^{-3}, $[O_2] = 6.5 \times 10^{16}$ molecules cm^{-3}
Upper limit = 3.0×10^{-11} $molecule^{-1}$ cm^3 s^{-1}, lower limit = 1.5×10^{-12} $molecule^{-1}$ cm^3 s^{-1}

B: $[IC_4H_6OH] = 2.1 \times 10^{13}$ molecules cm^{-3}, $[NO] = 9.6 \times 10^{14}$ molecules cm^{-3}, $[O_2] = 6.5 \times 10^{16}$ molecules cm^{-3}
Upper limit = 3.0×10^{-11} $molecule^{-1}$ cm^3 s^{-1}, lower limit = 1.5×10^{-12} $molecule^{-1}$ cm^3 s^{-1}.

$(2.3\pm2.0) \times 10^{-12}$ cm^3 s^{-1}derived from OH cycling experiments on isoprene.[66]

The reaction of NO with peroxy radical is a crucial reaction in butadiene oxidation as its rate constant is a key factor in determining the relative importance of the NO-peroxy reaction and the peroxy-peroxy self and cross reactions. Under moderate to high concentrations of NO, consistent with urban environments, the peroxy radical reacts with NO to produce an energized nitrite species, which decomposes to form an alkoxy radical and NO_2 with a small fraction forming stable nitrate species.[76] These nitrates are stable compounds and are removed from the atmosphere via dry and wet deposition as well as long range transport,[15] thus causing removal of NOx from atmosphere. Organic nitrates can also undergo photolysis, reaction with OH radical and unsaturated nitrates can further react with O_3 and NO_3. These processes also cause removal of NOx from atmosphere. However, under low NOx conditions, such as the Amazon rain forest; peroxy radicals primarily undergo reaction with HO_2[89] or participate in self/cross reactions with other peroxy radicals.[84] The rate constant for the NO reaction with peroxy radical to produce NO_2 and alkoxy radical (k_7) has a moderate sensitivity under our experimental conditions, but we are insensitive to the channel producing nitrate (k_8). Thus, we selectively determine k_7, and have assumed a value of 7% for the nitrate yield based on previous studies.[33] For the overall reaction of NO with the peroxy radicals, we have determined a rate constant of $1.5\,^{+1.0}_{-0.6} \times 10^{-11}$ cm^3 s^{-1}. Figure IV-X shows the best fit (solid line) to the data obtained by using the above mentioned value for ($k_7 + k_8$) and the dashed lines represent upper and lower limits of 2.5×10^{-11} $molecule^{-1}$ cm^3 s^{-1} and 9.0×10^{-12} $molecule^{-1}$ cm^3 s^{-1} respectively. To our knowledge, this rate constant has not been reported for butadiene, although several studies have measured this rate constant for

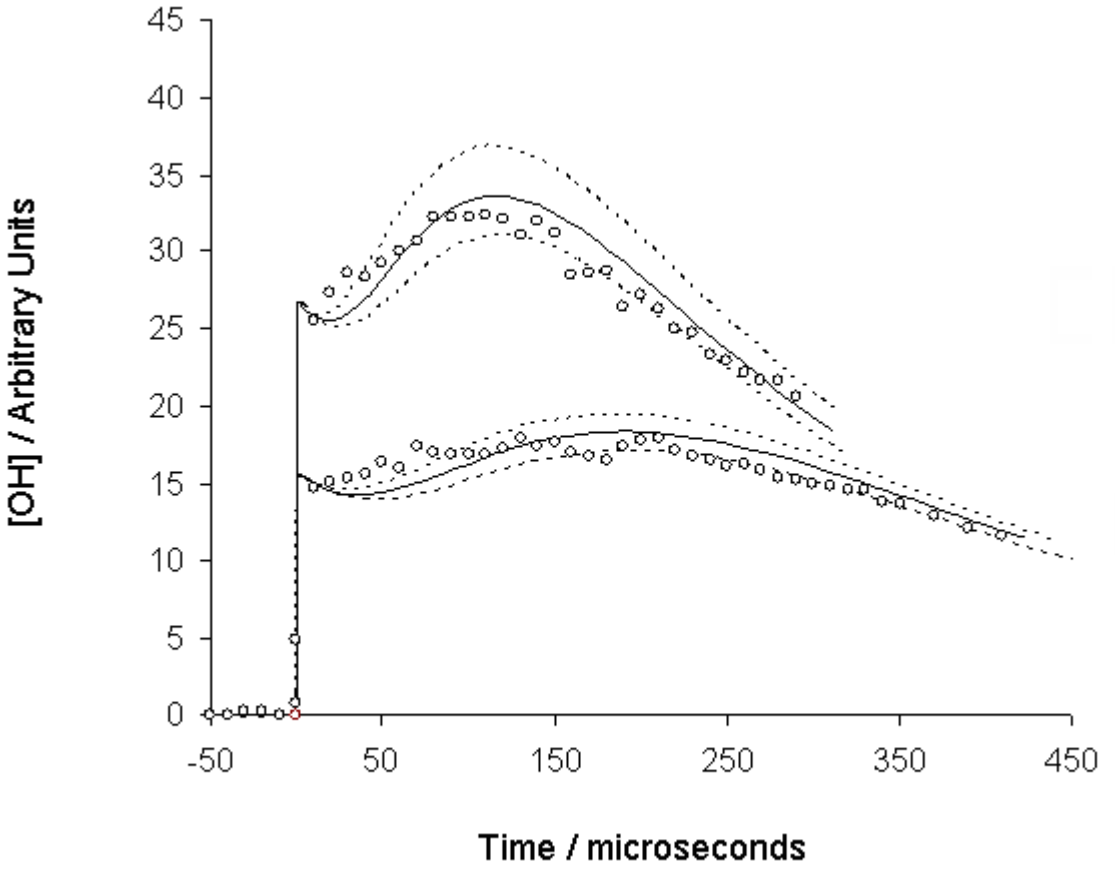

Figure IV-IX. Dashed lines indicate the rate constants for estimated error range for O_2 addition to hydroxyl alkyl radical.

A: $[IC_4H_6OH] = 3.0 \times 10^{13}$ molecules cm^{-3}, $[NO] = 1.9 \times 10^{15}$ molecules cm^{-3}, $[O_2] = 6.5 \times 10^{16}$ molecules cm^{-3}
Upper limit = 1.4×10^{-12} molecule^{-1} cm^3 s^{-1}, lower limit = 4.0×10^{-13} molecule^{-1} cm^3 s^{-1}

B: $[IC_4H_6OH] = 3.0 \times 10^{13}$ molecules cm^{-3}, $[NO] = 9.6 \times 10^{14}$ molecules cm^{-3}, $[O_2] = 6.5 \times 10^{16}$ molecules cm^{-3}
Upper limit = 1.4×10^{-12} molecule^{-1} cm^3 s^{-1}, lower limit = 4.0×10^{-13} molecule^{-1} cm^3 s^{-1}.

analogous systems. Zhang and co workers performed a theoretical study on NO addition to isoprene peroxy radical and found overall rate constant varying from 3.0×10^{-12} cm^3 s^{-1} to 2.0×10^{-11} cm^3 s^{-1} depending on the specific isomer[76] and our reported rate constant lies within this range. Our rate constant also agrees well with the value of $(1.4\pm0.2) \times 10^{-11}$ cm^3 s^{-1} obtained by Maricq et al.[90] for NO + $CH_3(CO)O_2$ reaction and is also close to the value of 2×10^{-11} cm^3 s^{-1} recommended by NASA-JPL[70] for the same reaction. Our value is slightly higher than the range of $(9.0\pm3.0) \times 10^{-12}$ cm^3 s^{-1} obtained by Park et al.[66]

Reaction k_{13}, which corresponds to the decomposition of activated alkoxy radicals, is predicted to be fast compared to the timescale of the experiment.[66] This reaction is described as 'prompt' in the reaction mechanism and the experiment is insensitive to its absolute values for values higher than 1.0×10^6 s^{-1}. The reaction rate constants k_4, k_5 and k_6 in Table IV-II correspond to relative branching ratios of different peroxy radicals. Reaction 4 corresponds to the branching to form β-hydroxy peroxy radicals, which subsequently reacts with NO to form β-hydroxy alkoxy radicals and decompose to form acrolein and formaldehyde molecules. Reaction 5 corresponds to the branching to form *Z*-δ-hydroxy peroxy radicals which undergo prompt 1-5 hydrogen transfer reaction followed by hydrogen abstraction by oxygen to form 4-hydroxy-2-butenal and HO_2. Finally, reaction 6 describes the branching of the (*E*)-δ- hydroxyl alkoxy radical which reacts with oxygen by hydrogen abstraction to form 4-hydroxy-2-butenal and HO_2 as its end products.[26] Due to the inherent symmetry of 1,3-butadiene, both the (*E*)- and the (*Z*)- forms of δ- hydroxyl alkoxy radical lead to the same final product. Thus, although 4-hydroxy-2-butenal has been detected in end product studies,[26]

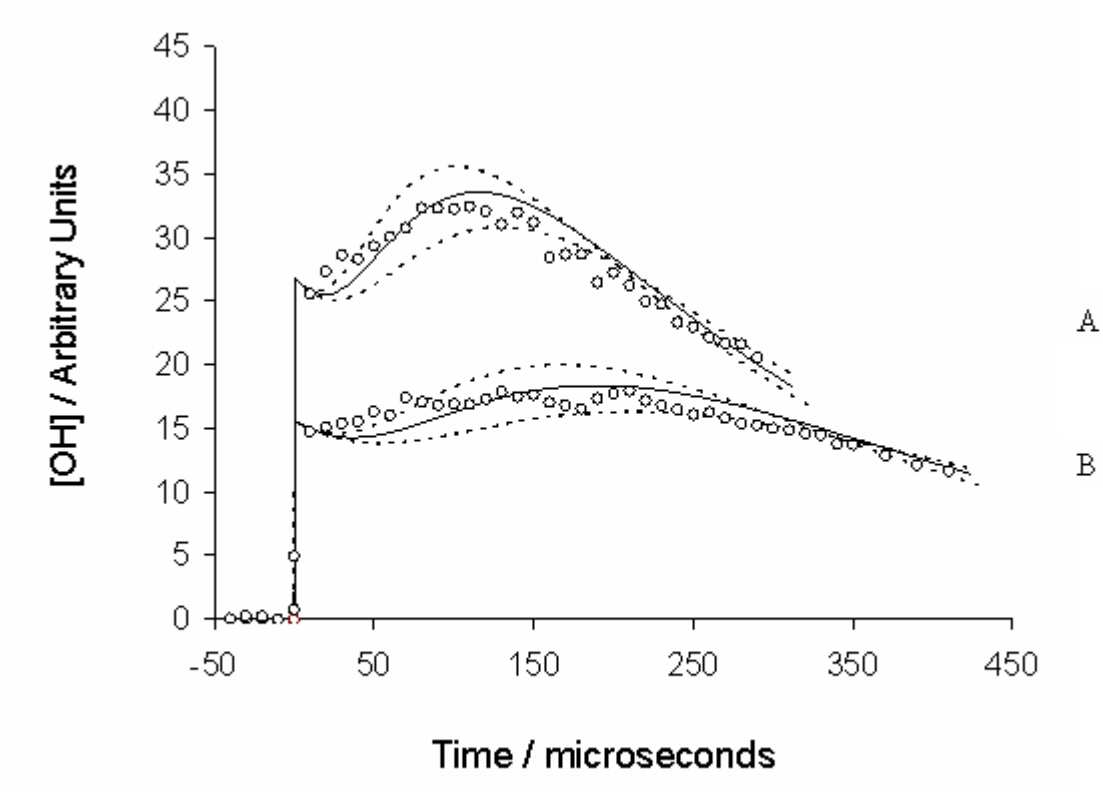

Figure IV-X. Dashed lines indicate the rate constants for estimated error range for NO reaction with hydroxyl alkyl peroxy radical rate ($k_7 + k_8$).

A: $[IC_4H_6OH] = 3.0 \times 10^{13}$ molecules cm^{-3}, $[NO] = 1.9 \times 10^{15}$ molecules cm^{-3}, $[O_2] = 6.5 \times 10^{16}$ molecules cm^{-3}
Upper limit = 2.5×10^{-11} molecule^{-1} cm^3 s^{-1}, lower limit = 9.0×10^{-12} molecule^{-1} cm^3 s^{-1}

B: $[IC_4H_6OH] = 3.0 \times 10^{13}$ molecules cm^{-3}, $[NO] = 9.6 \times 10^{14}$ molecules cm^{-3}, $[O_2] = 6.5 \times 10^{16}$ molecules cm^{-3}
Upper limit = 2.5×10^{-11} molecule^{-1} cm^3 s^{-1}, lower limit = 9.0×10^{-12} molecule^{-1} cm^3 s^{-1}.

the branching between the two channels has not been measured nor calculated. A branching of 0.74 for the *β*-hydroxy alkoxy channel provides a good fit to the data and is based on the results of isotopic studies described in the following section. As in case of isoprene, the *E*- and *Z*- forms of the *δ*- hydroxyl alkoxy radical are expected to have equivalent branching due to the very low barrier of *E*/*Z* inter-conversion,[46] and therefore we have assumed that the same is true for 1,3-butadiene. However, our sensitivity analysis predicts that OH cycling experiments are not a sensitive test of the branching (reaction 5 and 6) necessiting isotopically labeled cycling experiments.

We note that the inclusion of a minor contribution (<4%) from the inner OH addition channel eliminates the short term decay exhibited by the simulation but does not alter the long term behavior (Figure IV-XI).

II. OD cycling from a deuterated precursor. As shown in Figure IV-VI, if the OH group is replaced by an OD group, then the *β*-hydroxy peroxy radical and the (*Z*)- isomer of the *δ*-hydroxy peroxy radical both lead to the formation of OD while the (*E*)- isomer of the *δ*-hydroxy peroxy radical yields OH. Therefore, the detection of OD from a deuterated precursor should result in lower signals as compared to the previous OH cycling experiments using a non deuterated precursor. It is this decrease in signal that corresponds to the yield of the (*E*)-*δ*- hydroxyl peroxy channel. For this isotopic study, the precursor molecule was deuterated by dissolving it into D_2O and shaking for ~30 minutes followed by extraction and purification of the organic compound. The LIF cell and the inlet lines were passivated by flowing D_2O for several hours to reduce H/D exchange by the hydrogen at surfaces.

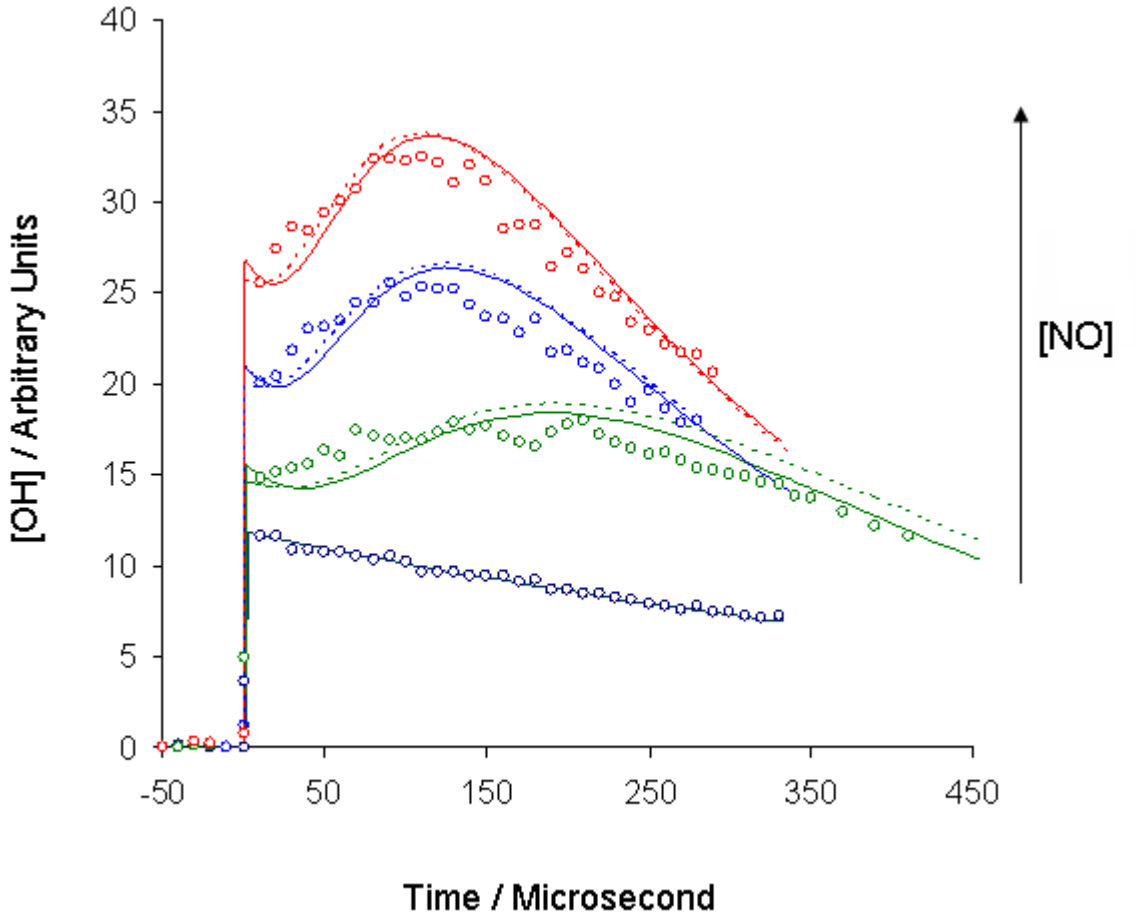

Figure IV-XI. OH fluorescence intensity plotted against reaction time at multiple NO concentrations. Symbols represent experimental data and solid lines represent the fits using the reaction mechanism and rate constants in Table IV-II while dashed lines indicate the simulations using a minor contribution of OH cycling from inner OH addition channel. The individual plots have been shifted vertically for clarity. $[IC_4H_6OH] = 3.0 \times 10^{13}$ molecules cm^{-3}, $[O_2] = 6.5 \times 10^{16}$ molecules cm^{-3}. The lowest plot was taken in the absence of NO.

Figure IV-XII shows the OD signal obtained following the photolysis of the deuterated precursor. The prompt rise due to the spontaneous dissociation of the nascent Hydroxyalkyl radical to form OD and 1,3-butadiene is followed by a slight rise and decay. The data is very similar to the data from non isotopic studies (Figure IV-V), yet with a smaller cycling signal relative to the prompt rise due to the absence of contribution of OD signal from the (*E*)-*δ*- hydroxyl peroxy channel. This decrease in the cycling signal over prompt rise provides a quantitative measure of the branching of the (*E*)-*δ*-hydroxyl peroxy channel. The dashed line is the simulation assuming no (*E*)-*δ*- hydroxyl peroxy channel formation, whereas the solid line represents the best fit to this data corresponding to a branching of 13% for the (*E*)-*δ*- hydroxyl peroxy channel. This measurement provides an upper limit to the branching of the *(E)*-*δ*-peroxy channel there may be alternative chemistry not included in the model that is capable of producing OH from a deuterated precursor. Given the predicted equal branching for the *E*- and *Z*-isomers,[46] results in an overall branching for the *δ*- hydroxyl peroxy channel of 26%. This value matches very well with the overall branching of 25% for the *δ*-hydroxy peroxy channel reported by Jenkin and co-workers.[84] An error analysis of this simulation fits to data provides an estimated error range of ± 5% for the branching of the *E*- channel, which provides an overall branching of 26±10 % for the *δ*-hydroxy peroxy channel.

Although the observation of OH from a deuterated precursor in the analogous isoprene system provided direct evidence of the *E*-channel, the low S/N in the current system precluded OH detection.

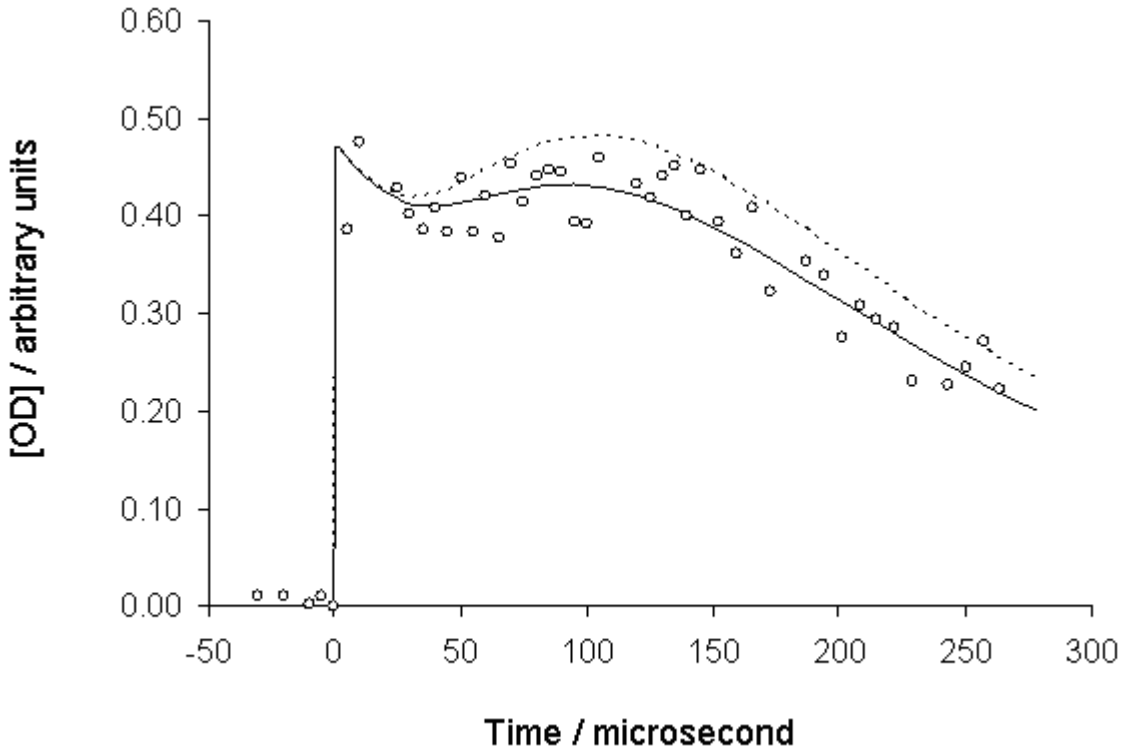

Figure IV-XII. OD cycling from deuterated precursor.
$[IC_4H_6OD] = 4.0 \times 10^{13}$ molecules cm^{-3}, $[NO] = 1.9 \times 10^{15}$ molecules cm^{-3}, $[O_2] = 3.3 \times 10^{16}$ molecules cm^{-3}
The best fit was obtained for a branching of 13% for the *E*-*δ*-hydroxy peroxy channel.

D. Predicted First Generation End Product Distribution

Based on the 26±10 % branching to the *δ*-hydroxy peroxy channel, and assuming an initial branching of 0.87:0.13 for isomer I and II (Figure IV-I)[84] and a nitrate yield of 7%, we predict a yield of (21±9)% for 4-hydroxy-2-butenal in close agreement to the value of (23±10) % reported by Berndt *et al*. in a product study of the 1,3-butadiene-OH oxidation.[26] Our value is also very close to the product yield of (25^{+15}_{-10}) % obtained by Baker and co workers in their end product study.[91] Combining the current results for the dominant channel (Channel I in Figure IV-I) with our previous results for the minor channel[9] of OH-1,3-butadiene oxidation chemistry, we can predict the end product distribution assuming a nitrate yield of 7%. The results are given in Table IV-III.

Table IV-III. Summary of end product distributions (in percentage yield) predicted by the branching ratios determined in this study, assuming initial branching ratios of 0.87:0.13 for □hydroxyl alkyl radicals I and II (Figure1). Included for comparison are the end product distributions reported in other studies.

End Product	Current study	Berndt[26]	Baker[91]	Tuazon[33]	Sprengnether[86]
Organic Nitrate	7[a]	6±2		7±3	11±6
Acrolein	63±10	59±6	58±10	58±4	69±7
4-hydroxy-2-butenal	21±9	23±10	25^{+15}_{-10}		
3-butenal (C_4 carbonyl)	9				
HCHO	63±10	64±8		62±5	69±10
Furan		4.6±1.4		3-4	1.9±0.2

[a] The current study was insensitive to the nitrate yield and the value of 7% recommended by Tuazon et al. was adopted.[33]

The yields of nitrate, acrolein, 4-hydroxy-2-butenal and formaldehyde are predicted to be 7%, 63±10%, 21±9% and 63±10% respectively. These predicted yields are very close to those found in other studies and lie within the mutual error limits. It is worth noting that since acrolein and HCHO are co-products from the same reaction they should be formed in equal yield as predicted by our model. Berndt et al.[26] and Tuazon and co workers[33] have reported slightly higher yield for HCHO compared to acrolein. Although the acrolein and HCHO yields are within their mutual error limits, the authors noted that there may be additional pathways leading to the formation of HCHO.[26,33] Our predicted yield for acrolein is slightly higher than values reported by Berndt et al.[26] and Tuazon et al.[33] but is very close to their HCHO yields. The wall-less studies conducted by Sprengnether[86] also reported equal yields for HCHO and acrolein, in good agreement with our values. On this basis, we suggest that there may be no additional pathways to the formation of HCHO. Berndt et al.[26] and Tuazon and co workers[33] also reported a furan yield of 3-4%, resulting from a faction of the *Z*-*δ*-hydroxy alkoxy channel via cyclization. Wall-less experiments on the OH initiated oxidation of isoprene did not detect furan[86] suggesting that furan derivatives result from secondary reactions. However, the same group reported a low yield (1.9%) for furan from 1,3-butadiene oxidation, suggesting that a small fraction of *Z*-*δ*-hydroxy alkoxy channel may lead to furan. The current study only measures the branching ratio of the *E*-*δ*-hydroxy alkoxy channel and is not sensitive to a minor channel leading to furan. The C_4 carbonyl 3-butenal to our knowledge has not been reported. However, the analogous C_5 carbonyl compound arising from similar chemistry from isoprene has been detected previously.[8] Berndt et al. carried out the most comprehensive end product analysis but did not observe 3-butenal.[26] However, their

product yields account for 94% of reacted carbon including 4.6% of furan yield. Considering the combined uncertainties of product yields, and the fact that furan yield is most likely to be less than 4.6%, the formation of 3-butenal cannot be ruled out by the studies of Berndt et al.[26] The theoretical and experimental study of Greenwald et al. has predicted the formation of the 3-butenal from the minor channel of OH-1,3-butadiene oxidation[9] and we have used the reported branching ratios from that work.

E. Conclusions

We have reported the first isomeric selective study on the dominant channel of OH radical initiated oxidation of 1,3-butadiene. Laser photolysis of the mono deuterated/non deuterated iodohydrin precursor molecule leads to the formation of a single isomer, the major addition adduct of OH-1,3-butadiene reaction, and OH/OD cycling experiments in the presence of NO and O_2 provides valuable information about the oxidation mechanism. We have employed sensitivity analysis to confirm that the experimental conditions were suitable for the determination of the isomeric selective rate constants. We have determined the rate constant of O_2 addition to the hydroxyl alkyl radical to be $7^{+7.0}_{-3.0} \times 10^{-13}$ cm^3 s^{-1} and we find a value of $1.5^{+1.0}_{-0.6} \times 10^{-11}$ cm^3 s^{-1} for the overall reaction rate constant of the hydroxyl peroxy radical with NO. Isotopic cycling experiments permits quantification of the branching for the *E*-*δ*- hydroxyl peroxy channel and we find an upper limit for the branching to be (13±5) %. This isomeric selective kinetic study, together with a previous study[13] on the minor channel of the 1,3-butadiene oxidation present a clear overall picture of butadiene oxidation under high NOx condition relevant to most parts of continental US.

CHAPTER V

HYDROXYL RADICAL INITIATED OXIDATION OF 1,3-BUTADIENE: DETERMINATION OF THE INITIAL BRANCHING*

A. Introduction

In the initial step of oxidation, the OH radical adds to 1,3-butadiene giving rise to two different hydroxy alkyl radicals (Figure V-I). This process has been studied previously and an overall rate constant of $(6.98\pm0.28) \times 10^{-11}$ s^{-1} $molecule^{-1}$ cm^3 has been reported.[25] The oxidative chemistry of the hydroxy alkyl radical obtained by OH addition to the outer carbon of 1,3-butadiene is distinct from the inner addition.[9,92] The outer hydroxy alkyl radical reacts with molecular oxygen by addition reaction to form a peroxy radical[92] whereas the inner hydroxy alkyl radical reacts with molecular oxygen by hydrogen abstraction mechanism to produce a C4 carbonyl compound.[9] Both reaction pathways regenerate OH radical (Figure V-II) whose concentration can be monitored using Laser Induced Fluorescence (LIF). The time dependence of OH radical concentration is sensitive to the oxidation mechanism, and a judicious choice of reactant concentrations with careful modeling can provide detailed mechanistic information. The two reaction pathways have recently been studied individually using photolytic precursors to generate the specific OH-adduct isomers. There have also been end product

---

* Parts of this chapter are preprinted with permission from "OH Initiated Oxidation of 1,3-Butadiene in the Presence of O_2 and NO" Ghosh, B.; Park, J.; Anderson, K.; North, S. W. *Chem. Phys. Lett.*, **2010,** *Accepted*

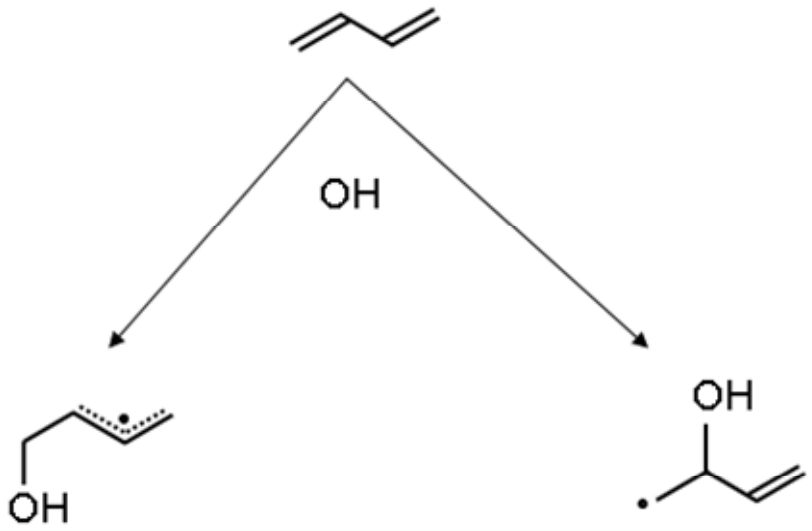

Figure V-I. Initial branching of hydroxyalkyl radicals followed by the reaction of OH radical with 1,3-butadiene.

studies using FTIR and mass spectrometric techniques which find acrolein, HCHO and 4-hydroxy-2-butenal as the major products.[26] However, there has been no study focused on assessment of the branching ratio between the outer and the inner hydroxy alkyl radicals. Since the two radicals have very different chemistry and lead to different final products, the initial branching is an important factor in controlling the end product distribution, and hence ozone production and the formaldehyde yield. We report the first OH cycling experiments performed on 1,3-butadiene and the analysis of the data, given the insight from previous isomeric selective studies, allows an estimation of the initial branching. Based on the reported branching, we predict end product yields and provide a condensed chemical mechanism for the OH-1,3-butadiene oxidation under high NOx conditions.

B. Results and Discussion

In the first section, we describe the results obtained from the study of the initial reaction of OH radical with 1,3-butadiene and the determination of the rate constant. In the next section, we discuss the results of OH cycling experiments on 1,3-butadiene, and address the relative branching in between the minor and the major addition channels (Figure 1).

I. OH+1,3-butadiene reaction. The rate constant for the OH addition reaction to 1,3-butadiene was measured using LP-LIF technique. Laser photolysis of H_2O_2 at 248 nm results in the formation of OH and the decay of OH in the presence of 1,3-butadiene was monitored by monitoring the decay in the integrated OH fluorescence intensity using LIF technique. The concentration of H_2O_2 was typically maintained around 4×10^{13} cm^{-3} and

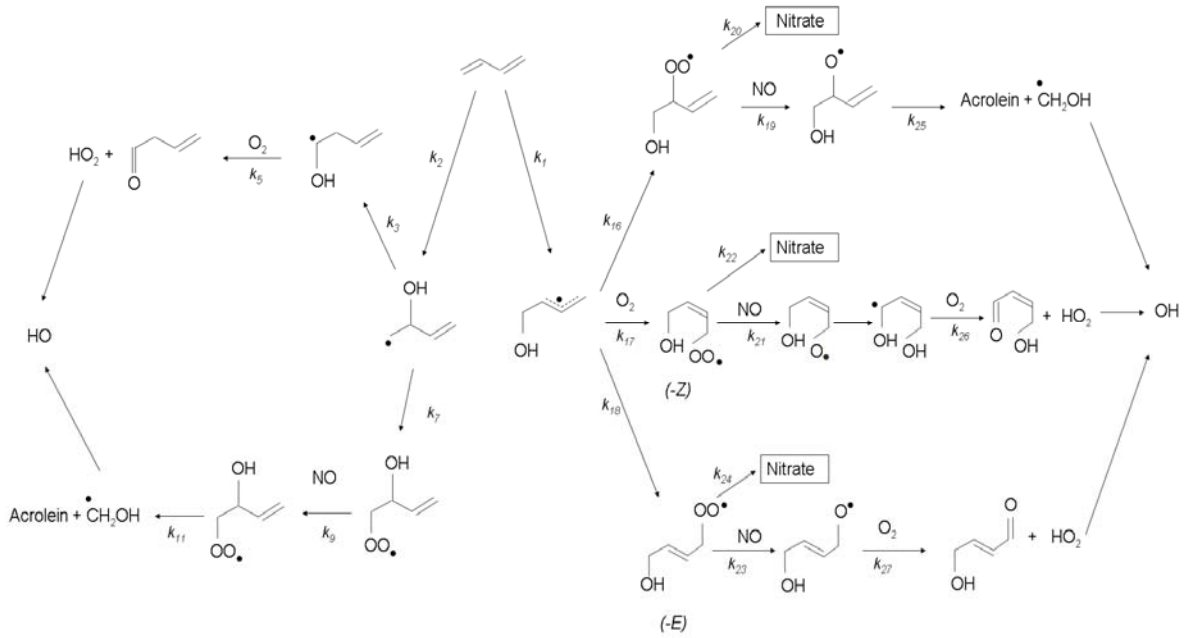

Figure V-II. Schematic diagram of OH cycling in 1,3-butadiene oxidation, for both hydroxyalkyl isomers.

the estimated OH concentration was typically 9×10^{10} cm^{-3} based on reported H_2O_2 absorption cross section[68] and photolysis laser power at 248 nm. Table V-I summarizes the experimental conditions employed in this study. Figure V-III shows OH decay curves for different concentrations of 1,3-butadiene. Pseudo first order rate constants (k^I) were obtained from the slope of the logarithmic plots. A linear least square fit of the pseudo first order rate constants versus 1,3-butadiene concentrations yields a value of $(7.0 \pm 0.3) \times 10^{-11}$ $molecule^{-1}$ cm^3 s^{-1} for the bimolecular rate constant k^{II} (Figure V-IV). The error bars correspond to 1 standard deviation from the least square regression.

Table V-I. Summary of the experimental conditions applied in this study.

[1,3-butadiene] 10^{14} molecules/cm^3	[NO] 10^{14} molecules/ cm^3	[O_2] 10^{16} molecules/ cm^3
OH + 1,3-butadiene		
1.2	0	0
2.4	0	0
3.6	0	0
4.9	0	0
7.3	0	0
OH + 1,3-butadiene + NO + O_2		
2.1	3.1	3.3
2.1	6.2	3.3
2.1	9.3	3.3
2.1	13	3.3

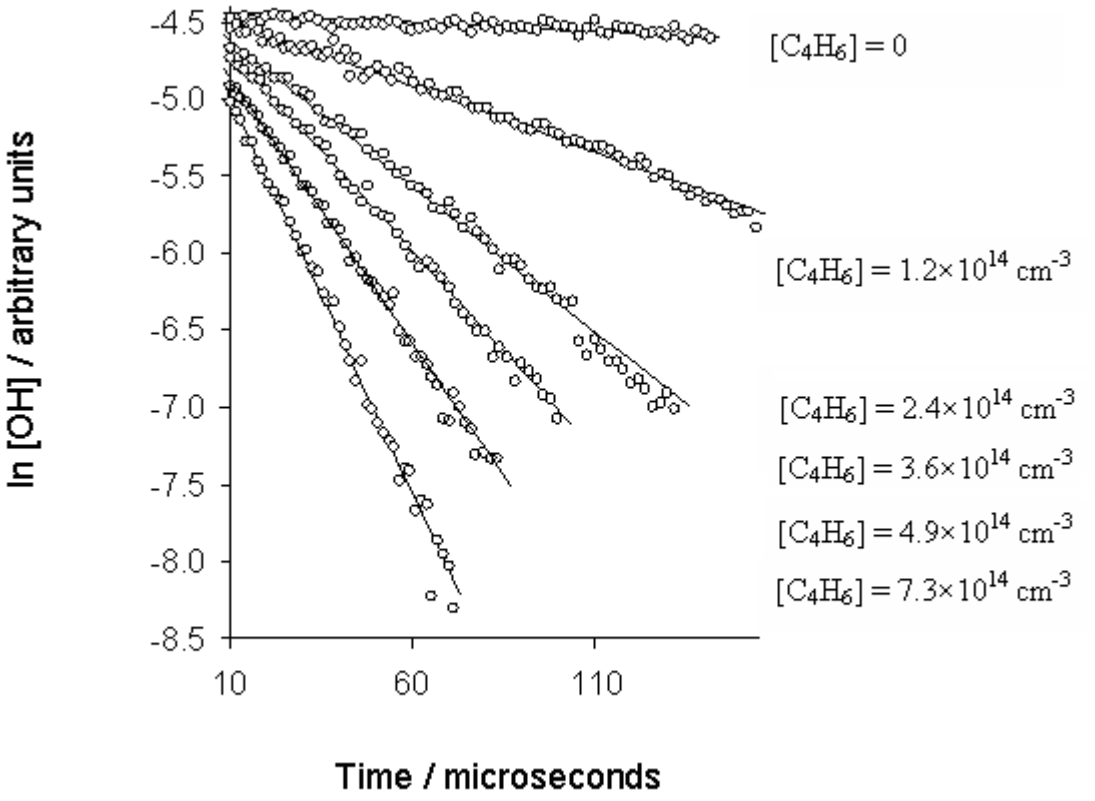

Figure V-III. Pseudo first order decays of measured OH signal for several 1,3-butadiene concentrations.

This value for the rate constant is in excellent agreement with previous studies in the high pressure limit and matches a previous report of Vimal et. al [25] who used discharge flow system coupled with resonance fluorescence/laser-induced fluorescence detection of OH to obtain a value of (6.98±0.28) × 10^{-11} molecule^{-1} cm^3 s^{-1} at 300 K and 5 torr pressure. Our value is also in good agreement with values of (6.83±0.24) × 10^{-11} molecule^{-1} cm^3 s^{-1} reported at 298 K and 1 torr pressure using a relative rate discharge flow technique[30] and (6.85±0.69) × 10^{-11} molecule^{-1} cm^3 s^{-1}measured by Atkinson et al. in 50 Torr of argon using the flash photolysis-resonance fluorescence technique.[93]

II. OH cycling from 1,3-butadiene in the presence of NO and O_2. The hydroxy alkyl radical produced by OH addition to 1,3-butadiene reacts with O_2 either by hydrogen abstraction to form a C4 carbonyl compound and HO_2 (isomer II) or by addition reaction to form a peroxy radical (isomer I). In the polluted atmosphere with high NO concentration, the peroxy radical reacts with NO to form alkoxy radical, which then either dissociate or reacts with oxygen to form different end products and HO_2. The reaction of HO_2 with NO regenerates OH radical (Figure V-II). Figure V-V shows a representative data set obtained from OH cycling experiments at a 1,3-butadiene concentration of 2.11×10^{14} molecules cm^{-3}, [O_2] = 3.3 × 10^{16} molecules cm^{-3}, and [NO] varied from 3.1 × 10^{14} molecules cm^{-3} to 1.3 × 10^{15} molecules cm^{-3}. The circles represent the data points and the solid lines represent the best fit simulation to the data. In the absence of NO, the OH signal exhibits a pseudo first order decay with a bimolecular rate constant of (7.0±0.3) × 10^{-11} molecule^{-1} cm^3 s^{-1} due to the reaction with1,3-butadiene. In the presence of NO, the early time OH signal exhibits an exponential decay until the onset of cycling (~ 100 μs). At this time, the decay rate decreases due to the regeneration

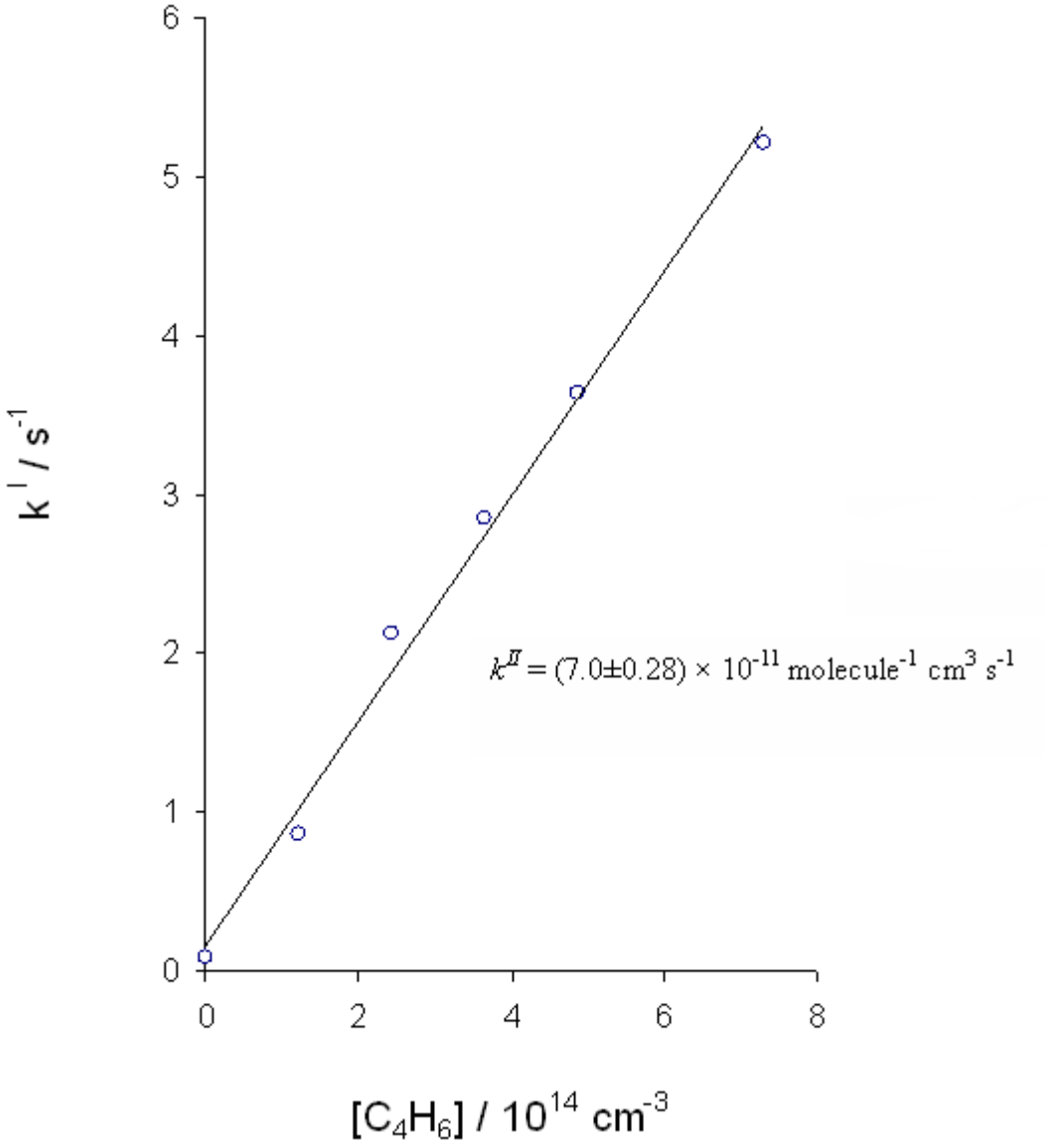

Figure V-IV. Bimolecular rate constant for OH+1,3-butadiene reaction at 50 torr, and 298 K.

TABLE V-II. Reaction mechanism and corresponding rate constants (298 K) employed in simulation of the experimental data.

Reaction				Rate Constant	Ref	Comment
k_1	C_4H_6+HO	→	1-HOC_4H_6	6.1×10^{-11}	a	Radical I and II branching(Fig. 1)
k_2	C_4H_6+HO	→	2-HOC_4H_6	0.9×10^{-11}	a	
k_3	2-HOC_4H_6	→	alpha-HOC_4H_6	7×10^{-11}	9	Oxidation chemistry of hydroxy alkyl radical II (Fig. 1)
k_4	2-HOC_4H_6	→	beta-HOC_4H_6	3×10^{-11}	9	
k_5	alpha-HOC_4H_6 + O_2	→	alpha-OC_4H_6+HO_2	3.3×10^{-11}	9	
k_6	alpha-HOC_4H_6 + NO	→	alpha-HOC_4H_6NO	2.2×10^{-11}	9	
k_7	beta-HOC_4H_6 + O_2	→	beta-$OHC_4H_6O_2$	2.3×10^{-12}	9	
k_8	beta-HOC_4H_6 + NO	→	beta-HOC_4H_6NO	2.2×10^{-11}	9	
k_9	beta-$OHC_4H_6O_2$+ NO	→	beta-OHC_4H_6O+NO_2	1.4×10^{-11}	9	
k_{10}	beta-$OHC_4H_6O_2$+ NO	→	beta-$OHC_4H_6ONO_2$	8.4×10^{-13}	9	
k_{11}	beta-OHC_4H_6O	→	HCHO+OHC_3H_4	Prompt	9	
k_{12}	beta-OHC_4H_6O+NO	→	beta-OHC_4H_6ONO	3×10^{-11}	9	
k_{13}	OHC_3H_4+ O_2	→	OC_3H_4+HO_2	3×10^{-11}	9	
k_{14}	OHC_3H_4+ NO	→	OHC_3H_4NO	3×10^{-11}	9	
k_{15}	1-HOC_4H_6+NO	→	1-HOC_4H_6NO	2.0×10^{-11}	92	Oxidation chemistry of hydroxy alkyl radical I (Fig. 1)
k_{16}	1-HOC_4H_6 + O_2	→	*β*-$HOC_4H_6O_2$	5.25×10^{-13}	92	
k_{17}	HOC_4H_6 + O_2	→	*Z*-$HOC_4H_6O_2$	8.75×10^{-14}	92	
k_{18}	HOC_4H_6 + O_2	→	*E*-$HOC_4H_6O_2$	8.75×10^{-14}	92	
k_{19}	*β*-$HOC_4H_6O_2$ + NO	→	*β*-HOC_4H_6O + NO_2	1.4×10^{-11}	92	
k_{20}	*β*-$HOC_4H_6O_2$ + NO	→	*β*-$HOC_4H_6ONO_2$	8.4×10^{-13}	92	
k_{21}	*Z*-$HOC_4H_6O_2$ + NO	→	*Z*-OHC_4H_5OH + NO_2	1.4×10^{-11}	92	
k_{22}	*Z*-$HOC_4H_6O_2$ + NO	→	*Z*-$HOC_4H_6ONO_2$	8.4×10^{-13}	92	
k_{23}	*E*-$HOC_4H_6O_2$ + NO	→	*E*-OHC_4H_6O + NO_2	1.4×10^{-11}	92	
k_{24}	*E*-$HOC_4H_6O_2$ + NO	→	*E*-$HOC_4H_6ONO_2$	8.4×10^{-13}	92	
k_{25}	*β*-HOC_4H_6O	→	CH_2OH+OC_3H_4	Prompt	92	
k_{26}	Z-OHC_4H_5OH+O_2	→	HO_2+OC_4H_5OH	1.0×10^{-11}	92	
k_{27}	Z-OHC_4H_5OH+NO	→	Z-OHC_4H_5OHNO	3.0×10^{-11}	92	
k_{28}	E-HOC_4H_6O+O_2	→	E-OHC_4H_5O+HO_2	1.0×10^{-11}	92	
k_{29}	E-HOC_4H_6O+NO	→	E-HOC_4H_6ONO	3.0×10^{-11}	92	
k_{30}	CH_2OH + O_2	→	CH_2O + HO_2	9.8×10^{-12}	92	
k_{31}	CH_2OH + NO	→	CH_2OHNO	1.2×10^{-11}	92	
k_{32}	HO_2+NO	→	OH+NO_2	1.2×10^{-11}	88	
k_{33}	OH + NO	→	HONO	9.4×10^{-13}	68	

of OH, finally reaching steady state at long times. At higher NO concentration, OH cycling is established at earlier times and there is a long time decay due to NO termination reactions.

A numerical program KINTECUS[60] was used to simulate the data using the model comprised of 33 reactions, as described in Table V-II, as well as to perform sensitivity analysis. The model describes the detailed oxidative chemistry of the two hydroxy alkyl radical isomers (I and II in Figure V-I) under high NOx conditions. The distinct chemistry of these isomers has been studied previously by Greenwald et al[9] and Ghosh et al.[92] using photolytic precursors that afford isolation of individual isomeric pathways. Both the hydroxyalkyl isomers I and II undergo a series of reactions to regenerate OH radicals, however the rate of OH cycling from isomer II is considerably faster than from isomer I. This is a result of the experimental conditions employed which ensures that the rate determining step for OH regeneration from isomer II (k_5 [O_2]) is faster than that from isomer I (k_{19} [NO]). A higher branching ratio for isomer II will thus result in greater OH cycling, affecting the shape of the OH concentration time profile. The main focus of current study was to determine the relative contribution of these two isomeric pathways, i.e. the relative branching ratios of the rate constants k_1 and k_2. We find that small changes in the branching ratio between these two rate constants have a profound effect on the simulations. The other rate constants have been fixed to values reported previously by Ghosh *et al.*[92] and Greenwald *et al.*[9] Thus we employed only a single parameter in the simulation, the relative branching between $k_1$and k_2. The most satisfactory fit to the experimental data was obtained for a branching ratio of 0.87 for k_1. An error analysis of this simulation to data provides an estimated error range of ± 0.08

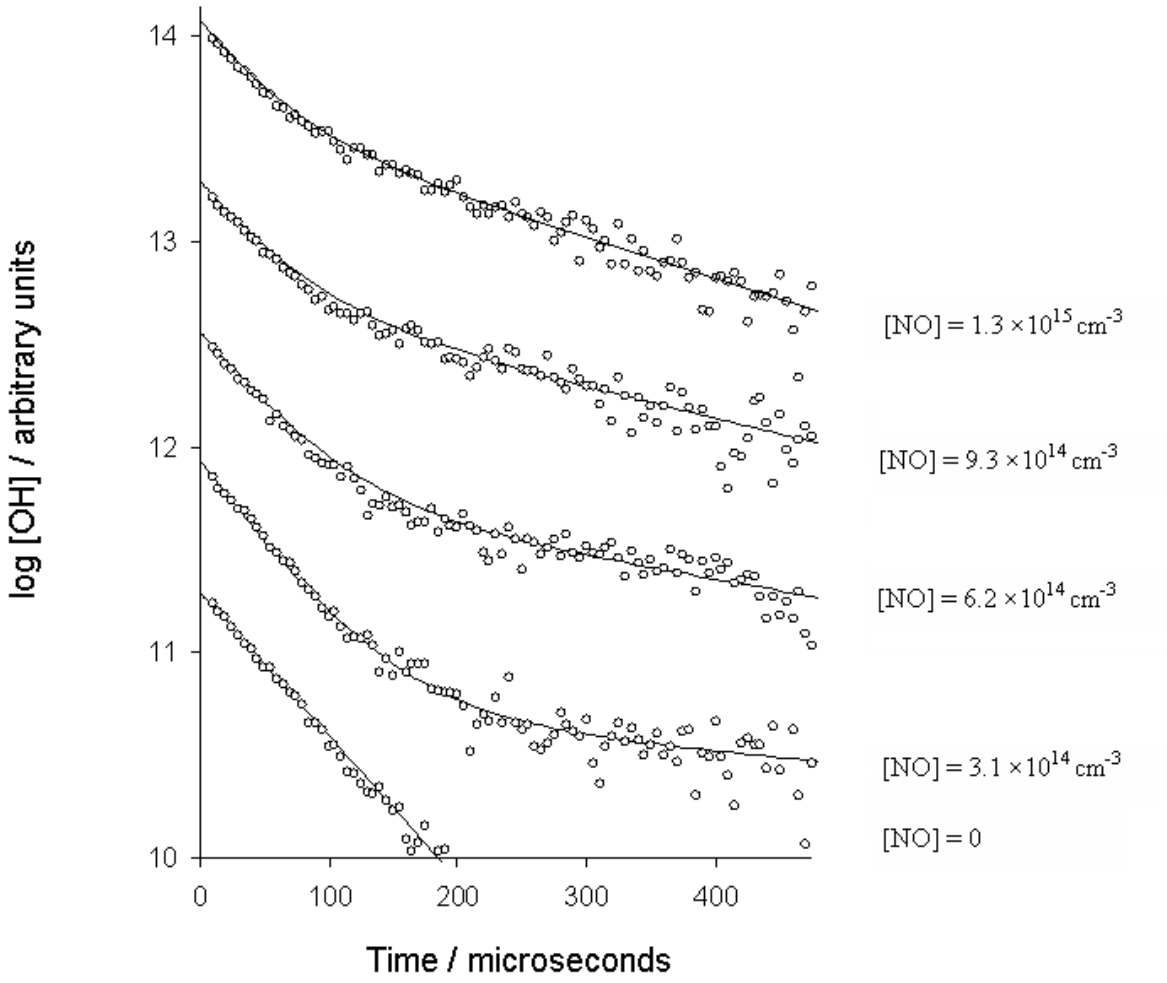

Figure V-V. OH decays at different NO concentrations. Circles represent experimental data, and lines represent the fits using the reaction mechanism and rate constants in Table V-II with $[C_4H_6]$ = 2.11×10^{14} cm^{-3} and $[O_2]$ =3.27×10^{16} cm^{-3}.

for the branching of the outer channel which represents two standard deviations. Figure V-VI shows the best fit obtained for the OH cycling data with a yield of 87% for isomer I and the corresponding error limit of ±8%. There has been only one other estimation of this branching, reported by Jenkin et. al.[84] Based on their study of peroxy radical kinetics using laser flash photolysis/UV absorption spectrometry, they estimated a branching of 0.87 for the radical I channel, in excellent agreement with our value.

C. Predicted First Generation End Product Distribution

Based on the branching of 0.87:0.13 for isomers I and II, we can predict end product yields given the chemistry of the individual radical pathways.[9,92] The results are tabulated in Table V-III.

TABLE V-III. Summary of end product distributions (in percentage yield) predicted by using the branching ratio of 0.87±0.08:0.13±0.08 for outer: inner addition channel (Figure V-I), as determined in current study. Included for comparison are the end product distributions reported in other studies.

End Product	Current study	Tuazon[33]	Sprengnether[86]		Berndt [26]	Baker[91]
			445 torr	750 torr		
Organic Nitrate	6	7±3	11±6	11	6±2	
Acrolein	64±12	58±4	69±7	54	59±6	58±10
4-hydroxy-2-butenal	21±11				23±10	25^{+15}_{-10}
3-butenal (C_4 carbonyl)	8±6					
HCHO	64±12	62±5	69±10	58	64±8	

The estimated product yields for acrolein, 4-hydroxy-2-butenal, 3-butenal (C_4 carbonyl) and HCHO are (64±12) %, (21±11) % and (8±6) %, and (64±12) %. These product yields are well within the range of the values reported in previous product studies.[26,33,86,91] Our acrolein yield is within the range of (54-69)% as reported in the literature.[26,33,86] Our reported acrolein yield is slightly higher than the yields of (59±6)% and (58±4)%, as reported by Berndt et al.[26] and Tuazon et al.[33] respectively, is similar to their reported HCHO yields of (62±5) % and (64±8) %. Since HCHO and acrolein are co-product of the same reaction, they should be formed in equal yields. From their "wall less" experiments, Sprengnether and co-workers reported equal yield for acrolein and HCHO at lower pressure (445 torr), and slightly higher HCHO yields at higher pressure (750 torr).[86] Our reported yield of (21±11)% for 4-hydroxy-2-butenal matches very well with the only two others reported yields of 23.0±10 and 25^{+15}_{-10} as determined by Berndt et. al[26] and Baker et. al[91] respectively. The C_4 carbonyl 3-butenal, to our knowledge, has never been reported; however its C5 analogue has been reported in case of isoprene oxidation.[8] End product analysis studies account for about 80-90% of carbon balance in the OH initiated oxidation of 1,3-butadiene[26] and we believe that the C4 carbonyl compound may account for some of the missing carbon balance. Based on our current understanding, we can build a condensed chemical mechanism for OH radical initiated oxidation of 1,3-butadiene under high NOx condition.

1,3-butadiene + OH = 0.06 $RONO_2$ + 0.64 Acrolein + 0.3 BUPD + 0.64 HCHO

+ 0.94 HO_2 + 0.86 NO2

where,

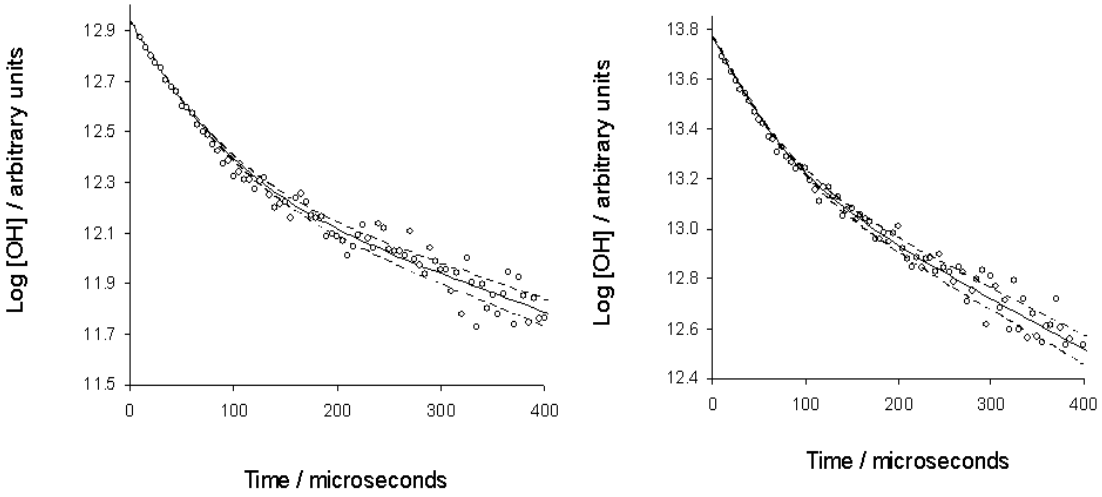

Figure V-VI. OH decays at different NO concentrations. Circles represent experimental data, solid lines represent the best fits using a branching of 0.87 for the radical I. Dashed lines indicate the estimated error range for the initial branching in between the outer and inner isomers (k_1 and k_2). The outer branching is founded to be 0.87±0.08

A: $[C_4H_6] = 2.11\times10^{14}$ cm^{-3}, $[O_2] = 3.27\times10^{16}$ cm^{-3}, $[NO] = 3.1\times10^{14}$ cm^{-3}

B: $[C_4H_6] = 2.11\times10^{14}$ cm^{-3}, $[O_2] = 3.27\times10^{16}$ cm^{-3}, $[NO] = 1.3\times10^{15}$ cm^{-3}.

$RONO_2$ = Organic nitrate (assuming 6% nitrate yield)

BUPD = First generation products other than Acrolein= C4 carbonyl (8%)

4-hydroxy-2-butenal (22%)

NO_2 = Total NO_2 formed from NO

D. Conclusions

The OH radical initiated oxidation of 1,3-butadiene was studied in high NOx condition by using LP-LIF technique. The rate constant for the reaction of OH radical with 1,3-butadiene was measured to be $(7.0\pm0.3)\times10^{-11}$ s^{-1} $molecule^{-1}$ cm^3. Analysis of OH cycling experiments permits the determination of the branching in between the outer and inner OH-1,3-butadiene adduct isomers. The branching of the outer isomeric channel was found to be 0.87±0.08. The current study provides a comprehensive model for oxidation of 1,3-butadiene under high NOx condition, and the model was used to predict the distribution of the first generation end products.

CHAPTER VI

CONCLUSIONS

A. Concluding Remarks

This dissertation has described *Isomeric Selective* experiments to develop and refine the tropospheric oxidation mechanisms of unsaturated hydrocarbons. Isolating individual isomeric pathways in the oxidation chemistry provides detailed insight into the oxidation processes, which was ultimately used to express hydrocarbon oxidation using condensed mechanism, suitable for use in atmospheric models.

We have extended a novel synthetic approach to synthesize photolytic precursors by adding an iodine atom and an OH group across one of the double bonds of isoprene. Laser photolysis exclusively resulted in the formation of the dominant OH-isoprene adduct isomer. The further oxidation of this isomer under high NOx conditions lead to OH generation and the OH radical concentrations were monitored over the reaction time scale using Laser Induced Fluorescence (LIF) technique. The simulation of time dependent OH signal led to the development of a detailed chemical model for the oxidation of the dominant channel for OH addition to isoprene. Furthermore, the use of isotopically labeled precursor afforded the first clear experimental evidence of the *E*-*δ*-peroxy radical pathway and its formation yield was measured to be (10±3) %. Since the values of the intermediate rate constants for this major channel are similar to the values obtained in non isomeric studies of isoprene oxidation, we predict that the other outer addition channel would have similar kinetic parameters associated with the OH-initiated oxidation. Hence, this study would account for approximately 20% of missing carbon

balance in isoprene-OH oxidation and a condensed model including the chemistry of the *δ*-peroxy channel should provide a comprehensive description of isoprene-OH chemistry at high NO*x* conditions.

The OH radical initiated oxidation of 1,3-butadiene has not been as extensively studied as that of isoprene. We have employed a similar isomeric selective approach to examine the oxidation mechanism for 1,3-butadiene. The use of photolytic precursor resulted in isolation of the dominant addition channel of 1,3-butadiene oxidation and afforded the measurement of isomeric selective rate constants. Isotopically labeled studies lead to the measurement of the *E*-*δ*-hydroxyperoxy isomeric pathway and its formation yield was measured to be (13±5) %. This provides a mechanistic pathway for the formation of 4-hydroxy-2-butenal as a first generation end product with a reported formation yield of about 25%.

Finally, we have determined the branching ratio of the initial OH-1,3-butadiene adducts. By modeling the OH cycling data using previously obtained kinetic information on the individual isomeric pathways, we calculated the branching ratios of the individual OH addition channels. We find that the outer OH-1,3-butadiene adduct has a formation yield of (89±9) %. Using this branching ratio with the reported oxidation chemistry of the individual pathways, we can express the 1,3-butadiene oxidation under high NOx conditions using a condensed chemical mechanism.

We have used isomeric selective approach to examine OH initiated oxidation of unsaturated hydrocarbons. Our measured branching ratios of different pathways within the oxidation mechanism provide great insight into the tropospheric chemistry of volatile organic compounds and would help in improving the atmospheric models.

B. Future Directions

The studies described in this thesis have greatly enhanced our knowledge of alkene oxidation under high NOx conditions, however their oxidation in low NOx environments remain poorly understood. Under such conditions, many competing reactions take place involving the peroxy radical intermediates, and the chemistry is significantly more complicated. Peroxy radicals can react with HO_2 or undergo self/cross reactions with itself or other peroxy radicals leading to a variety of hydroperoxides, alcohols, and carbonyl compounds (Figure I-II). The relative branching between these different competitive reactions can vary for different isomers and isomeric selective strategy can be extended to unsaturated hydrocarbon oxidation under low NOx conditions to isolate individual isomeric pathways, making the oxidation mechanism simpler and providing important insight into the oxidation mechanism. Since OH cycling would be minimum under low NOx conditions, monitoring the peroxy radical concentrations using their global absorbance (at 270 nm or 280 nm)[43,94] via UV absorption spectroscopy or Cavity Ringdown Spectroscopy (CRDS) can be useful in understanding peroxy radical chemistry. Isoprene oxidation products, under low NOx conditions, are expected to account for about 58% of SOA formation globally through the formation of diol and tetrol compounds.[20-22] Accurate formation yields of diols and tetrols are yet to be reported, and they can be measured using mass spectrometric studies. Recent field campaign studies in pristine environment of Amazonian rain forest, with chemistry largely dominated by isoprene oxidation, have revealed large OH concentrations, which remains unexplained by our current understanding of isoprene oxidation under such conditions.[95] Alternate isoprene oxidation mechanisms have been proposed based on

computational studies,[96] however experimental verifications of such models are yet to obtain. Time dependent mass spectrometric techniques like Chemical Ionization Mass Spectrometry (CIMS) or the time resolved mass spectrometry apparatus at the Advanced Light Source can be used in monitoring and quantification of species of interest, for example OH, HO_2, and ROOH that can greatly enhance our understanding of oxidation processes under low NOx conditions.

The tropospheric oxidation chemistry of aromatic compounds is poorly understood. These hydrocarbons are emitted into the atmosphere primarily from anthropogenic sources and can account for up to 44% of urban VOC mixture in various parts of the world.[97] Toluene, which is a major component of gasoline (up to 35% by volume) reacts with OH radical upon release into the atmosphere. Although the initial reaction of toluene with OH radical has been well studied, much of the remaining oxidation mechanism has not been clearly understood and over 40% of carbon balance is yet to be determined.[98] The proposed oxidation mechanisms involve multiple intermediates, however the branching ratios, and even existence of different intermediates are yet to be confirmed. Isomeric selective approach can be used to isolate individual isomeric pathways and studies using the principle of OH cycling can be employed to understand the oxidation mechanism. Any such experiments must be performed under high O_2 conditions in the laboratory due to the slow rate of reactions of the aromatic-OH adduct, which provides an experimental challenge for using LIF technique as the fluorescence is effectively quenched by O_2. Detection of OH using absorption techniques like Cavity Ringdown Spectroscopy can be useful in studying such chemical processes.

REFERENCES

(1) Wang, Y. H.; Jacob, D. J.; Logan, J. A. *J. Geophys. Res. [Atmos.]* **1998**, *103*, 10757.

(2) Gery, M. W.; Whitten, G. Z.; Killus, J. P.; Dodge, M. C. *J. Geophys. Res. [Atmos.]* **1989**, *94*, 12925.

(3) Carter, W. P. L. *Atmospheric Environment Part A-General Topics* **1990**, *24*, 481.

(4) Yarwood, G.; Rao, S.; Yocke, M.; Whitten, G. Z. *Updates to the Carbon Bond Chemical Mechanism: CB05. Final Report to the US EPA, RT-0400675* **2005**.

(5) Carter, W. P. L. *Implementation of the SAPRC-99 Chemical Mechanism into the Models-3 Framework. Report to the United States Environmental Protection Agency* **2000**.

(6) Luecken, D. J.; Phillips, S.; Sarwar, G.; Jang, C. *Atmos. Environ.* **2008**, *42*, 5805.

(7) Faraji, M.; Kimura, Y.; McDonald-Buller, E.; Allen, D. *Atmos. Environ.* **2008**, *42*, 5821.

(8) Greenwald, E. E.; Ghosh, B.; Anderson, K. C.; Dooley, K. S.; Zou, P.; Selby, T.; Osborn, D. L.; Meloni, G.; Taatjes, C. A.; Goulay, F.; North, S. W. *J. Phys. Chem. A* **2010**, *114*, 904.

(9) Greenwald, E. E.; Park, J.; Anderson, K. C.; Kim, H.; Reich, B. J. E.; Miller, S. A.; Zhang, R. Y.; North, S. W. *J. Phys. Chem. A* **2005**, *109*, 7915.

(10) Chameides, W. L.; Fehsenfeld, F.; Rodgers, M. O.; Cardelino, C.; Martinez, J.; Parrish, D.; Lonneman, W.; Lawson, D. R.; Rasmussen, R. A.; Zimmerman, P.; Greenberg, J.; Middleton, P.; Wang, T. *J. Geophys. Res. [Atmos.]* **1992**, *97*, 6037.

(11) Guenther, A.; Hewitt, C. N.; Erickson, D.; Fall, R.; Geron, C.; Graedel, T.; Harley, P.; Klinger, L.; Lerdau, M.; McKay, W. A.; Pierce, T.; Scholes, B.; Steinbrecher, R.; Tallamraju, R.; Taylor, J.; Zimmerman, P. *J. Geophys. Res. [Atmos.]* **1995**, *100*, 8873.

(12) Martin, R. S.; Westberg, H.; Allwine, E.; Ashman, L.; Farmer, J. C.; Lamb, B. *J. Atmos. Chem.* **1991**, *13*, 1.

(13) Wiedinmyer, C.; Friedfeld, S.; Baugh, W.; Greenberg, J.; Guenther, A.; Fraser, M.; Allen, D. *Atmos. Environ.* **2001**, *35*, 1001.

(14) Poschl, U.; von Kuhlmann, R.; Poisson, N.; Crutzen, P. J. *J. Atmos. Chem.* **2000**, *37*, 29.

(15) Chen, X. H.; Hulbert, D.; Shepson, P. B. *J. Geophys. Res. [Atmos.]* **1998**, *103*, 25563.

(16) Engardt, M. *J. Atmos. Chem.* **2008**, *59*, 61.

(17) Wang, D.; Bormann, F. H.; Karnosky, D. F. *Environ. Sci. Technol.* **1986**, *20*, 1122.

(18) Horowitz, L. W.; Liang, J. Y.; Gardner, G. M.; Jacob, D. J. *J. Geophys. Res. [Atmos.]* **1998**, *103*, 13451.

(19) Sasaki, K.; Saito, T.; Lämsä, M.; Oksman-Caldentey, K. M.; Suzuki, M.; Ohyama, K.; Muranaka, T.; Ohara, K.; Yazaki, K. *Plant Cell Physiol.* **2007** *48*.

(20) Claeys, M.; Graham, B.; Vas, G.; Wang, W.; Vermeylen, R.; Pashynska, V.; Cafmeyer, J.; Guyon, P.; Andreae, M. O.; Artaxo, P.; Maenhaut, W. *Science* **2004**, *303*, 1173.

(21) Kroll, J. H.; Ng, N. L.; Murphy, S. M.; Flagan, R. C.; Seinfeld, J. H. *Geophys. Res. Lett.* **2005**, *32*.

(22) Liao, H.; Henze, D. K.; Seinfeld, J. H.; Wu, S. L.; Mickley, L. J. *J. Geophys. Res. [Atmos.]* **2007**, *112*.

(23) United States Environmental Protection Agency. Locating and Estimating Air Emissions from Sources of 1, -. B. *EPA-454/R-96-008; Office of Air Quality Planning and Standards:Research Triangle Park,NC,* **1996**.

(24) Duffy, B. L.; Nelson, P. F. *Atmos. Environ.* **1997**, *31*, 3877.

(25) Vimal, D.; Pacheco, A. B.; Iyengar, S. S.; Stevens, P. S. *J. Phys. Chem. A* **2008**, *112*, 7227.

(26) Berndt, T.; Boge, O. *J. Phys. Chem. A* **2007**, *111*, 12099.

(27) Cote, I. L.; Bayard, S. P. *Environ. Health Perspect.* **1990**, *86*, 149.

(28) United States Environmental Protection Agency. Health Assessment of 1, -. B. *EPA/600/P-98/001F; Office of Research and Development: Washington, DC,* **2002.**

(29) Kligerman, A. D.; Doerr, C. L.; Milholland, V. S.; Tennant, A. H. *Toxicology* **1996**, *113*, 336.

(30) Li, Z. J.; Nguyen, P.; de Leon, M. F.; Wang, J. H.; Han, K. L.; He, G. Z. *J. Phys. Chem. A* **2006**, *110*, 2698.

(31) Liu, X. Y.; Jeffries, H. E.; Sexton, K. G. *Atmos. Environ.* **1999**, *33*, 3005.

(32) Notario, A.; Le Bras, G.; Mellouki, A. *Chem. Phys. Lett.* **1997**, *281*, 421.

(33) Tuazon, E. C.; Alvarado, A.; Aschmann, S. M.; Atkinson, R.; Arey, J. *Environ. Sci. Technol.* **1999**, *33*, 3586.

(34) Fehsenfe.Fc; Evenson, K. M.; Broida, H. P. *Rev. Sci. Instrum.* **1965**, *36*, 294.

(35) Monson, R. K.; Fall, R. *Plant Physiol.* **1989**, *90*, 267.

(36) Sharkey, T. D.; Singsaas, E. L. *Nature* **1995**, *374*, 769.

(37) Sharkey, T. D.; Wiberley, A. E.; Donohue, A. R. *Annals of Botany* **2008**, *101*, 5.

(38) Greenwald, E. E.; North, S. W.; Georgievskii, Y.; Klippenstein, S. J. *J. Phys. Chem. A* **2007**, *111*, 5582.

(39) Atkinson, R.; Baulch, D. L.; Cox, R. A.; Crowley, J. N.; Hampson, R. F., Jr.; Kerr, J. A.; Rossi, M. J.; Troe, J. *Summary of Evaluated Kinetic and Photochemical Data for Atmospheric Chemistry. IUPAC Subcommittee on Gas Kinetic Data Evaluation for Atmospheric Chemistry; Blackwell: London* **2002**.

(40) Chuong, B.; Stevens, P. S. *J. Phys. Chem. A* **2000**, *104*, 5230.

(41) Kleindienst, T. E.; Harris, G. W.; Pitts, J. N. *Environ. Sci. Technol.* **1982**, *16*, 844.

(42) Lei, W. F.; Zhang, R. Y.; McGivern, W. S.; Derecskei-Kovacs, A.; North, S. W. *Chem. Phys. Lett.* **2000**, *326*, 109.

(43) Jenkin, M. E.; Hayman, G. D. *Journal of the Chemical Society-Faraday Transactions* **1995**, *91*, 1911.

(44) Tuazon, E. C.; Atkinson, R. *Int. J. Chem. Kinet.* **1989**, *21*, 1141.

(45) Park, J.; Jongsma, C. G.; Zhang, R. Y.; North, S. W. *Phys. Chem. Chem. Phys.* **2003**, *5*, 3638.

(46) Dibble, T. S. *J. Phys. Chem. A* **1999**, *103*, 8559.

(47) Lei, W. F.; Zhang, R. Y. *J. Phys. Chem. A* **2001**, *105*, 3808.

(48) Park, J.; Stephens, J. C.; Zhang, R. Y.; North, S. W. *J. Phys. Chem. A* **2003**, *107*, 6408.

(49) Atkinson, R.; Aschmann, S. M.; Tuazon, E. C.; Arey, J.; Zielinska, B. *Int. J. Chem. Kinet.* **1989**, *21*, 593.

(50) Kwok, E. S. C.; Atkinson, R.; Arey, J. *Environ. Sci. Technol.* **1995**, *29*, 2467.

(51) Lloyd, A. C.; Atkinson, R.; Lurmann, F. W.; Nitta, B. *Atmos. Environ.* **1983**, *17*, 1931.

(52) Paulson, S. E.; Flagan, R. C.; Seinfeld, J. H. *Int. J. Chem. Kinet.* **1992**, *24*, 79.

(53) Paulson, S. E.; Seinfeld, J. H. *J. Geophys. Res. [Atmos.]* **1992**, *97*, 20703.

(54) Tuazon, E. C.; Atkinson, R. *Int. J. Chem. Kinet.* **1990**, *22*, 1221.

(55) Zhao, J.; Zhang, R. Y.; Fortner, E. C.; North, S. W. *J. Am. Chem. Soc.* **2004**, *126*, 2686.

(56) Dibble, T. S. *J. Phys. Chem. A* **2002**, *106*, 6643.

(57) Zhao, J.; Zhang, R. Y.; North, S. W. *Chem. Phys. Lett.* **2003**, *369*, 204.

(58) Fan, J. W.; Zhang, R. Y. *Environ. Chem.* **2004**, *1*, 140.

(59) Snider, B. B.; Duvall, J. R. *Tetrahedron Lett.* **2003**, *44*, 3067.

(60) Ianni, J. C. *Kintecus Windows* **2002**, *Version 2.80*.

(61) Miller, A. M.; Yeung, L. Y.; Kiep, A. C.; Elrod, M. J. *Phys. Chem. Chem. Phys.* **2004**, *6*, 3402.

(62) Zhang, D.; Zhang, R.; North, S. W. *J. Phys. Chem. A* **2003**, *107*, 11013.

(63) Atkinson, R. *J. Phys. Chem. Ref. Data* **1997**, *26*, 215.

(64) Blitz, M.; Pilling, M. J.; Robertson, S. H.; Seakins, P. W. *Phys. Chem. Chem. Phys.* **1999**, *1*, 73.

(65) Deng, W.; Wang, C. J.; Katz, D. R.; Gawinski, G. R.; Davis, A. J.; Dibble, T. S. *Chem. Phys. Lett.* **2000**, *330*, 541.

(66) Park, J.; Jongsma, C. G.; Zhang, R. Y.; North, S. W. *J. Phys. Chem. A* **2004**, *108*, 10688.

(67) Pagsberg, P.; Munk, J.; Anastasi, C.; Simpson, V. J. *J. Phys. Chem.* **1989**, *93*, 5162.

(68) DeMore, W. B.; Sander, S. P.; Golden, D. M.; Hampson, R. F.; Kurylo, M. J.; Howard, C. J.; Ravishankara, A. R.; Kolb, C. E.; Molina, M. J. *Chemical Kinetics and Photochemical Data for Use in Stratospheric Modeling. JPL Publ. 02-25; Jet Propulsion Lab: Pasadena, CA* **2003**.

(69) Forster, R.; Frost, M.; Fulle, D.; Hamann, H. F.; Hippler, H.; Schlepegrell, A.; Troe, J. *J. Chem. Phys.* **1995**, *103*, 2949.

(70) Sander, S. P.; Friedl, R. R.; Golden, D. M.; Kurylo, M. J.; Moortgat, G. K.; Wine, P. H.; Ravishankara, A. R.; Kolb, C. E.; Molina, M. J.; Finlayson-Pitts, B. J.; Huie, R. E.; Orkin, V. L. *Chemical Kinetics and Photochemical Data for Use in Stratospheric Modeling. JPL Publ. 06-2; Jet Propulsion Lab: Pasadena, CA* **2006**.

(71) Steinfeld, J. I.; Francisco, J. S.; Hase, W. L. *Chemical Kinetics and Dynamics*, Prentice Hall International.

(72) Lotz, C.; Zellner, R. *Phys. Chem. Chem. Phys.* **2001**, *3*, 2607.

(73) Lei, W. F.; Zhang, R. Y.; McGivern, W. S.; Derecskei-Kovacs, A.; North, S. W. *J. Phys. Chem. A* **2001**, *105*, 471.

(74) Zhang, D.; Zhang, R. Y.; Church, C.; North, S. W. *Chem. Phys. Lett.* **2001**, *343*, 49.

(75) Koch, R.; Siese, M.; Fittschen, C.; Zetzsch, C. **1995**, *In a contribution to the EUROTRAC subproject LACTOZ*, 268.

(76) Zhang, D.; Zhang, R. Y.; Park, J.; North, S. W. *J. Am. Chem. Soc.* **2002**, *124*, 9600.

(77) Carter, W. P. L.; Atkinson, R. *Int. J. Chem. Kinet.* **1996**, *28*, 497.

(78) Dibble, T. S. *J. Phys. Chem. A* **2004**, *108*, 2199.

(79) Paulot, F.; Crounse, J. D.; Kjaergaard, H. G.; Kroll, J. H.; Seinfeld, J. H.; Wennberg, P. O. *Atmos. Chem. Phys.* **2009**, *9*, 1479.

(80) Carter, W. P. L.; Darnall, K. R.; Graham, R. A.; Winer, A. M.; Pitts, J. N. *J. Phys. Chem.* **1979**, *83*, 2305.

(81) Ohta, T.; Bandow, H.; Akimoto, H. *Int. J. Chem. Kinet.* **1982**, *14*, 173.

(82) Washida, N. *J. Chem. Phys.* **1981**, *75*, 2715.

(83) Taraborrelli, D.; Lawrence, M. G.; Butler, T. M.; Sander, R.; Lelieveld, J. *Atmos. Chem. Phys.* **2009**, *9*, 2751.

(84) Jenkin, M. E.; Boyd, A. A.; Lesclaux, R. *J. Atmos. Chem.* **1998**, *29*, 267.

(85) Ghosh, B.; Bugarin, A.; Connel, B.; North, S. W. *J. Phys. Chem. A* **2010**, *114*, 2553.

(86) Sprengnether, M.; Demerjian, K. L.; Donahue, N. M.; Anderson, J. G. *J. Geophys. Res.-Atmos.* **2002**, *107*, 13.

(87) Atkinson, R.; Baulch, D. L.; Cox, R. A.; Hampson, R. F.; Kerr, J. A.; Troe, J. *J. Phys. Chem. Ref. Data* **1989**, *18*, 881.

(88) Glaschickschimpf, I.; Leiss, A.; Monkhouse, P. B.; Schurath, U.; Becker, K. H.; Fink, E. H. *Chem. Phys. Lett.* **1979**, *67*, 318.

(89) King, M. D.; Thompson, K. C. *Atmos. Environ.* **2003**, *37*, 4517.

(90) Maricq, M. M.; Szente, J. J. *J. Phys. Chem.* **1996**, *100*, 12374.

(91) Baker, J.; Arey, J.; Atkinson, R. *Environ. Sci. Technol.* **2005**, *39*, 4091.

(92) Ghosh, B.; Bugarin, A.; Connel, B.; North, S. *J. Phys. Chem. A* - **2010,** *114,* 5299.

(93) Atkinson, R.; Perry, R. A.; Pitts, J. N. *J. Chem. Phys.* **1977**, *67*, 3170.

(94) Boyd, A. A.; Flaud, P. M.; Daugey, N.; Lesclaux, R. *J. Phys. Chem. A* **2003**, *107*, 818.

(95) Butler, T. M.; Taraborrelli, D.; Fischer, C. B. H.; Harder, H.; Martinez, M.; Williams, J.; Lawrence, M. G.; Lelieveld, J. *Atmos. Chem. Phys.* **2008**, *8*, 4529.

(96) Peeters, J.; Nguyen, T. L.; Vereecken, L. *Phys. Chem. Chem. Phys.* **2009**, *11*, 5935.

(97) Jang, M. S.; Kamens, R. M. *Environ. Sci. Technol.* **2001**, *35*, 3626.

(98) Atkinson, R. *Atmospheric Environment Part A-General Topics* **1990**, *24*, 1.

VITA

Name:	Buddhadeb Ghosh
Address:	Department of Chemistry, Texas A&M University PO Box 30012, College Station, TX 77842
Email Address:	buddhadeb09@gmail.com
Education:	B.Sc. Chemistry, Calcutta University, 2003
	M.Sc. Chemistry, Indian Institute of Technology (IIT), Bombay, 2005
	Ph.D. Chemistry, Texas A&M University, 2010